ABSTRACT

Title of Document:	FUNCTIONALIZATION OF SURFACES USING PHOTOLITHOGRAPHY AND OTHER TECHNIQUES
	Kathleen Marie Monaco, Doctor of Philosophy, 2011
Directed By:	Professor John T. Fourkas Department of Chemistry and Biochemistry

Coated materials are encountered on a daily basis, and are a part of almost everything manufactured today. Despite their ubiquity, investigations on their chemical functionality and structure still provide interesting research potential. This dissertation investigates two kinds of coatings, polymeric and self-assembled monolayers (SAMs).

The polymeric coatings investigated are in the form of photoresists that are used to create substrates for laser ablation. Adjusting the composition of the

photoresists leads to the formation of unique structures during this laser ablation. Another application of photoresists that was studied is the creation of transferable microstructures on a flexible substrate. These microstructures, in the form of arches, are created using multiphoton absorption polymerization.

The creation of a patterned SAMs substrate with the potential application as a microarray was explored. Photolithography and soft lithography approaches were tested to create these amine-functionalized surfaces. In addition, silicon nitride surfaces were investigated as a suitable substrate for alkylphosphonate SAMs. A variety of surface techniques including sum frequency generation and X-ray photoelectron spectroscopy were employed to study these surfaces and ultimately the presence of a multilayer, more than one monolayer, was found.

FUNCTIONALIZATION OF SURFACES USING PHOTOLITHOGRAPHY AND OTHER TECHNIQUES

By

Kathleen Marie Monaco

Dissertation submitted to the Faculty of the Graduate School of the
University of Maryland, College Park, in partial fulfillment
of the requirements for the degree of
Doctor of Philosophy
2011

Advisory Committee:
Professor John T. Fourkas, Chair
Professor Sang Bok Lee
Professor Janice Reutt-Robey
Professor Neil Blough
Professor Sheryl H. Ehrman

Dedication

This work is dedicated to

Florence “Gram” Buran.

I’ve finally finished that book.

Acknowledgements

I would like to thank my friends and family for all of their continued love and support. Professor John Fourkas for being a wonderful advisor and always having an endless list of ideas. Dr. Christopher Rivera for being an amazing editor, I could not have written this dissertation without his help and encouragement. Dr. Linjie Li for being a great mentor and his ability to solve any problems that arise in lab.

Dr. George Kumi for all of his help in lab and preparation for candidacy. Dr. Rafael Gattass for his "today is a great day for science" attitude and meticulous presentation editing. Dr. Terry Ding, Xiaoxiao He and Katherine Manfred for their help collecting and processing SFG spectra. Dr. Farah Dawood and Chad Ropp for providing silicon nitride coated slides, and all their guidance with the phosphonate project.

I would like to thank my friend Yunbo Shi, he and I joined the Fourkas group at the same time and had many great experiences. Mike Stocker for his Labview editing, crossword solving and spelling abilities. Floyd Bates and Jarrett Leeds for all their great discussions in lab. Juliet Znovena and Sheree Ibrahim for encouraging me to join the Fourkas group and getting me started on great projects once I became a member.

Also, many thanks goes to the past and present members of the Fourkas group for making and keeping it such an enjoyable place to work: Dr. Qin Zhong, Dr. Erez Gershgoren, Hana Hwang, Meghan Driscoll, Sijia Qin, Sanghee Nah, Xiaoyu Sun,

Alison Sikorsky, John Bender, Dr. Samrat Dutta, Dr. Carlos Toro, Soner Erduran, Pearl Horng, and George Hao.

I would also like to thank Dr. Karen Gaskell for all her XPS expertise and analysis. Tim Maugel for his help with the SEM. Dr. Liwei Yuan and Dr. Qingnan Liu in the Mullin group for their help with the Nd:YAG laser and finally the Sita lab, particularly Brendan Yonke and Emily Trunkely for providing dry solvents for these experiments.

Last but not least, I would like to thank the Graduate Assistance in Areas of National Need (GAANN) fellowship committee for selecting me and providing support for a year of research.

Table of Contents

List of Tables

List of Figures

Chapter 1: Introduction to Photoresists and SAMs

1.1 Introduction

Coated materials are encountered on a daily basis, and are a part of almost everything manufactured today. Common coatings include paint (e.g., applied to the exterior of a building) and corrosion-inhibiting coatings used in automobile manufacturing.[1] On a smaller scale, coatings are commonly used to develop devices on silicon wafers in the semiconductor industry.[2] In biological research, conductive coatings are often applied to specimens to assist in visualization during scanning electron microscopy.[2, 3] From the macroscale to the microscale, coatings can be found on almost everything encountered today, but the chemical nature (including structure and functionality) of even relatively simple coatings provides interesting research potential.

The types of coatings available vary as much as their applications, with each form, such as self-assembled monolayers (SAMs) and thin polymer films, having its own strengths and weaknesses. Each of these coatings can be introduced for unique applications and can modify the functionality of a surface or substrate.[4, 5] For example, a conducting polymer film of polyaniline has show promise in preventing corrosion on iron and steel surfaces, while a long-chain thiol SAM has been shown to protect a gold surface from degradation in a basic solution.[6, 7]

This dissertation will look specifically at polymeric coatings in the form of photoresists and SAMs of chlorosilanes and alkylphosphonates. Photoresists have tailorable properties that are of particular interest for this dissertation. The control over the degree of cross-linking in a photoresist leads to interesting formations, discussed in Chapter 3, when laser ablation is performed on UV-cured films. Alkylphosphonate SAMs offer a way to decrease adhesion of particles in microfluidic channels created on silicon nitride surfaces, while chlorosilane-derived SAMs are investigated for their compatibility with microarrays. Described in the next sections are overviews of photoresists and SAMs, with a focus on specific applications for their use.

1.2 Photoresists

Photoresists are light-sensitive materials that contain a mixture of monomers and a photosensitive compound. In a process known as photolithography, these photoresists are exposed to a light source through a mask, creating a pattern.[8] After exposure to light, the pattern can be revealed in a series of development steps.[8] The mask contains opaque and transparent areas that control which areas on the photoresist get exposed. Photoresists can be used to create polymer films, which can be used as a new substrate, or they can be patterned to create a wide range of structures, from simple two-dimensional lines to complex 3D formations.

Photoresists can be made of many materials, and the type of material is typically chosen for a specific application. Photoresists come in two varieties or tones, negative and positive.[9, 10] In negative-tone photoresists, areas exposed to a

light source become hardened and will remain intact during and after development.[10, 11] In positive-tone photoresists, areas exposed to the light source become more soluble and will wash away during development.[10] Some of the more popular photoresists include phenol formaldehyde monomers mixed with diazonaphyhoquinone (Novolacs/DNQ), which forms a positive-tone resist, and epoxy-based photoresists such as SU-8 which are negative-toned.[12, 13]

For a negative-tone, epoxy-based photoresist, the generation of an acid occurs upon exposure to UV light.[11] This acid serves as a catalyst for cross-linking the epoxy monomers during post-exposure heating.[11] For positive-tone photoresists, exposure to UV will break down the cross-linking within the polymer, causing these areas to become more soluble.[10] This increase in solubility allows for removal of these areas in subsequent development steps. In either case, chemical reactions are initiated upon light exposure within the photoresist, allowing for visualization of a structure after development.

Development steps are unique for each photoresist and generally consist of a series of solvent rinses that will dissolve or remove any unpolymerized photoresist.[9] Some photoresists, such as SU-8 and PerMX 3000, require additional baking steps, after exposure and prior to development to ensure complete cross-linking of the monomers.[11, 14, 15]

Traditional photolithography is a single-photon (linear absorption) process meaning that photon absorption and subsequent polymerization will occur throughout the entire exposed region. This type of photolithography is useful for patterning large areas in a short amount of time, and is most commonly used for the creation of

integrated circuits, but other devices such as optical wave guides have also been fabricated.[8, 16] Fabricating lines in an SU-8 photoresist has been used as a method to create channels for microfluidic and microelectromechanical systems (MEMS) devices.[17, 18] The melting of photoresists has been shown to create microlenses, and in other work, the usage of photoresists to create microarrays for biological studies has been achieved.[19, 20]

Alternative forms of photolithography, such as multiphoton absorption polymerization (MAP), have been used in the creation of 3D microstructures in photoresists.[21-23] MAP uses a femtosecond laser to induce polymerization within a small area of a photoresist. It does so by confining excitation to the small focal area of a microscope objective.[22] Within the focal volume, the simultaneous absorption of two or more photons occurs, inducing polymerization only within that small area.[22] Programming a movable sample stage and shutter controls the location of polymerization within the photoresist.

MAP has advantages over traditional, single-photon photolithography, in that complex 3D structures can be easily created without the use of an expensive set of masks.[23] Additionally, alterations of a structure can be easily performed with MAP by making changes to the stage movement.[23] With traditional photolithography, a different mask would be required for each needed change. Additionally, MAP can create undercut and curved structures that would be challenging using traditional photolithographic techniques.[22] However, since MAP is a serial process, each structure needs to be created individually, which can lead to long processing times.[23]

MAP has been able to create functional microgears that rotate when optically trapped.[24] Other devices created using MAP include photonic crystals and coils.[25,26] Even miniaturized versions of familiar structure such as the Venus de Milo and a bull have been created to highlight the wide range of possibilities for structure creation using MAP (Figure 1.1).[27, 28]

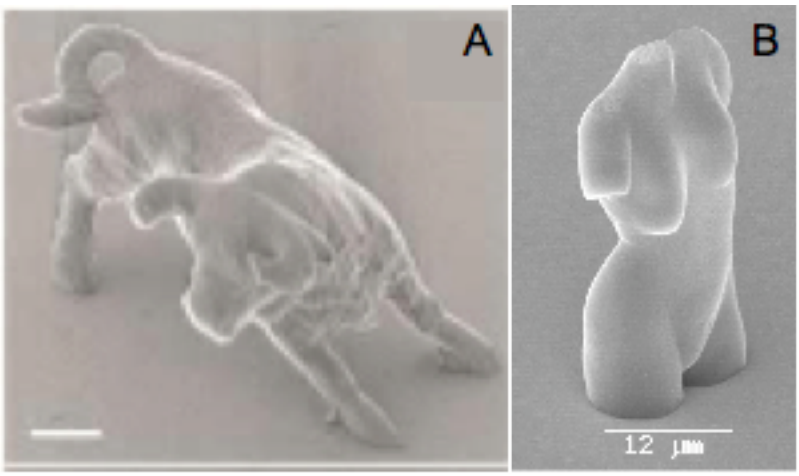

Figure 1.1 A) A MAP fabricated microbull created by Kawata et al.[28] Reproduced from reference 28. **B)** A MAP fabricated Venus do Milo created by Serbin et al.[27] Reproduced from reference 27.

In this dissertation, Chapters 2 and 3 detail laser ablation of a UV cured photoresist on glass; while Chapter 4 discusses laser ablation on more complex 3D structures created using MAP. The use of a solid photoresist is tested for compatibility with MAP in Chapter 5.

1.3 Self-Assembled Monolayers

SAMs are thin layers, usually nanometer thickness, of organized molecules that are strongly bound to a surface.[29, 30] They can be created from solution or vapor-phase deposition, and can contain, any of a multitude of different functionalizations.[30] Typical SAMs contain molecules with a headgroup that bonds to the substrate, a backbone of varying length, and a functionalized endgroup (Figure 1.2).[5, 30] Attractive features of SAMs are that they are easy to apply and headgroups and endgroups can be tailored to fit a specific need.[30, 31]

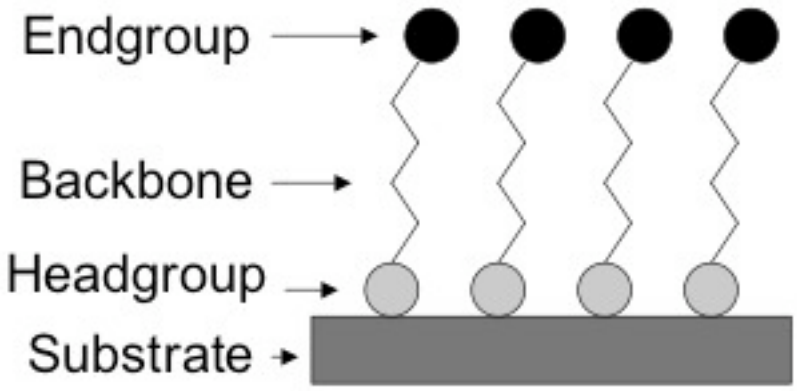

Figure 1.2 An illustration of the components of a self-assembled monolayer.[30] Adapted from reference 30.

The headgroups should be chosen so that there is an affinity or reactivity towards the substrate.[30] The self-assembly process is spontaneous and transitions from a phase in which molecules are randomly deposited on the substrate to a phase in which the molecules are ordered in a way to maximize van der Waals interactions.[5, 32] Many factors that can affect this organization, such as temperature and the solvents used.[5, 30, 32] The resultant SAM is typically ordered, often with a

slight tilt angle. For example, the average tilt angle, relative to the surface normal, for thiols on metals is 30°.[5]

Another common SAM is octadecyltrichlorosilane (OTS) on glass, forming a monolayer with a tilt angle of ≤ 20°.[30] OTS bonds to the substrate through silanol groups to form an Si-O-Si network.[30, 33] These silanol groups get introduced to the substrate through an activation step, such as acid washing or plasma cleaning.[33]

The endgroups consist of functional groups that are chosen based on the intended application of the coating.[31] Hydrophobic or hydrophilic properties can be introduced to a substrate or a specific reactive group can be incorporated.[30, 34] Endgroups can also be chosen to provide a docking site for specific target, which has far-reaching applications for biosensors.[29]

The large variety of endgroups that can be used in SAMs are matched by the number of applications. As mentioned above, biosensors employ SAMs, often alkanethiols on a gold surfaces, to immobilize cells or enzymes for further investigation with surface techniques such as atomic force microscopy (AFM).[29, 34, 35] In a separate experiment utilizing SAMs, AFM probes were coated with an amino silane monolayer to which a ligand was attached.[35] These coated probes were then employed in the study of ligand binding interactions with receptors on a substrate.[35]

SAMs can also be modified after formation. Using traditional wet chemistry or techniques such as photolithography allows access to surfaces with multiple functionalities.[5, 36] Phenyltrichlorosilane is one example of a photosensitive SAM that can be removed photolithographically.[36] Soft lithography has also been shown as a way to pattern SAMs.[37] By functionalizing a substrate with a SAM (e.g., thiols)

and then using a flexible stamp to ink the substrate (e.g., gold) with a reactive molecule, a patterned surface can be achieve.[37] These kinds of patterning techniques can ultimately be used to create spot arrays used to study proteins.[33]

To study SAMs and other coatings, methods to analyze surfaces are needed. These methods range from spectroscopies, such as infrared absorption spectroscopy (IR), X-ray photoelectron spectroscopy (XPS), sum-frequency generation (SFG) spectroscopy and surface-enhanced Raman spectroscopy (SERS), to microscopy-based ones such as AFM and scanning tunneling microscopy (STM).[30] Spectroscopic techniques provide information on the chemical structure of a layer and microscopy techniques can probe the uniformity of a layer as well as directly imaging the surface.[30] Continued research on SAMs will lead to improved and new applications. In this dissertation XPS, SFG and AFM will be used to characterize alkylphosphonate layers on silicon nitride.

1.4 Dissertation Overview

As described above, the work contained in this dissertation uses coatings to study and pattern surfaces. The techniques and materials used in the experiments are different for each chapter and will be described in the introduction at the beginning of each chapter. Below is a brief summary of what will be presented in each chapter.

Chapter 2 illustrates laser ablation on UV-cured acrylate photoresists. Discussed is the observation of the laser ablation threshold decreasing near areas that have been previously ablated. Chapter 3 examines laser ablation on less cross-linked acrylate photoresists. A detailed discussion on the formation of raised dots with holes

in the center is presented with results suggesting that ablation and polymerization are occurring simultaneously.

Working examples, improved using laser ablation, of acrylate structures created using MAP are shown in Chapter 4. These examples include microcantilevers for which ablation is used to circumvent stiction effects, and ring-and-post structures in which ablation is used to remove the ring from the post. Chapter 4 also discusses the effect that stiction, the unintentional sticking of objects, has on microstructures. Preliminary data are presented for the modification with a perfluorostearic acid solution designed to reduce stiction.

Continuing the work done with photoresists, Chapter 5 highlights the use of an epoxy-based photoresist, PerMX 3000, for MAP fabrication. PerMX 3000 is unique because it is a solid photoresist and can be transferred to a substrate after exposure to a light source. PerMX 3000 also becomes flexible upon heating, and transfer to a curved substrate is demonstrated.

Switching to coatings created with SAMs, Chapter 6 looks at the creation of a patterned amine substrate. Approaches to develop this patterned substrate using photolithography, as well as soft lithography, are explored. This patterned amine substrate has the potential for use as a microarray, and experiments detailing the resistance of hydrophobic coatings in solvents used during DNA synthesis are presented.

Chapter 7, investigates the creation of alkylphosphonate SAMs on the surface of silicon nitride. XPS measurements were made to confirm the presence of the deposited layer, while SFG measurements suggested there was not a well-ordered

layer on the substrate. SEM, AFM and additional XPS experiments were conducted and suggest that a multilayer is formed on the silicon nitride surface. The final chapter, Chapter 8, provides a summary of each chapter and offers suggestions for future work.

References

1. Weiss, K. D., Paint and coatings: A mature industry in transition. *Prog. Polym. Sci.* **1997,** *22* (2), 203-245.

2. Nie, Z. H.; Kumacheva, E., Patterning surfaces with functional polymers. *Nat. Mater.* **2008,** *7* (4), 277-290.

3. Echlin, P., *Handbook of Sample Preparation for Scanning Electron Microscopy and X-Ray Microanalysis*. Springer: 2009.

4. Lewis, J., Material challenge for flexible organic devices. *Mater. Today* **2006,** *9* (4), 38-45.

5. Love, J. C.; Estroff, L. A.; Kriebel, J. K.; Nuzzo, R. G.; Whitesides, G. M., Self-assembled monolayers of thiolates on metals as a form of nanotechnology. *Chem. Rev.* **2005,** *105* (4), 1103-1169.

6. Biallozor, S.; Kupniewska, A., Conducting polymers electrodeposited on active metals. *Synth. Met.* **2005,** *155* (3), 443-449.

7. Kumar, A.; Biebuyck, H. A.; Whitesides, G. M., Patterning self-assembled monolayers- applications in materials science *Langmuir* **1994,** *10* (5), 1498-1511.

8. Chiu, G. L.-T.; Shaw, J. M., Optical lithography: introduction. *IBM J. Res. Dev.* **1997,** *41* (1-2), 3-6.

9. Adams, T. M.; Layton, R. A., *Introductory MEMS: Fabrication and Applications*. Springer: 2010.

10. Mortini, B., Photosensitive resists for optical lithography. *C. R. Phys.* **2006,** *7* (8), 924-930.

11. Shaw, J. M.; Gelorme, J. D.; LaBianca, N. C.; Conley, W. E.; Holmes, S. J., Negative photoresists for optical lithography. *Ibm Journal of Research and Development* **1997,** *41* (1-2), 81-94.

12. Reiser, A.; Huang, J. P.; He, X.; Yeh, T. F.; Jha, S.; Shih, H. Y.; Kim, M. S.; Han, Y. K.; Yan, K., The molecular mechanism of novotak-diazonaphthoquinone resists. *Eur. Polym. J.* **2002,** *38* (4), 619-629.

13. Abgrall, P.; Conedera, V.; Camon, H.; Gue, A. M.; Nguyen, N. T., SU-8 as a structural material for labs-on-chips and microelectromechanical systems. *Electrophoresis* **2007,** *28* (24), 4539-4551.

14. DuPont, DuPont PerMX 3000 Photodielectric dry film adhesive technical data sheet. DuPont, Ed. DuPont: 2010.

15. Microchem, SU-8 3000 Permanent Epoxy Negative Photoresist Microchem, Ed.

16. Ma, H.; Jen, A. K. Y.; Dalton, L. R., Polymer-based optical waveguides: Materials, processing, and devices. *Adv. Mater.* **2002,** *14* (19), 1339-1365.

17. Becker, H.; Gartner, C., Polymer microfabrication methods for microfluidic analytical applications. *Electrophoresis* **2000,** *21* (1), 12-26.

18. Zhang, J.; Tan, K. L.; Hong, G. D.; Yang, L. J.; Gong, H. Q., Polymerization optimization of SU-8 photoresist and its applications in microfluidic systems and MEMS. *J. Micromech. Microeng.* **2001,** *11* (1), 20-26.

19. Daly, D.; Stevens, R. F.; Hutley, M. C.; Davies, N., The manufacture of microlenses by melting photoresist. *Meas. Sci. Technol.* **1990,** *1* (8), 759-766.

20. McGall, G.; Labadie, J.; Brock, P.; Wallraff, G.; Nguyen, T.; Hinsberg, W., Light-directed synthesis of high-density oligonucleotide arrays using semiconductor photoresists. *Proc. Natl. Acad. Sci. U. S. A.* **1996,** *93* (24), 13555-13560.

21. Li, L.; Fourkas, J. T., Multiphoton polymerization. *Mater. Today* **2007,** *10* (6), 30-37.

22. LaFratta, C. N.; Fourkas, J. T.; Baldacchini, T.; Farrer, R. A., Multiphoton fabrication. *Angew. Chem.-Int. Edit.* **2007,** *46* (33), 6238-6258.

23. Sun, H. B.; Kawata, S., Two-photon photopolymerization and 3D lithographic microfabrication. In *Nmr - 3d Analysis - Photopolymerization*, Springer-Verlag Berlin: Berlin, 2004; Vol. 170, pp 169-273.

24. Maruo, S.; Ikuta, K.; Korogi, H., Force-controllable, optically driven micromachines fabricated by single-step two-photon micro stereolithography. *J. Microelectromech. Syst.* **2003,** *12* (5), 533-539.

25. Seet, K. K.; Mizeikis, V.; Matsuo, S.; Juodkazis, S.; Misawa, H., Three-dimensional spiral-architecture photonic crystals obtained by direct laser writing. *Adv. Mater.* **2005,** *17* (5), 541-+.

26. LaFratta, C. N.; Li, L. J.; Fourkas, J. T., Soft-lithographic replication of 3D microstructures with closed loops. *Proc. Natl. Acad. Sci. U. S. A.* **2006,** *103* (23), 8589-8594.

27. Serbin, J.; Egbert, A.; Ostendorf, A.; Chichkov, B. N.; Houbertz, R.; Domann, G.; Schulz, J.; Cronauer, C.; Frohlich, L.; Popall, M., Femtosecond laser-induced two-photon polymerization of inorganic-organic hybrid materials for applications in photonics. *Opt. Lett.* **2003,** *28* (5), 301-303.

28. Kawata, S.; Sun, H. B.; Tanaka, T.; Takada, K., Finer features for functional microdevices - Micromachines can be created with higher resolution using two-photon absorption. *Nature* **2001,** *412* (6848), 697-698.

29. Chaki, N. K.; Vijayamohanan, K., Self-assembled monolayers as a tunable platform for biosensor applications. *Biosens. Bioelectron.* **2002,** *17* (1-2), 1-12.

30. Schreiber, F., Structure and growth of self-assembling monolayers. *Prog. Surf. Sci.* **2000,** *65* (5-8), 151-256.

31. Guo, L. Y.; Zhao, Y. P., Effect of chain length of self-assembled monolayers on adhesion force measurement by AFM. *J. Adhes. Sci. Technol.* **2006,** *20* (12), 1281-1293.

32. Schwartz, D. K., Mechanisms and kinetics of self-assembled monolayer formation. *Annu. Rev. Phys. Chem.* **2001,** *52*, 107-137.

33. Onclin, S.; Ravoo, B. J.; Reinhoudt, D. N., Engineering silicon oxide surfaces using self-assembled monolayers. *Angew. Chem.-Int. Edit.* **2005,** *44* (39), 6282-6304.

34. Schreiber, F., Self-assembled monolayers: from 'simple' model systems to biofunctionalized interfaces. *J. Phys.-Condes. Matter* **2004,** *16* (28), R881-R900.

35. Ebner, A.; Wildling, L.; Zhu, R.; Rankl, C.; Haselgrubler, T.; Hinterdorfer, P.; Gruber, H. J., Functionalization of probe tips and supports for single-molecule recognition force Microscopy. In *Stm and Afm Studies On*, Springer-Verlag Berlin: Berlin, 2008; Vol. 285, pp 29-76.

36. Herzer, N.; Hoeppener, S.; Schubert, U. S., Fabrication of patterned silane based self-assembled monolayers by photolithography and surface reactions on silicon-oxide substrates. *Chem. Commun.* **2010,** *46* (31), 5634-5652.

37. Xia, Y. N.; Zhao, X. M.; Whitesides, G. M., Pattern transfer: Self-assembled monolayers as ultrathin resists. *Microelectron. Eng.* **1996,** *32* (1-4), 255-268.

Chapter 2: Laser Ablation of Acrylate Polymers

2.1 Introduction

Polymers are invaluable materials in science and technology because their properties can be adjusted to meet many specific applications.[1, 2] The ability to control the final properties of a polymer, such as flexibility or chemical functionality, lends itself to many applications in materials science and microelectromechanical systems (MEMS).[2] Since the first reports of laser ablation on a polymer in 1982, the laser ablation of polymer films has become an important tool for creating and ablating microstructures.[3, 4]

Laser ablation is defined as the use of a laser to remove material from a surface. Ablation using a focused laser beam allows for precise control over the creation of 2D microstructures by etching the surface of the polymer film.[5] Laser ablation has been demonstrated on the surface of many polymers, such as polyimide, polycarbonate, polymethylmethacrylate and Teflon, to name a few.[6]

Commercially, ablation is used at IBM in microchip module preparation to create holes in polyimide.[7] The creation of holes in polymers is also useful in the field of microfluidics.[8] Additionally, laser ablation allows for the creation of high-aspect-ratio structures within a polymer.[9] This technique can only be performed one sample at a time however, and thus it requires long processing times for large areas.

Before laser ablation can be carried out, polymer films must first be created. In this chapter, traditional photolithography is used to create polymer films. One common method of photolithography utilizes light to polymerize monomers that have been blended with a photosensitive species.[10] This photosensitive blend of monomers and photoinitiator is known as a photoresist. Photoresists are commercially available or can be made in-house. Many monomers can potentially be used, such as epoxies and acrylates, and can be blended with a photoinitiator suitable for the wavelength of the available light source.[11]

In the work presented in this chapter, photoresists were made in-house with a blend of acrylate monomers and the photoinitiator Lucirin TPO-L. Lucirin TPO-L is a liquid, which allows for easy mixing with the liquid monomers. Tri- and pentaacrylate monomers were chosen for their fast polymerization times and high degree of cross-linking. Once a photoresist has been created, it is then exposed to a light source in order for polymerization to take place.

This polymerization can happen via a radical or cationic mechanism.[12] In the former, radicals are formed and begin reacting with the monomers, causing them to cross-link and polymerize. In cationic polymerization, the exposure to light forms an acid, which helps initiate cross-linking. In both kinds of polymerization, longer exposure leads to increased cross-linking, which in turn leads to larger polymerized regions. By controlling which areas within the photoresist are exposed, patterned polymer films can be created.

In traditional photolithography this spatial control is obtained through the use of a mask. A mask consists of a piece of glass, or another transparent material,

patterned with areas that inhibit transmission. The mask is placed between the light source and the photoresist, thereby restricting certain areas of the photoresist to light exposure. Subsequent development steps can then reveal the patterns. This method of photolithography typically uses single-photon absorption, which allows for an entire layer of photoresist to be cured in one exposure.[13]

Once a solidified polymer structure or substrate is created, laser ablation can be performed. By scanning the laser over the surface of a polymer film, recessed regions within the polymer will appear. The mechanism by which ablation occurs is still not well understood, but it is generally agreed that the energy from the laser pulses is converted to electronic excitations.[6, 14] Following the electronic excitations, bonds within the material break, but it is still debated by what means this bond scission occurs.[6]

The traditional pathways by which this energy transfer occurs are suggested to be photochemical and photothermal.[6, 14] In the photochemical pathway, the electronic energy directly breaks the bonds within the polymer, while in the photothermal model the electronic energy increases the temperature within a small area of the polymer, causing the bonds to break.[6, 14, 15] More recent models suggest that a combination of both pathways is the most probable mechanism of ablation.[6, 14, 16]

Previous studies in our group concluded that the monomer SR368 enhances polymer ablation, which suggests that the decomposition method of SR368 is similar to that of polyimide (PI) (Figure 2.1).[5] Studies on PI performed by Kuper *et al.* have

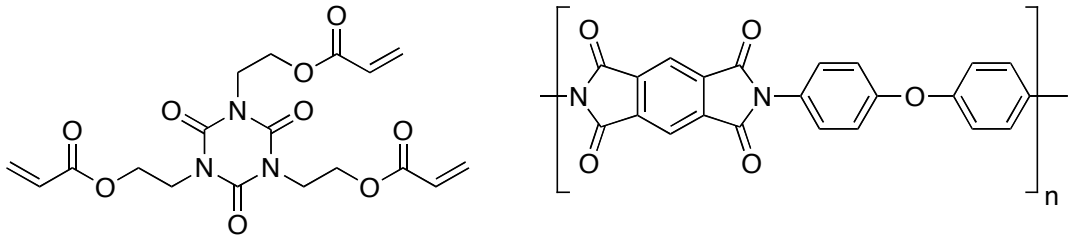

SR368 Polyimide

Figure 2.1 Chemical structures of SR368 and Polyimide.

shown that as the wavelength increases from 248 nm to 351 nm, ablation behavior becomes consistent with a photothermal model.[17] In addition, photothermal ablation is also associated with surface swelling, which will be important to this work.[6] Based on the current literature it is believed that the photothermal pathway dominates ablation in acrylate polymers.[6, 14]

Laser ablation is also known to have an incubation period, i.e. a period of time between when the polymer is first exposed to the laser beam and when ablation first takes place.[18, 19] During this incubation time, the energy deposited is believed to modify the polymer both chemically and physically.[20] Laser power can be used to adjust the incubation time, with higher powers leading to lower incubation times.[19]

Previous work in the Fourkas group has looked at characterizing structures created using femtosecond laser ablation of acrylate polymer films.[5] Additionally, the Fourkas group has demonstrated that laser ablation can be used to create patterns for use in microcontact printing.[5] This chapter examines both the resolution of lines created with laser ablation using higher numerical aperture (NA) objectives and the threshold power required for ablation.

The determination of how close two lines can be placed to one another before the two lines become one larger feature is also important, as this property will

partially determine the number of passes needed to create broader lines and ablated areas. Careful investigation of this parameter is needed in each individual system in order to optimize and minimize the time needed to complete the ablation process. In this chapter both a line resolution study and hole ablation experiment are used to study some the critical aspects of the ablation process, including the line spacing and ablation mechanism. These experiments also demonstrate the ability for fine control of the ablation process.

2.2 Experimental Setup

Ablation sample preparation involves coating a photoresist onto a functionalized substrate. This coating can be applied by either sandwiching the photoresist between two glass substrates or by spin coating a film. In either case films are subsequently polymerized by exposure to UV light. These cured samples are then used for laser ablation.

2.2.1 Resin Preparation

Two acrylate monomer blends were used in these studies: ethoxylated (6) trimethylolpropane triacrylate (SR499 Sartomer)/tris (2-hydroxy ethyl) isocyanurate triacrylate (SR368 Sartomer) and dipentaerythritol pentaacrylate (SR399 Sartomer)/tris (2-hydroxy ethyl) isocyanurate triacrylate (SR368 Sartomer) (Figure 2.2). SR368, which tends to crystallize, was heated prior to use for efficient mixing. The prepolymer blends were mixed with 3 percent by weight of a commercial photoinitiator, Lucirin TPO-L (BASF), to make the photoresists.

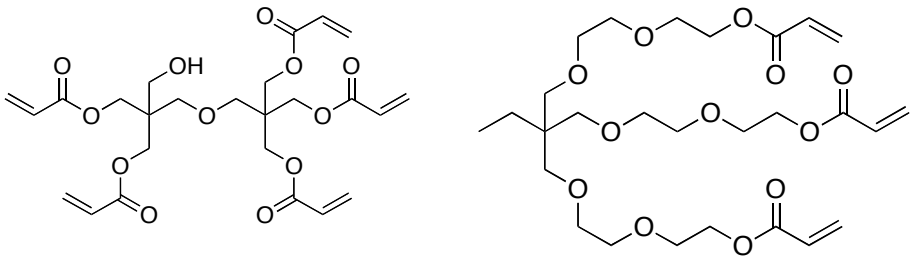

SR399 SR499

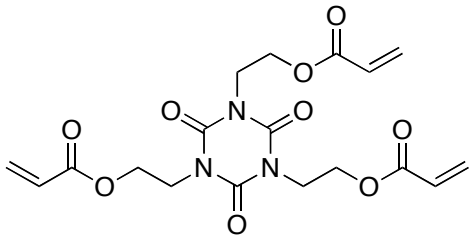

SR368

Figure 2.2 Components of the acrylate prepolymer resins.

Blends of these acrylate monomers were created to tailor the properties of the cured polymer. For example, to create a strong and stable polymer, a blend of SR368, which promotes hardness, and SR499, which reduces shrinkage, can be used. SR399 is a pentaacrylate polymer and therefore has two more reactive sites that can be used if further functionalization of the polymer is needed after fabrication. Specific blends of monomers used in this study can be found in Table 2.1.

Photoresist	Prepolymer Blend (wt. %)	Photoinitiator Concentration
I	55.3% SR499/41.7% SR368	3% TPO-L
II	53.8% SR399/43.2% SR368	3% TPO-L

Table 2.1 The prepolymer acrylate blends used to create the photoresists used in this study.

2.2.2 Substrate Preparation

Substrates were functionalized with acrylate groups to promote adhesion of the polymer. To prepare glass substrates (#2 coverslips, Corning) for coating, slides were sonicated three times, once each for 3 minutes in acetone (Production Grade, BDH), isopropyl alcohol (99% Reagent Grade, Pharmco-Aapar), and distilled water, followed by oxygen plasma cleaning (Harrick plasma cleaner/sterilizer, Model PDC-32G). The slides were exposed to an oxygen plasma for 4 minutes at 300 mtorr, resulting in a hydroxylated, hydrophilic surface. The substrates were then immersed directly in an acrylate silane solution for at least 12 hours, rinsed in ethyl alcohol, and then dried at 95 °C. The solution consisted of 93 vol% ethyl alcohol (200 proof, Pharmco-Aapar), 5 vol% distilled water, and 2 vol% (3-acryloxypropyl) trimethoxysilane (95%, Gelest, Inc.).

2.2.3 Single-Photon Polymerization

The single-photon curing of samples was performed with a UV lamp (Black Ray, UV lamp Model B 100). With the exception of the 0.3% TPO-L blends, all samples were exposed long enough for complete polymerization to occur. No further processing was required prior to ablation. Specific details of the sample development times and the UV curing process can be found in Appendix A.

2.2.4 Ablation Setup

Laser ablation was carried out using an upright microscope setup that has been described previously.[21] Briefly, a linearly-polarized, ~200 femtosecond Ti:Sapphire

laser (Coherent MIRA 900-F), tuned to 800 nm, was focused through an objective on an upright microscope. Tuning to 800 nm allows for two or more photons to excite the photoinitiator. The laser is focused onto a sample that is mounted to a programmable stage (LEP MAC5000) that is controlled using Labview. A CCD camera (COHU 4915-2000/0000) attached to the microscope allows for observation of the ablation process.

2.2.5 Polydimethylsiloxane (PDMS) Molding

Once an ablated surface is created a mold can be made to generate an inverted image of the ablated surface. This image provides information about the texture and depth of the ablated surfaces. PDMS (Dow Corning) is a commercially-available elastomer kit that comes in two parts: base and curing agent. The two liquids were combined in a 10:1 ratio of base to curing agent, mixed well and degassed. A few drops of the degassed PDMS were placed directly onto the ablated surface to create a thin film. These samples were then cured for 45 minutes at 95 °C. After curing, the PDMS mold was peeled away gently, revealing a negative of the ablated surface.

2.3 Results and Discussion

2.3.1 Resolution

Ablated lines were created on the surface of a UV-cured acrylate polymer (Figure 2.3). The properties of these lines depend on several factors, including the laser power, the objective used to create the lines and the polymer blend. Previous work demonstrated that smaller structures could be created with higher NA

objectives.[5] Line resolutions of 2.4 μm and 1.7 μm can be achieved with a 10× and 20× objectives respectively. It was also demonstrated that the finest resolution of 1.3 μm could be achieved with a 40× air (NA =0.75) objective.[5]

This similar experiment was employed to study the differences in line resolution among a 20× air (NA=0.5), 40× air (NA=0.75) and 40× oil-immersion (NA=1.3) objectives in photoresist I. Line measurements were taken between the white edges of each ablated line using the SEM. Consistent with the previously observed trend, the line created with the lower numerical aperture is wider, with a width of 1.1 μm (Figure 2.3A) although significantly narrower than in the study mentioned above. Similarly, the line made with the 40× air objective is 900 nm wide compared to 1.3 μm (Figure 2.3B). Average feature sizes as low 600 nm could be obtained with a 40× oil immersion (NA=1.3) objective (Figure 2.3C). This apparent improvement of the resolution here with respect to the earlier work is presumably due to differences in laser power and pulse duration, as well as the scanning speed used to create the lines, but the overall trends agree nicely.

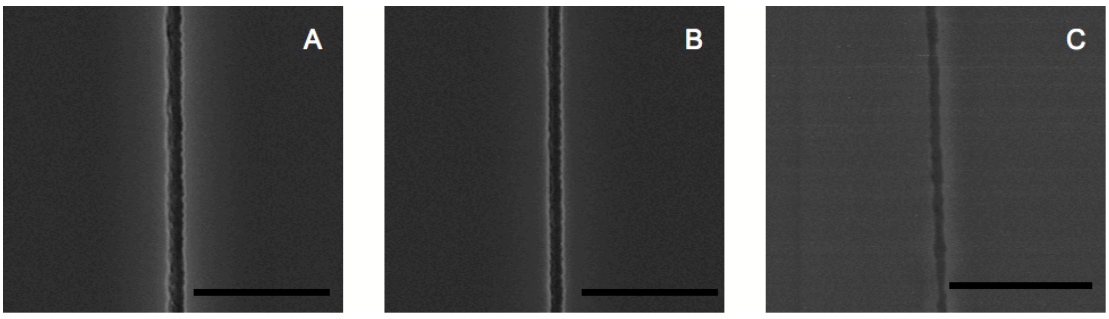

Figure 2.3. Lines created in UV cured acrylate polymer surfaces using photoresist I. Line width decreases with increasing numerical aperture of the objective used to create the lines. Scale bar equal to 10 microns **A)** Line created with 20×, 0.5 NA objective. **B)** Line created with 40× air, 0.75 NA objective. **C)** Line created with 40× oil-immersion, 1.3 NA objective.

The line spacing using a 20× objective at 175 mW was also examined by creating a series of lines with increasingly smaller spaces between each line. A distance of 3 μm was revealed to be the spacing limit for this configuration (Figure 2.4). At separations of less than 3 μm, lines overlap to form one feature. Although only one objective was used in this investigation, a similar study should be performed prior to fabrication of larger structures (a study that was previously performed in our laboratory[5]) to ensure optimal processing times. However, we can tentatively estimate that overlap occurs at a line spacing of approximately 3× the singly ablated line widths.

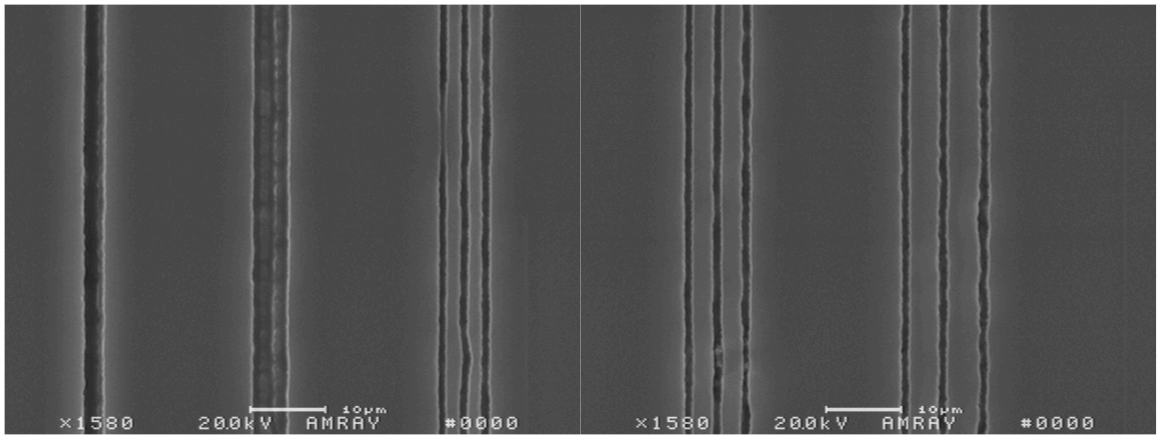

Figure 2.4 Spacing study on lines created in photoresist I. Five sets of 3 lines were created with a spacing of, moving from left to right 1, 2, 3, 4 and 5μm.

To investigate the texture of an ablated line in photoresist I using a 20× objective, PDMS molds were made from an ablated surface (Figure 2.5A). Examination of the molds revealed several areas in which ablation was not perfectly consistent. These areas appear as the fainter, narrower regions in both the ablated lines and the molds, but overall the ablated lines appear relatively smooth (Figure 2.5B). The removal of some of the molded and ablated lines occurs during the molding process when the mold has not completely detached from the ablated surface. This effect can be seen in the lower two lines in Figures 2.5A and B.

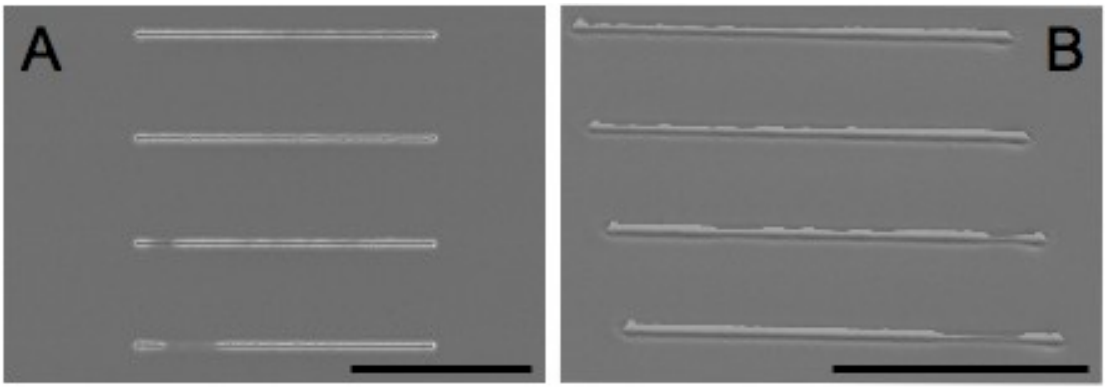

Figure 2.5 Ablated lines created for molding. **A)** The polymer ablated surface. The dark areas on the lower two lines are filled with PDMS that remained attached after molding. Scale bar equal to 100 μm. **B)** The PDMS mold of the ablated surface. Scale bar equal to 100 μm.

Optimal ablation conditions were investigated by studying powers vs. scanning velocities. Powers ranged from 300 mW to 150 mW and velocities ranged from 1600 μm/s to 25 μm/s. Three lines were created for each parameter, and the stage began moving as soon as the polymer was exposed to the laser. If ablation was seen for the entire length of all three lines, it was considered full ablation. If a portion of one of the lines was missing it was considered partial and if no ablation was seen at

all it was considered none. The ablated sample can be seen in Figure 2.6A and a chart with the ablation conditions is presented in Figure 2.6B. It was determined that at powers of 300 mW and 250 mW, ablation occurs with every velocity. At 250 mW partial ablation was observed for velocities higher than 200 μm/s. Below 200 μm/s, full ablation was observed. No ablation was seen using 150 mW at velocities of 200 μm/s and above, and below this combination only partial ablation was observed. It is intuitively obvious that at higher powers and lower velocities ablation is more likely to be consistently observed since the surface is exposed to greater number of photons, and these results are consistent with this logic. While not surprising, this result demonstrates our ability to control ablation conditions precisely and it constitutes an important metric for optimizing processing under these condition.

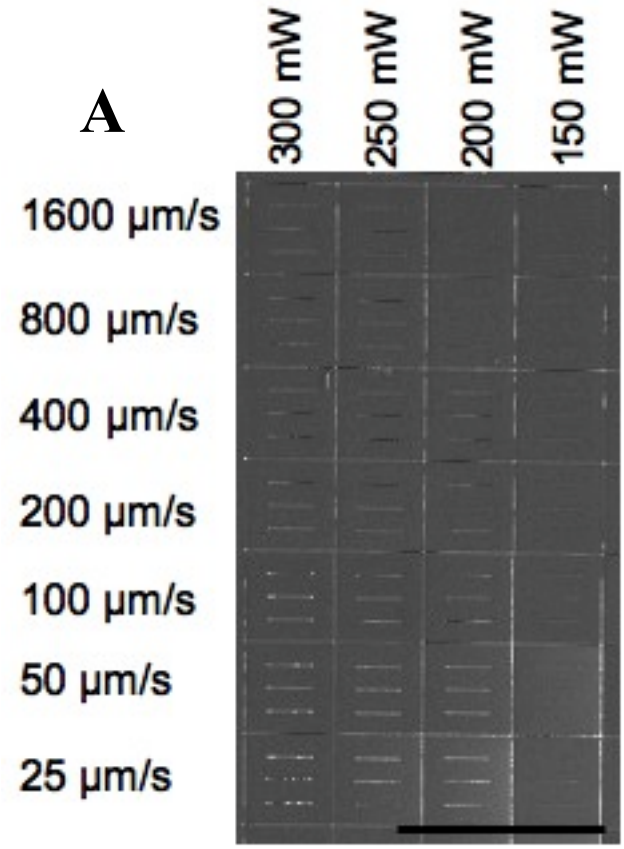

B	300 mW	250 mW	200 mW	150 mW
1600 µm/s	Full	Full	Partial	None
800 µm/s	Full	Full	Partial	None
400 µm/s	Full	Full	Partial	None
200 µm/s	Full	Full	Partial	None
100 µm/s	Full	Full	Full	Partial
50 µm/s	Full	Full	Full	None
25 µm/s	Full	Full	Full	Partial

Figure 2.6 Power vs. velocity study to optimize ablation conditions. **A)** The ablated polymer surface. Scale bar is equal to 0.5 mm **B)** A chart of the ablation seen in A. Full ablation is when ablation was always observed, partial for when only some areas were ablated and none for when no ablation was observed.

2.3.2 Crossing lines

It was observed that creating ablation features near areas that had been previously ablated required shorter incubation times. To investigate this observation, a 250 µm long line was created at 500 µm/s in a UV-cured polymer (photoresist II) surface at high power. Lines were then ablated perpendicular to the existing line with decreasing powers (Figure 2.7A). The perpendicular lines moved from right to left

and no time for incubation was included. It was observed that at higher powers (200 mW and above) ablated lines appear before and after the previously ablated line. At powers of 160 mW and 120 mW ablation started only after reaching the already ablated line and at 80 mW only a small mark can be seen where crossing occurred (Figure 2.7B).

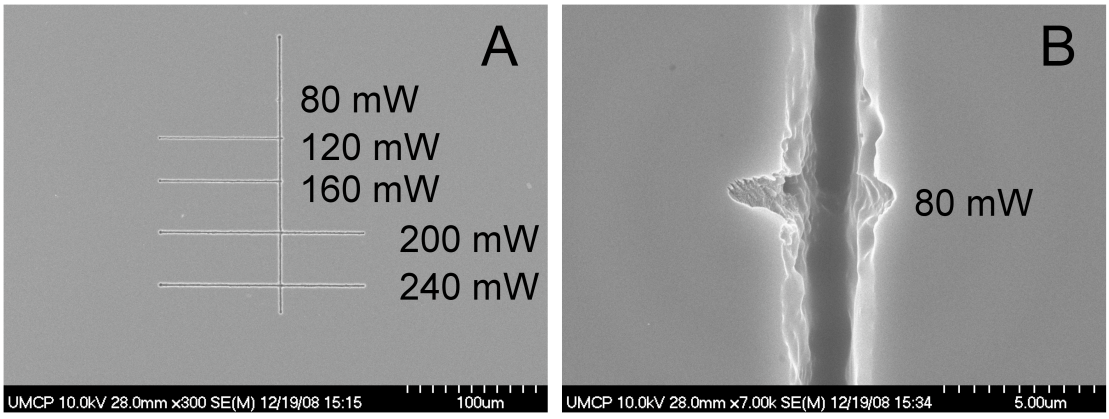

Figure 2.7 A) An SEM image of a series of ablated horizontal lines crossing an ablated vertical line. Laser power was increased for each horizontal line from bottom to top, and the laser was scanned from right to left. **B)** A close up of the mark made by the 80 mW laser pass.

These results indicate that there is a threshold power at which ablation will occur, no matter the location. In this case the threshold power is above 200 mW. Below this power, no ablation can be seen on a clean polymer film, suggesting that the power is below the threshold power for ablation at this velocity, devoid of incubation. At powers below the ablation threshold for clean polymer, ablation can be seen only after crossing a previously ablated line. As seen for 80 mW ablation, even powers that cannot sustain ablation at the given conditions show some effect near the previously ablated line. It is clear that the initial ablation is physically creating a rough line in the surface. Near the edges of the line however, the ablation

threshold appears to be lowered. It is reasonable to imagine that that near the edges of the ablated line there is a region in which chemical modification of the polymer has occurred (possibly partial ablation) which essentially weakens the polymer this and decreases the threshold. It is also possible that the rougher edges and small particle released by the primary ablation could act similarly to a fuse by catalyzing ablation due to the already modified surface.

To test if a rougher surface is responsible for the induced ablation, a razor blade was used to create a line in a UV cured polymer and lines were then ablated perpendicular to it (Figure 2.8A). Again, at higher powers (≥ 200 mW) ablation occurs on both sides of the line. At 160 mW three lines were created. Two of these lines started ablating just after the razor line, and one started right before the razor line (Figure 2.8B). Another ablated line created with 140 mW of power also began after the razor scratch (Figure 2.8B). This effect could be an indication that the razor line created a favorable surface to initiate ablation, although some areas may have been raised or lowered sufficiently to actually prevent ablation. Evidence for this latter phenomenon can be seen in Figure 2.8C, where at 240 mW the ablated line seems to disappear in sections of the razor line. It can also be seen that a significant amount of debris (circle Figure 2.8C) was created on the polymer surface after scratching. It is possible that the line appearing after the scratch at 160 mW and 140 mW were initiated by the particles of debris (Figure 2.8B), supporting the proposed fuse-like mechanism.

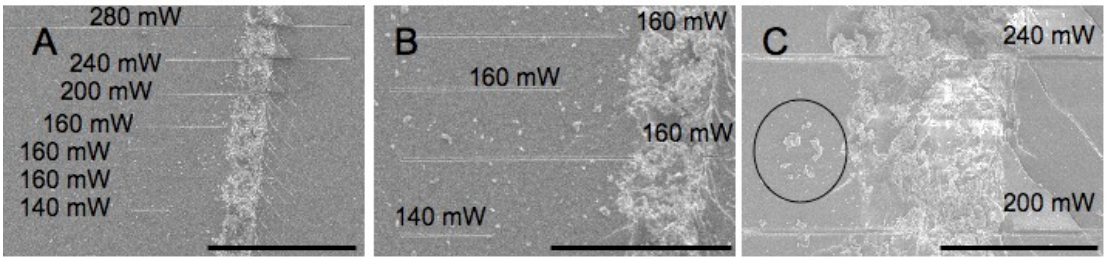

Figure 2.8 A) An SEM image of a series of horizontal lines crossing a vertical line created by dragging a razor over the surface of a highly cross-linked polymer. The thin lines on the right of the razor line are stress fractures from the creation of the razor line. The ablated horizontal lines were created by scanning the laser from right to left. Scale bar equals 200 μm **B)** A close up of the lines created with 160 mW and 140 mW seen in Figure 2.6A. Scale bar equals 100 μm. **C)** A close up of Figure 2.6A highlighting the damage done by the razor line and the ablated lines created with 240 mW and 200 mW laser power. Scale bar equals 40 μm.

2.3.3 Mechanism Study

To investigate the ablation mechanism, laser ablation was used to create holes in a polymer surface. These holes had the same total laser exposure, but the length and number of individual exposures varied. The total laser exposure time was 1 s. Holes were created using either a continuous 1 s exposure or else the exposure time was broken up into 10 groups of 0.1 s with a time of 100 s gap between each exposure. Observing smaller holes created with the interrupted exposure would suggest that a thermal mechanism is operative, because any heat that built up in the polymer would have time to dissipate between exposures. If holes created with one exposure of 1 s and 10 exposures of 0.1 s appear the same, it would suggest that a photochemical mechanism dominates the ablation.

Figure 2.9A shows 4 holes created with 1 exposure of 1 s and Figure 2.9B shoes 4 holes created with 10 exposures of 0.1 s. Both sets of holes were created in

photoresist I. The sets of holes are the same size, which suggests a dominance of a photochemical mechanism for ablation. Repeating the same experiment in

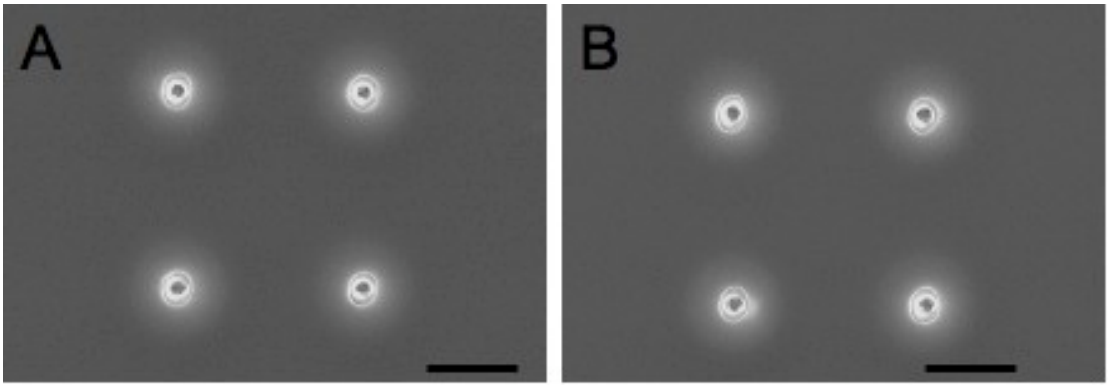

Figure 2.9 Ablated holes created in photoresist I. **A)** Ablated holes created using 1, 1 s exposure time. Scale bar equals 10 μm. **B)** Ablated holes created using 10, 0.1 s exposure time. The time between each exposure was 100 s. Scale bar equals 10 μm.

photoresist II revealed that there are slight differences between the two sets of holes. The holes created with one exposure of 1 s (Figure 2.10A). appear to have more damage on the polymer surface than the holes created with the 10, 0.1 s exposures (Figure 2.10B). This observation suggests that a thermal ablation mechanism may also contribute when using photoresist II. This difference maybe lie in the amount of cross-linking present in the polymer with photoresist II having 2 additional acrylate groups available for polymerization. This increase in cross-linking may require more laser exposure and heat generation to break apart the polymer.

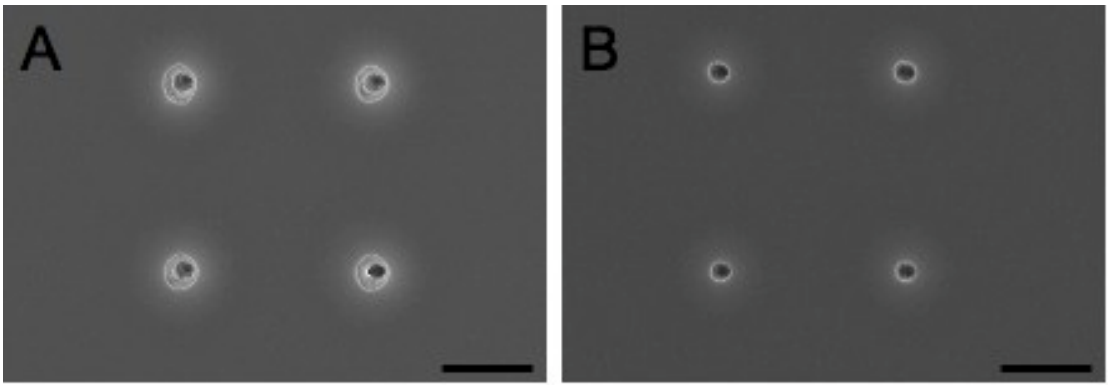

Figure 2.10 Ablated holes created in photoresist II. **A)** Ablated holes created using 1, 1 s exposure time. Scale bar equals 10 μm. **B)** Ablated holes created using 10, 0.1 s exposure time. The time between each pulse was 100 s. Scale bar equals 10 μm.

A control experiment was performed for each of the photoresists in which the polymer surface was exposed to only 1/10 of the total laser power (1 exposure for 100 ms). In photoresist I a small mark could be seen on the surface, but no ablation or hole was present. In photoresist II no mark could be seen on the polymer surface. Both polymers require longer than 100 ms of exposure to the laser to produce ablation (at powers of 200 mW for photoresist I and 220 mW for photoresist II).

2.4 Conclusions

The effects of ablation on cross-linked acrylate polymers have been described, and new average line widths of 600 nm created with the 40× oil-immersion objective (1.3 NA) were reported. Experiments showed that the minimum line spacing for a given set of conditions is 3 microns. Powers and velocities that ablation could be observed at were investigated and it was shown that as power increases and velocity decreases the surface is more easily ablated. In addition, at powers of 250 mW and above, ablation could be seen at all velocities tested. Studies also indicate that

ablation near a roughened surface appears to decrease the threshold power required for ablation to start. These roughened areas could be created using laser ablation or with a razor. Initial mechanism studies suggest that the ablation occurs by a chemical mechanism in photoresist I, and a thermal mechanism in photoresist II.

Performing simple but very important characterization experiments allowed for fine control of the resultant ablation structures, such as line width. Knowledge from these characterization experiments also assisted in optimizing processing times for future studies. Obviously, there are many combinations of photoresists and laser parameters that can be tested. From the small portion of combinations studied here, a general recipe for performing consistent ablation in photoresist I would be to use the 20× objective with 250 mW of power at a velocity at around 200 μm/s. If a smaller line width is needed the objective used could be changed to a 40× air or oil-immersion objective with a higher numerical aperture.

References

1. LaFratta, C. N.; Fourkas, J. T.; Baldacchini, T.; Farrer, R. A., Multiphoton fabrication. *Angew. Chem.-Int. Edit.* **2007,** *46* (33), 6238-6258.

2. Liu, C., Recent developments in polymer MEMS. *Adv. Mater.* **2007,** *19* (22), 3783-3790.

3. Kawamura, Y.; Toyoda, K.; Namba, S., Effective deep ultraviolet photoetching of poly methyl methacrylate by an excimer laser *Appl. Phys. Lett.* **1982,** *40* (5), 374-375.

4. Srinivasan, R.; Maynebanton, V., Self-developing photoetching of poly(ethylene-terephthalate) films by far ultraviolet excimer laser-radation *Appl. Phys. Lett.* **1982,** *41* (6), 576-578.

5. Baldacchini, T. Novel Techniques for the Fabrication of Two- and Three-Dimensional Microstructures. Boston College, 2004.

6. Lippert, T.; Dickinson, J. T., Chemical and spectroscopic aspects of polymer ablation: Special features and novel directions. *Chem. Rev.* **2003,** *103* (2), 453-485.

7. Lankard, J. R.; Wolbold, G., Excimer laser ablation of polyimide in a manufacturing facility. *Appl. Phys. A-Mater. Sci. Process.* **1992,** *54* (4), 355-359.

8. Gomez, D.; Tekniker, F.; Goenaga, I.; Lizuain, I.; Ozaita, M., Femtosecond laser ablation for microfluidics. *Opt. Eng.* **2005,** *44* (5), 8.

9. Zhang, Y.; Katoh, T.; Washio, M.; Yamada, H.; Hamada, S., High-aspect-ratio micromachining teflon by direct exposure to synchrotron-radiation *Appl. Phys. Lett.* **1995,** *67* (6), 872-874.

10. Shaw, J. M.; Gelorme, J. D.; LaBianca, N. C.; Conley, W. E.; Holmes, S. J., Negative photoresists for optical lithography. *IBM J. Res. Dev.* **1997,** *41* (1-2), 81-94.

11. Belfield, K. D.; Schafer, K. J.; Liu, Y. U.; Liu, J.; Ren, X. B.; Van Stryland, E. W., Multiphoton-absorbing organic materials for microfabrication, emerging optical applications and non-destructive three-dimensional imaging. *J. Phys. Org. Chem.* **2000,** *13* (12), 837-849.

12. Adams, T. M.; Layton, R. A., *Introductory MEMS: Fabrication and Applications*. Springer: 2010.

13. Sun, H. B.; Kawata, S., Two-photon photopolymerization and 3D lithographic microfabrication. In *Nmr - 3d Analysis - Photopolymerization*, Springer-Verlag Berlin: Berlin, 2004; Vol. 170, pp 169-273.

14. Dyer, P. E., Excimer laser polymer ablation: twenty years on. *Appl. Phys. A-Mater. Sci. Process.* **2003,** *77* (2), 167-173.

15. Cain, S. R., A photothermal model for polymer ablation - chemical modification *J. Phys. Chem.* **1993,** *97* (29), 7572-7577.

16. Sinkovics, B.; Gordon, P.; Harsanyi, G., Computer modelling of the laser ablation of polymers. *Appl. Therm. Eng.* **2010,** *30* (16), 2492-2498.

17. Kuper, S.; Brannon, J.; Brannon, K., Threshold behavior in polyimide photoablation: single-shot rate measurements and surface-temperature modeling *Appl. Phys. A-Mater. Sci. Process.* **1993,** *56* (1), 43-50.

18. Kuper, S.; Stuke, M., Femtosecond UV excimer laser ablation *Applied Physics B-Photophysics and Laser Chemistry* **1987,** *44* (4), 199-204.

19. Sutcliffe, E.; Srinivasan, R., Dynamics of UV laser ablation of organic polymer surfaces *J. Appl. Phys.* **1986,** *60* (9), 3315-3322.

20. Kuper, S.; Stuke, M., UV-excimer-laser ablation of polymethylmethacrylate at 248 nm - characterization of incubation sites with fourier-transform IR-spectroscopy and UV-spectroscopy. *Appl. Phys. A-Mater. Sci. Process.* **1989,** *49* (2), 211-215.

21. Kumi, G.; Yanez, C. O.; Belfield, K. D.; Fourkas, J. T., High-speed multiphoton absorption polymerization: fabrication of microfluidic channels with arbitrary cross-sections and high aspect ratios. *Lab Chip* **2010,** *10* (8), 1057-1060.

Chapter 3: Laser Ablation's Role in the Formation of Dots

3.1 Introduction

As discussed in Chapter 2, laser ablation is an important technique for creating microstructures in highly cross-linked polymer films. All of the microstructures shown in Chapter 2 were created in the plane of the polymer surface. An alternative method of laser ablation has also been developed to create raised conical structures on the surface of a polymer film.

As with the in plane ablation mechanism, the mechanism by which raised features are created is not clearly understood. Past studies have shown that introducing impurities onto a polymer surface and ablating leads to the creation of raised conical structures.[1] Periodic raised features with holes in the center also have been reported on polyimide when using circularly polarized light (Figure 3.1).[2] The

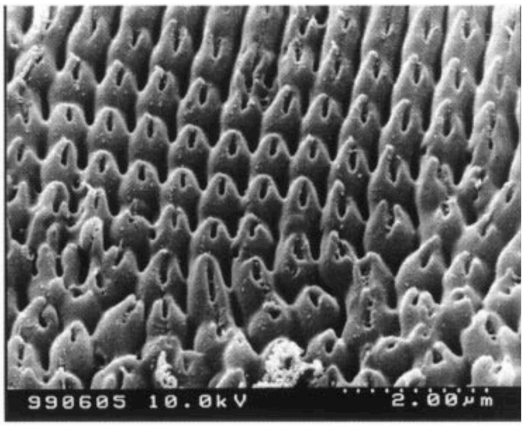

Figure 3.1 Periodic raised structures on polyimide created with a circularly-polarized 800 nm femtosecond Ti:Sapphire laser. Reproduced from reference 2.

creation of conical structures was presumed to be the result of diffraction effects coming from impurities in the sample, but no explanations were given for the presence of the hole in the center.[2, 3] Catry et al. speculated that holes with a slightly raised edge made in polymethylmethacrylate could be due to bubble formation under the substrate surface.[4] When the bubble breaks the material that is removed gathers around the edges and leaves a hole in the center.[4]

In this chapter, experimental results are discussed regarding the use of laser ablation to form raised polymer dots with a hole in the center. The initial creation of these dots was unintentional, but once it was found that they could be created a more completed understanding of how they form was sought.[5] These raised dots are created on less cross-linked acrylate polymer surfaces using the same materials as in Chapter 2. It is unknown how these dots form, but we believe that this less cross-linked polymer surface is a significant factor in the creation process observed and leads to concurrent polymerization and ablation.

3.2 Experimental Setup

Ablation sample preparation consisted of coating a photoresist onto a functionalized substrate. This coating can be applied by either sandwiching the photoresist between two glass substrates or by spin coating a film. Films were subsequently polymerized by exposure to UV light. These cured samples were then used for laser ablation.

3.2.1 Resin Preparation

Blends of ethoxylated (6) trimethylolpropane triacrylate (SR499 Sartomer)/tris (2-hydroxy ethyl) isocyanurate triacrylate (SR368 Sartomer) were used in these studies (Figure 3.2). These blends were created with concentrations ranging from 25 to 50 weight percent SR499 (Table 3.1). The prepolymer blends were mixed with 0.3% of a commercial photoinitiator, Lucirin TPO-L (BASF), to make the photoresists.

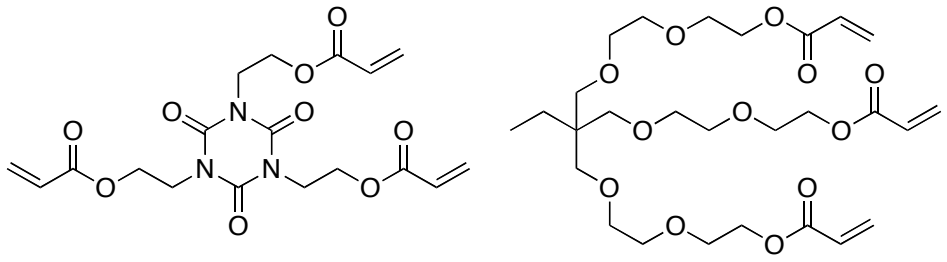

SR368 SR499

Figure 3.2 Components of the acrylate prepolymer resins.

Photoresist	Prepolymer Blend (wt. %)	Photoinitiator Concentration
III	50% SR499/50% SR368	0.3% TPO-L
IV	25% SR499/75% SR368	0.3% TPO-L
V	99.7% SR368	0.3% TPO-L

Table 3.1 List of the prepolymer acrylate blends used to create the photoresists used in this chapter.

3.2.2 Substrate Preparation

Substrates were functionalized with acrylate groups to promote adhesion of the polymer. To prepare glass substrates for coating, slides (#2 coverslips, Corning)

were sonicated three times, once each for 3 minutes in acetone (Production Grade, BDH), isopropyl alcohol (99% Reagent Grade, Pharmco-Aapar), and distilled water, followed by oxygen plasma cleaning (Harrick plasma cleaner/sterilizer, Model PDC-32G). The slides were exposed to an oxygen plasma for 4 minutes at 300 mtorr, resulting in a hydroxylated, hydrophilic surface. The substrates were then immersed in an acrylate silane solution for at least 12 hrs, rinsed in ethyl alcohol (200 proof, Pharmco-Aapar), and then dried at 95 °C. The solution consisted of 93 vol% ethyl alcohol, 5 vol% distilled water, and 2 vol% (3-acryloxypropyl) trimethoxysilane (95%, Gelest, Inc.).

3.2.3 Single-Photon Polymerization

The single-photon curing of samples was performed with a UV lamp (Black Ray, UV lamp Model B 100) with an exposure time of 5 minutes for most samples. No further processing was required prior to ablation. Specific details of the UV curing process can be found in Appendix B.

3.2.4 Ablation Setup

Laser ablation was carried out using an upright microscope setup that has been described previously.[6] Briefly, a linearly-polarized, ~200 femtosecond Ti:Sapphire laser (Coherent MIRA 900-F), tuned to 800 nm, was focused through an objective on an upright microscope. The laser is focused onto a sample that is mounted to a programmable stage (LEP MAC5000) that is controlled using Labview. A CCD camera (COHU 4915-2000/0000) attached to the microscope allows for observation

of the ablation process. After ablation, some samples are rinsed in ethyl alcohol (200 proof, Pharmco-Aapar) for at least 10 minutes followed by a 1 minute rinse in methyl alcohol (Reagent Grade, Pharmco-Aapar) with sonication. The rinsed samples are denoted as such throughout the chapter.

3.3 Results and Discussion

3.3.1 Dots

Three partially cross-linked acrylate films were created, each containing varying amounts of SR368. Ablation was performed to create dots on the surface of each polymer film at varying powers as listed below (Figure 3.3). The laser propagation was positioned perpendicular to the plane of the polymer film. For orientation purposes the surface of the polymer film is defined as the *x*,*y*-plane and the *z* axis perpendicular to the polymer surface.

Polymer films were exposed to the ablating laser until a dot formed; this process generally took ~1 s, but the exposure time can be longer as the laser power is decreased. Exposure times of 15 s and 1 min were also studied. In all photoresists it can be seen that at a specific laser power, as exposure times increased, the sizes of the dots increased as expected.

Besides differences in dot size based on laser power and exposure time, it was observed that as the percentage of SR368 in the sample increased, ablation of the samples yielded larger, more distinct features. Dots created in Photoresist V produced dots that were not pronounced and only slightly raised (Figure 3.3A). In samples created with photoresist IV, a pronounced raised region is present around the

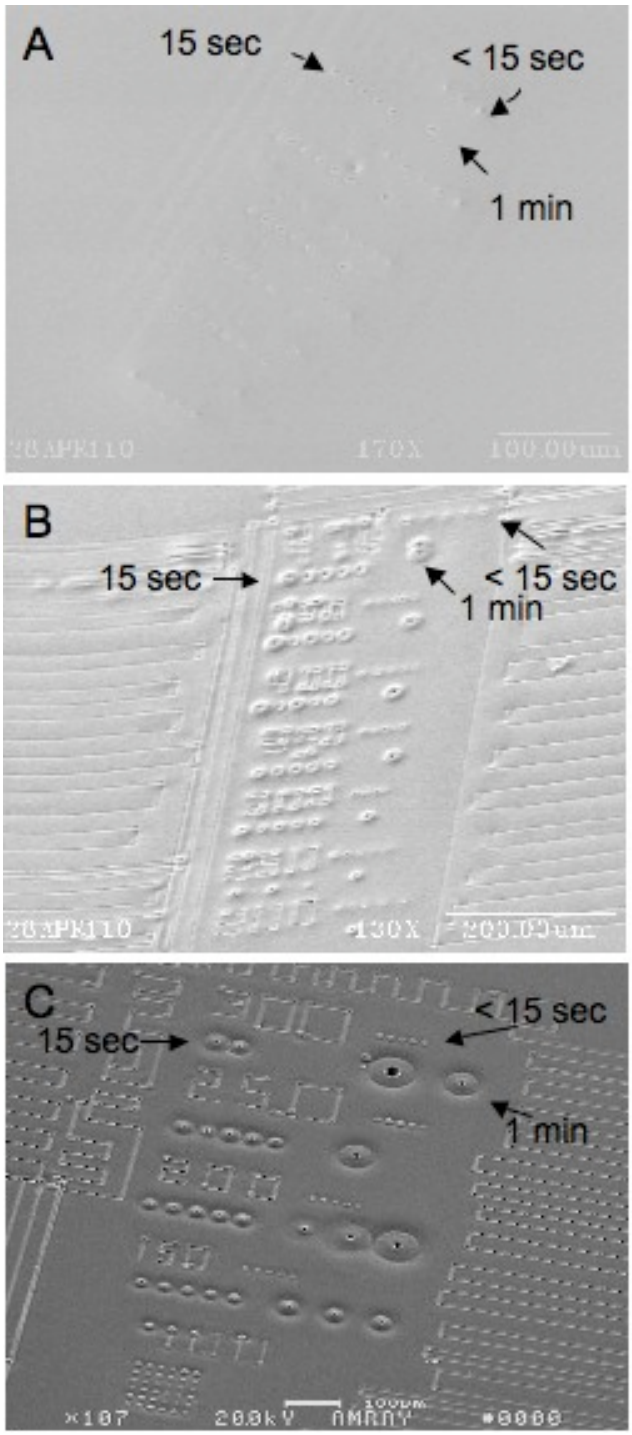

Figure 3.3 Three different blends of polymer were tested for their compatibility with ablation. Areas exposed for < 15 sec were exposed only until a dot formed, in most cases this took only a few seconds but it can take longer than 15 seconds. A) Photoresist III, powers used ranged from 490 mW to 250 mW. B) Photoresist IV, powers used ranged from 490 mW to 200 mW. C) Photoresist V, powers used range from 300 mW to 100 mW.

created dot (Figure 3.3B). Photoresist III yielded recessed regions centered around a dot that is slightly raised (Figure 3.3C).

As mentioned in Chapter 2, the suggested decomposition pathway for SR368 is similar to that of polyimide (PI). Since recessed regions around ablated features occur in pure SR368 but not in the blends, the amount of decomposition in the pure SR368 should be greater than in the blends (Figure 3.4A). Additionally, it is known that SR499 does not ablate well,[7] so presumably its presence in a blend with the SR368 can support the regions on the polymer surface that are being ablated and prevent the collapse of polymer (Figure 3.4B). For all dot experiments after this point, photoresist IV was used.

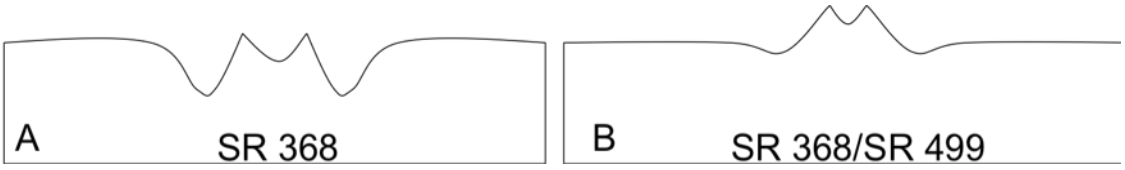

Figure 3.4 Schematic side view illustrations of what could be occurring at the surface of a polymer film during the creation of these dots. **A)** Photoresist V. **B)** Photoresist IV.

Further investigation into the creation of dots involved translation along the *z*-axis. The *z*-axis has a significant affect on ablation due to the changing position of the focal volume and thus the amount of polymer exposed to the laser beam (Figure 3.5). Additionally, ablation can be observed in a shorter amount of time when the beam is focused at the surface, but as the focal point is moved into the bulk of the polymer a longer time is required for ablation to become observable at the surface, influencing the dot structure.

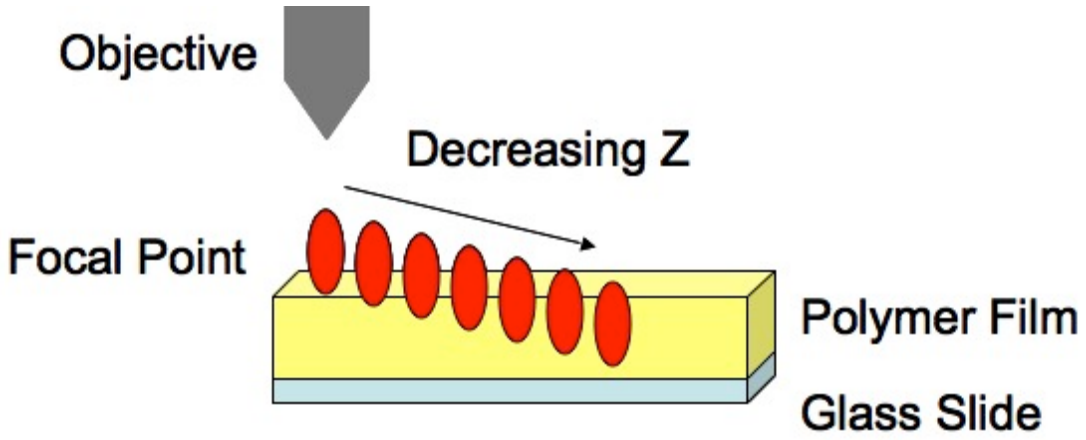

Figure 3.5 A schematic illustration of how moving the focal point affects the amount of polymer that interacts with the laser.

Dots were created in 3×3 arrays at the surface of a polymer film composed of photoresist IV by moving sequentially inwards toward the bulk. The same objective and power were used to create each set of dots and the exposure time was as long as needed until a dot appeared (usually less than 15 seconds). The dots created in the bulk polymer appear more sunken into the polymer than do the dots created at higher *z* values (Figure 3.6). This observation could indicate that ablation occurring in the bulk of the polymer (rather than at the surface) generates greater amounts of decomposition. This decomposition probably leads to the formation of volatile species such as CO, CO_2, HCN and H_2C_2, which have been identified as products formed during ablation of polyimide.[8] Also, due to its ability to reduce shrinkage, the addition of SR499 may help prevent the polymer film from sinking.

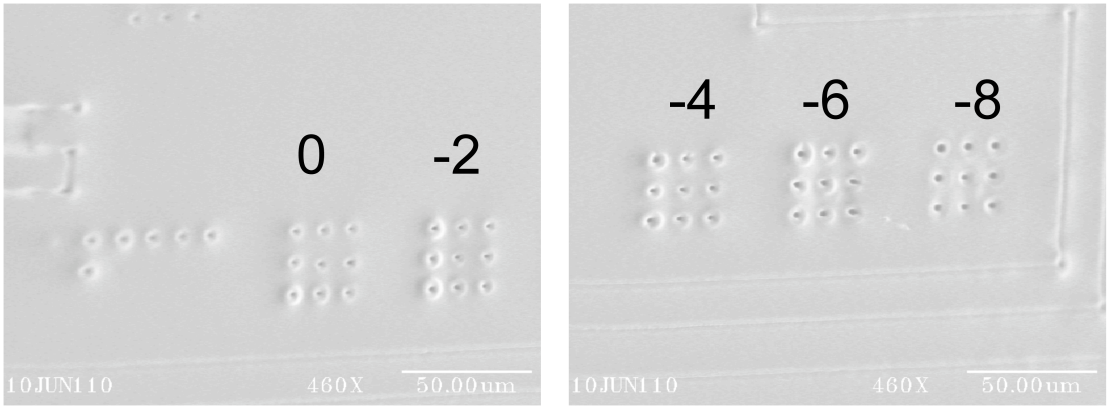

Figure 3.6 SEM image of dots created in photoresist IV with 175 mW of power. Adjusted the *z*-dimension so that the dots created from the film surface, 0, are moving further into the bulk polymer by two microns for each array.

To examine what lies under the polymer surface, another ablation experiment with varying *z*-positions was performed in which the sample was rinsed after ablation to remove unreacted monomers. Pronounced raised dots, each with a clean hole in the center, were observed (Figure 3.7). These dots appear to be of equal height regardless of the depth of the laser focus with which they are created. This observation indicates that what is observed at the polymer surface may not always accurately represent what is occurring within the polymer film.

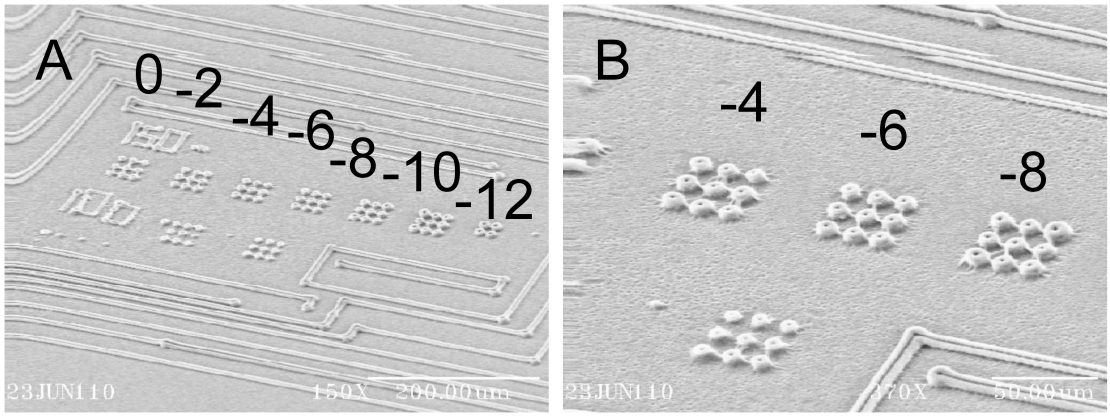

Figure 3.7 A *z* study performed using 150 mW of power in photoresist IV after washing. **A)** An SEM image of the samples created moving into the bulk of the polymer after washing. **B)** A close-up of three of arrays created at different *z* values.

Another interesting feature observed after washing the polymer film is that thin strands of polymer appear between adjacent dots. Another sample was created with the laser focus at only one *z* position close to the surface of the polymer film (Figure 3.8). The raised polymer dots can be seen clearly along with the thin strands of polymer connecting them. These polymer strands are not created intentionally. These strands are most likely due to proximity effects in which the ablating laser is scattered off already created structures causing areas outside the focal point to become exposed.[9, 10] This explanation also suggests that there will be a spacing limit after which the lines will no longer appear between the raised dots.

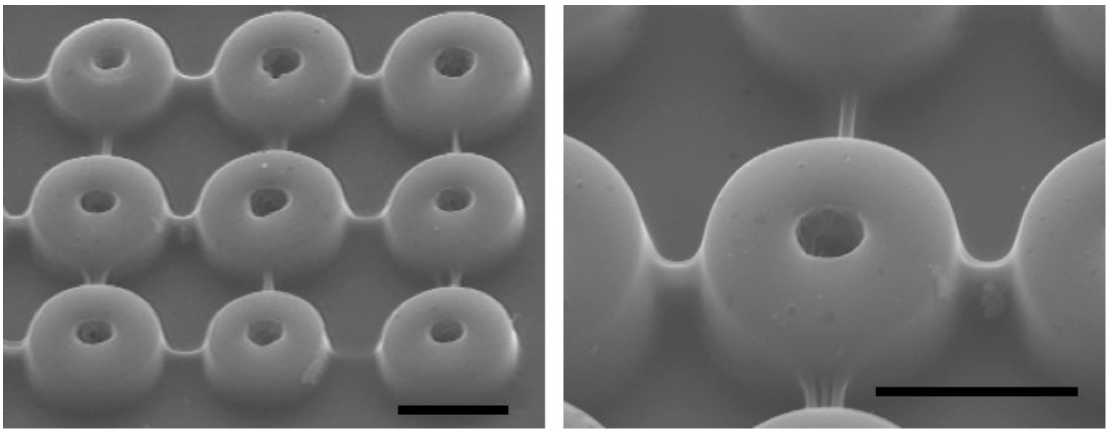

Figure 3.8 Ablated polymer dots after rinsing. Scale bars equal to 10 microns.

The spacing limit was investigated by increasing the distance between dots (Figure 3.9). It was revealed that at a line spacing greater than 16 μm, polymer strands no longer formed between the dots. Strands also appeared between dots that were created in a ring pattern with a 13 μm spacing (Figure 3.10A). Some of the dots

in the ring structure have shallower holes in the center this is due to the polymer not being exposed to the laser for a long enough time (Figure 3.10B).

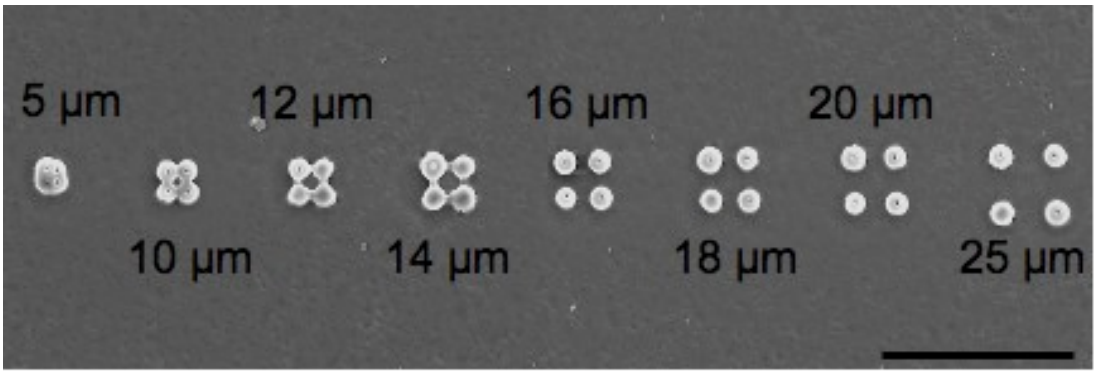

Figure 3.9 A spacing study in which the distance between each set of dots ranged from 5 µm to 25 µm. Scale bar equals 100 µm.

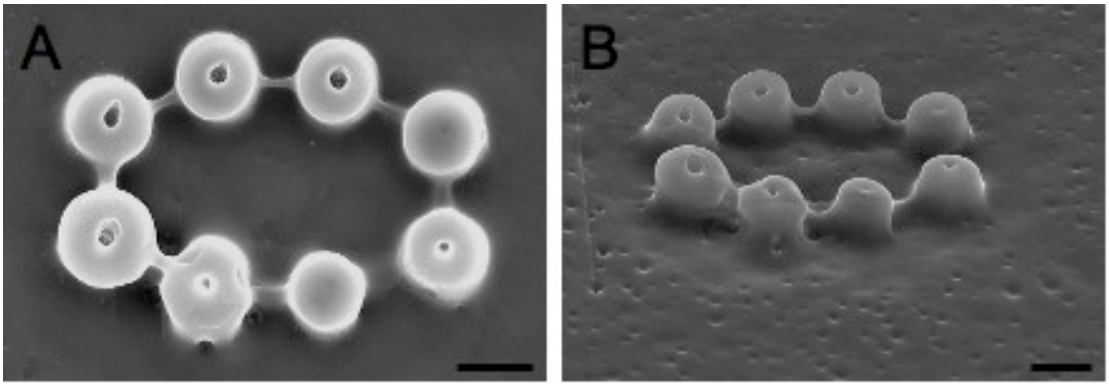

Figure 3.10 Dots formed with ablation in the form of a ring. The spacing between dots is 13 µm . **A)** A top down view of the dots. Scale bar equals 10 µm. **B)** A tilted (50°) view of the dots. Scale bar equals 10 µm.

The facts that the dots are raised and that connecting lines are created suggests that polymerization may be occurring concurrently with ablation. It is possible that the SR368 decomposes, as suggested by previous work,[7] while any unpolymerized monomers, either from SR499 or SR368, are cross-linked by the same exposure. If

these dueling processes occur at the same time in these less cross-linked films, it could potentially lead to the formation of a raised dot and ablation in the form of a hole in the center.

To examine the interiors of dots, ablation was used for cross-sectioning. The dots were created as above, washed and placed back on the microscope stage. Laser ablation was then used to remove half of the dot, leaving behind just the cross-section of the ablated dot (Figure 3.11A). Figure 3.11B indicates that the hole in the center of the dot goes to the polymer surface and that it tapers towards the surface.

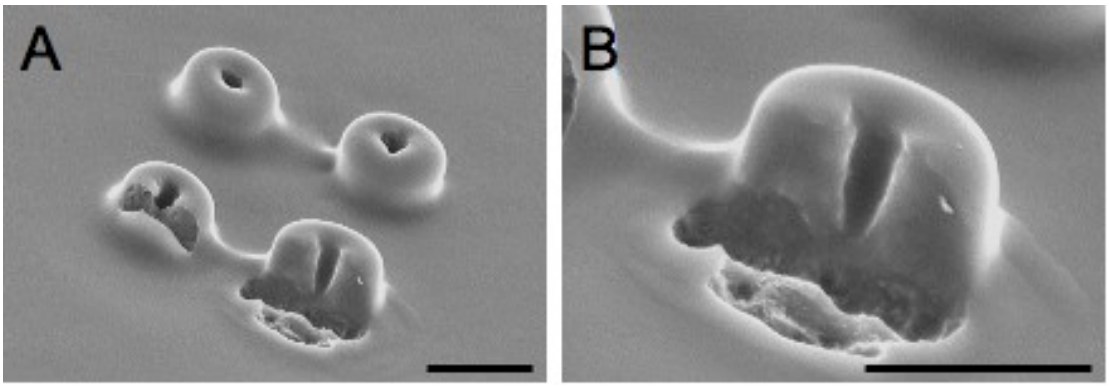

Figure 3.11 A cross-section of an ablated dot. **A)** A series of 4 ablated dots, 2 of which have been cross-sectioned using ablation. Scale bar equals 10 μm. **B)** A close-up of the cut dot in the lower right if Figure 3.11A. Scale bar equals 10 μm.

A power study was performed by exposing the surface of the polymer film using powers at which ablation can be observed and then decreasing towards powers at which ablation cannot be seen. After washing, it was revealed that there were features present that could not be seen on the optical microscope during fabrication (Figure 3.12). These features did not have a hole in the top, which suggests a power lower than the threshold for ablation was being used. Even though ablation cannot be

seen, a reaction occurs that polymerizes the monomers and creates these features. This observation provides strong evidence that powers below the ablation threshold induce further structural growth, resulting in the cone and donut shapes observed.

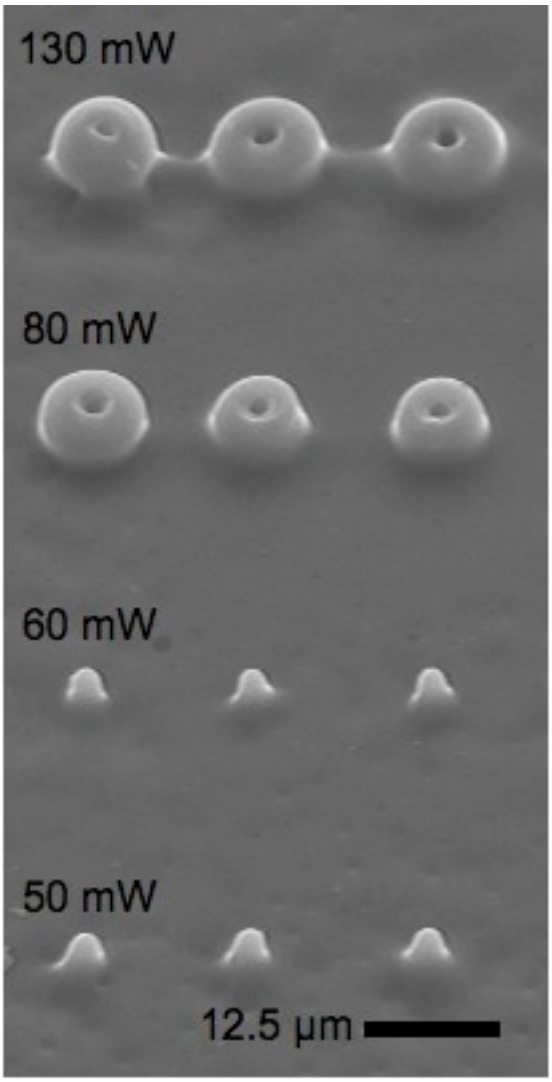

Figure 3.12 Raised dots created in a partially cross-linked polymer film.

3.3.2 Mechanism Study

The mechanism experiments described in Chapter 2 were tested with this resin blend as well and washed after ablation. In Figure 3.13A ablation was used to create dots with 1 exposure of 1s. (The first dot created is only half in the image due to a miscalculation during the ablation.) In Figure 3.13B ablation was used to create dots with 10 exposures of 0.1 ms each. The waiting time between each exposure was 100 s.

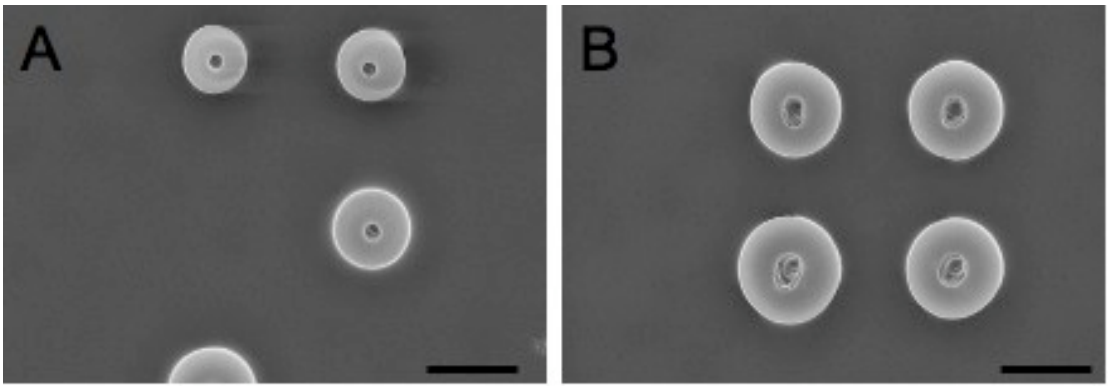

Figure 3.13 Ablation dots created in photoresist IV. **A)** Ablated holes created using a single, 1 s exposure time. Scale bar equals 10 μm. **B)** Ablated holes created using 10, 0.1 s exposure time. The time between each pulse was 100 s. Scale bar equals 10 μm.

Comparing Figure 3.13A to Figure 3.13B indicates that the dots formed from 10 exposures appear larger than those created with a single exposure. Additionally, the holes that formed within the dots appear to have a roughened surface with the 10 exposures while the single exposure holes appear much smoother. The appearance of larger dots with 10 exposures suggests that more polymerization is occurring in these structures than in the structures formed with a single exposure. This could be due to the decreased amount of cross-linking in this polymer blend which allows for a small

amount polymerization of monomers to occur after the laser exposure has ended. The structures created with the 10 exposures would be larger due to this extended polymerization occurring during, and slightly after, each exposure. A control study was performed using a single pulse of the 0.1 s and a small mark on the polymer surface was present but no ablation was observed. This indicates that a longer total exposure time is needed for ablation to be seen.

3.4 Conclusions

The creation of raised dots on partially cross-linked polymer films was described. These raised dots appear to be generated by a combination of polymerization and ablation. An ablated hole appears in the center (the most intense region) and polymerization occurs around the edges (the less intense region). Tests at low powers confirmed the presence of polymerization. A study on the mechanism of ablation indicated that the partially cross-linked films may allow for more polymerization to occur as a total exposure time is broken into smaller times (i.e. a single 1 s exposure vs. 10 exposures of 0.1 s).

References

1. Dyer, P. E.; Jenkins, S. D.; Sidhu, J., Development and origin of conical structures on XeCl laser ablated polyimide *Appl. Phys. Lett.* **1986,** *49* (8), 453-455.

2. Baudach, S.; Bonse, J.; Krautek, W., Ablation experiments on polyimide with femtosecond laser pulses. *Appl. Phys. A-Mater. Sci. Process.* **1999,** *69*, S395-S398.

3. Dyer, P. E.; Farley, R. J., Periodic surface-structures in the excimer laser ablative etching of polymers *Appl. Phys. Lett.* **1990,** *57* (8), 765-767.

4. Catry, C.; Jeuris, K.; Jackers, C.; Hofkens, J.; Bastin, L.; Gensch, T.; Grim, P. C. M.; De Schryver, F. C.; Van Damme, M., Confocal and scanning probe microscopy of surface modifications of thin polymer films induced by infrared diode laser irradiation. *Langmuir* **1999,** *15* (4), 1364-1372.

5. Znovena, J., Picture. Monaco, K., Ed. 2008; p 1.

6. Kumi, G.; Yanez, C. O.; Belfield, K. D.; Fourkas, J. T., High-speed multiphoton absorption polymerization: fabrication of microfluidic channels with arbitrary cross-sections and high aspect ratios. *Lab Chip* **2010,** *10* (8), 1057-1060.

7. Baldacchini, T. Novel Techniques for the Fabrication of Two- and Three-Dimensional Microstructures. Boston College, 2004.

8. Ortelli, E. E.; Geiger, F.; Lippert, T.; Wei, J.; Wokaun, A., UV-laser-induced decomposition of Kapton studied by infrared spectroscopy. *Macromolecules* **2000,** *33* (14), 5090-5097.

9. Parikh, M., Corrections to Proximity Effects in Electron-Beam Lithography .1. Theory *J. Appl. Phys.* **1979,** *50* (6), 4371-4377.

10. Chang, T. H. P., Proximity Effect in Electron-Beam Lithograpy. *Journal of Vacuum Science & Technology* **1975,** *12* (6), 1271-1275.

Chapter 4: The Reduction of Stiction on Polymer Structures

4.1 Introduction

In Chapters 2 and 3, traditional photolithographic methods were used to create polymer films for ablation. In this chapter another kind of photolithography, multiphoton absorption (MAP), is used to create 3D microstructures. MAP allows for an area within a photoresist to be polymerized while the areas surrounding it in three dimensions remain unpolymerized.[1] MAP uses two- or multi-photon absorption to induce polymerization only in a small region. This localization arises from the fact that the probability of the simultaneous absorption of two, or more, photons is highest in regions where the intensity is highest, such as the focal point of a microscope objective.[1, 2]

Being able to move the photoresist relative to the focal point of the objective allows for control over where the polymerization is occurring without the use of a mask. Polymerization using multiphoton absorption therefore allows for the creation of complex, 3D structures that are not achievable with traditional photolithography.[1, 3] However, because MAP is a serial process requiring that each structure is individually created, long processing times are required. Additionally, any structure created using MAP needs to be anchored to a substrate or it will wash away during development.

During development solvent rinses are utilized to remove any unpolymerized monomers and thus reveal the created microstructure. Unfortunately, during development microstructures can become attached to the substrate or to one another. This unintentional sticking is known as stiction.[4, 5] Stiction is due to the surface tension of the solvent which, as it evaporates, can strain a microstructure and pull it towards a substrate causing it to stick.[4-6] These effects are seen because the microstructure is small enough that it can fit inside a solvent droplet. Using solvents with a low surface tension as well as freeze drying structures has shown promise in reducing the amount of stiction seen.[4, 7, 8]

Finding ways to prevent stiction effects from occurring is important because once a microstructure becomes stuck there is no easy way to repair the device.[5, 6] In this chapter, laser ablation is shown to assist in circumventing of stiction effects on microstructures. Additionally, to help reduce the amount of stiction, a fluorinated solution was modified and tested on acrylate surfaces and applied to microwalls created with MAP. Preliminary experiments indicate that this fluorination applied to an acrylated surface is able to decrease the amount of adhesion. Ablation is also shown as a way to free a structure from a surface. MAP was used to create ring-and-post microstructures, and after fluorination ablation was used to cause the ring to fall down the post.

4.2 Experimental Setup

Ablation sample preparation involves coating a photoresist on a functionalized substrate. This coating can be applied by either sandwiching the photoresist between

two glass substrates or by spin-coating a film. Films are subsequently polymerized by exposure to UV light or MAP. These cured samples are then used for laser ablation.

4.2.1 Resin Preparation

Two acrylate prepolymer blends were used in these studies: ethoxylated (6) trimethylolpropane triacrylate (SR499 Sartomer)/tris (2-hydroxy ethyl) isocyanurate triacrylate (SR368 Sartomer) or dipentaerythritol pentaacrylate (SR399 Sartomer)/tris (2-hydroxy ethyl) isocyanurate triacrylate (SR368 Sartomer). The prepolymer blends were mixed with 3 percent by weight of a commercial photoinitiator, Lucirin TPO-L (BASF), to make the photoresists. Lucirin TPO-L has a suitable two-photon absorption cross-section at near infrared wavelengths for use with MAP as well as having a single-photon absorption cross-section compatible with traditional UV light sources.[9] The structures of the monomers used are show in Figure 4.1 and all polymer blends used are shown in Table 4.1.

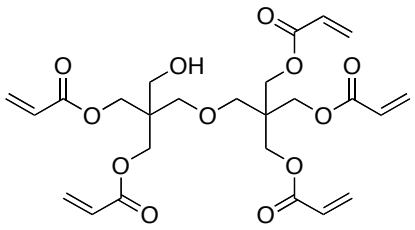

SR399

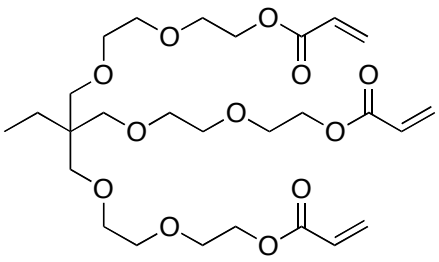

SR499

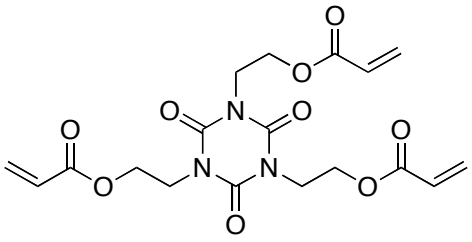

SR368

Figure 4.1 Components of the acrylate prepolymer resins.

Photoresist	Prepolymer Blend (wt. %)	Photoinitiator Concentration
I	55.3% SR499/41.7% SR368	3% TPO-L
II	55.8% SR399/43.2% SR368	3% TPO-L

Table 4.1 The prepolymer acrylate blends used to create the photoresists used in this chapter.

4.2.2 Substrate Preparation

Substrates were functionalized with acrylate groups to promote adhesion of the polymer. To prepare glass substrates (#2 coverslips, Corning) for coating, slides were sonicated three times, once each for 3 minutes in acetone (Production Grade, BHD), isopropyl alcohol (99% Reagent Grade, Pharmco-Aapar), and distilled water, followed by oxygen plasma cleaning (Harrick plasma cleaner/sterilizer, Model PDC-32G). The slides were exposed to an oxygen plasma for 4 minutes at 300 mtorr,

resulting in a hydroxylated, hydrophilic surface. The substrates were then immersed directly in an acrylate silane solution for at least 12 hrs, rinsed in ethyl alcohol (200 proof, Pharmco-Aapar), and then dried at 95 °C. The solution consisted of 93 vol% ethyl alcohol, 5 vol% distilled water, and 2 vol% (3-acryloxypropyl) trimethoxysilane (95%, Gelest, Inc.).

4.2.3 MAP

The MAP setup has been described in detail previously.[10] Presented here is a brief overview of the major components of the MAP system. MAP begins with an ~200 femtosecond Ti:Sapphire laser (Coherent MIRA 900-F), tuned to 800 nm. The beam is directed through a series of optics that can expand or contract the beam and control its pulse duration, power and polarization. The polarization used in these MAP experiments is linear.

The laser is directed into an inverted microscope (Zeiss Axiovert 135) and through a microscope objective. The beam is then focused into a photoresist that is mounted to a programmable stage (Physik Instrumente, P-563 3CD). This programmable stage is controlled using Labview software. To control when the laser interacts with a sample a mechanical shutter is used. By synchronizing the mechanical shutter with the programmable 3D stage, structures can be fabricated. Progress can be visually tracked on a CCD camera (COHU 4912-2010/0000) that is attached to the microscope.

After fabrication, samples are subjected to a series of solvent rinses to remove any unpolymerized photoresists. Samples consisting of the SR399/SR368 blend are

rinsed in dimethylformamide, for ~ 3 minutes, followed by a rinse in ethyl alcohol, for ~ 3 minutes. Samples created from SR499/SR368 are rinsed in ethyl alcohol only for ~ 3 minutes.

4.2.4 Ablation Setup

Laser ablation was carried out using an upright microscope setup that has been described previously and is similar to the setup for MAP.[11] Briefly, a linearly-polarized, ~200 femtosecond Ti:Sapphire laser (Coherent MIRA 900-F) was focused through an objective on an upright microscope. The laser is focused onto a sample that is mounted to a programmable stage (LEP MAC5000) that is controlled using Labview. A CCD camera (COHU 4915-2000/0000) attached to the microscope allows for observation of the ablation process.

4.2.5 Single-Photon Polymerization

The single-photon curing of samples was performed with a UV lamp (Black Ray, Model B 100). To create a flat polymer surface a drop of acrylate photoresist was sandwiched between an acrylate-functionalized coverslip and a silicon wafer. The silicon wafer was rinsed in acetone, isopropyl alcohol and ethyl alcohol and dried at 95°C prior to use. To maintain a constant thickness for each sample a spacer was placed between the acrylate-functionalized coverslip and the silicon wafer. The spacer consisted of 2, #2 coverslips held together by a piece of double stick tape. The setup was then UV cured for 10 minutes. After curing, the cured polymer was

carefully removed from the silicon wafer, while ensuring that it remained attached to the acrylate-functionalized coverslip, to reveal a flat polymer surface.

4.2.6 Fluorinated Coating

The addition of an optional fluorinated coating on MAP structures helps to prevent stiction. Immediately following development structures were placed in an 80% ethyl alcohol, 20% ethlyenediamine (≥ 99%, Sigma) solution for 30 min. The samples were rinsed in ethyl alcohol then transferred to a solution containing 4 mg perfluorostearic acid (97%, Alfa Aesar), 4.455 g pentafluorobenzene (98%, Alfa Aesar), 0.01 g methyl alcohol (Reagent Grade, Pharmco-Aapar), 16 mL ethyl alcohol for 1 hour. The pentafluorobenzene can be replaced with hexafluorobenzene (99%, SynQuest Labs) (Figure 4.2). Specific details regarding each sample can be found in Appendix C.

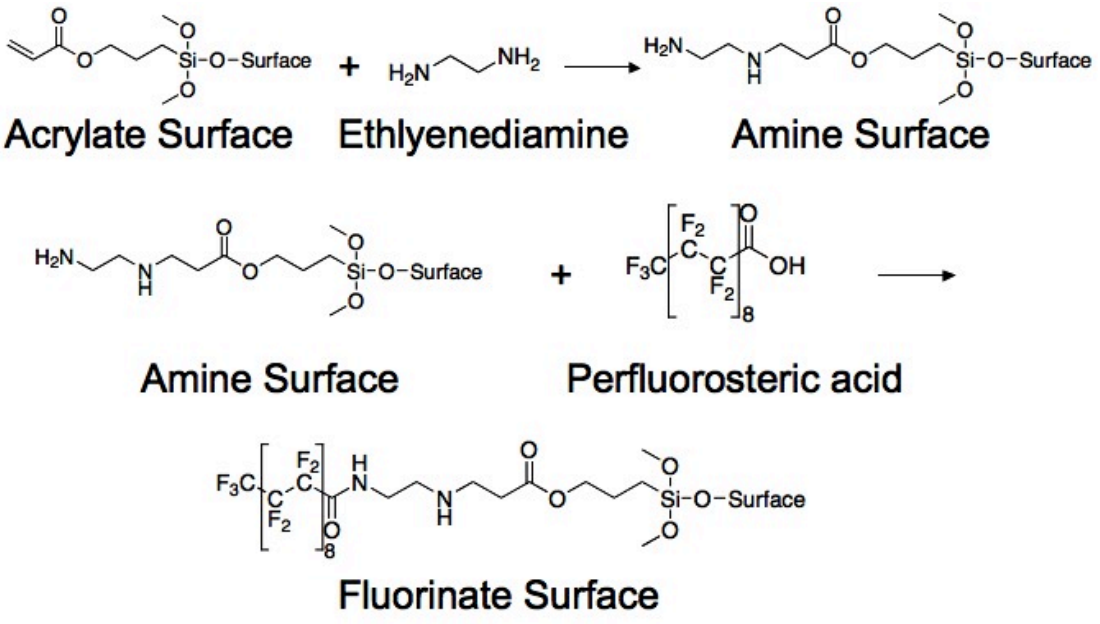

Figure 4.2 The chemistry used to fluorinate an acrylate surface.

In order to confirm the presence of the fluorinated groups on the surface of a substrate contact angle measurements were taken. The sessile drop method was used to measure contact-angles at room temperature between distilled water droplets and treated surfaces.[12] A contact-angle goniometer (Ramé-Hart Instrument Co., 100-00-115) was used to image a drop of distilled water from a micropipette, set to deliver 20 μL, onto a treated surface. The top of the drop was brought into focus in the goniometer and a digital image of the water drop was taken. The contact-angle, angle between the solid-liquid interface and the line tangent to the drop shape at the liquid-vapor interface, was measured using GIMP 2.6 (GNU Image Manipulation Program) software.

4.3 Results and Discussion

4.3.1 Ablation on Cantilevers

Microcantilevers are multipurpose tools that are commonly used in atomic force microscopy for mapping of surfaces and sensing chemical interactions.[13, 14] Previous work done in our group showed that ablation can be used to increase the arm length, or overhang, of a cantilever created using MAP.[15] Figure 4.3 shows three cantilever structures that were recreated from previous work to illustrate how ablation can be used to increase arm length.[15]

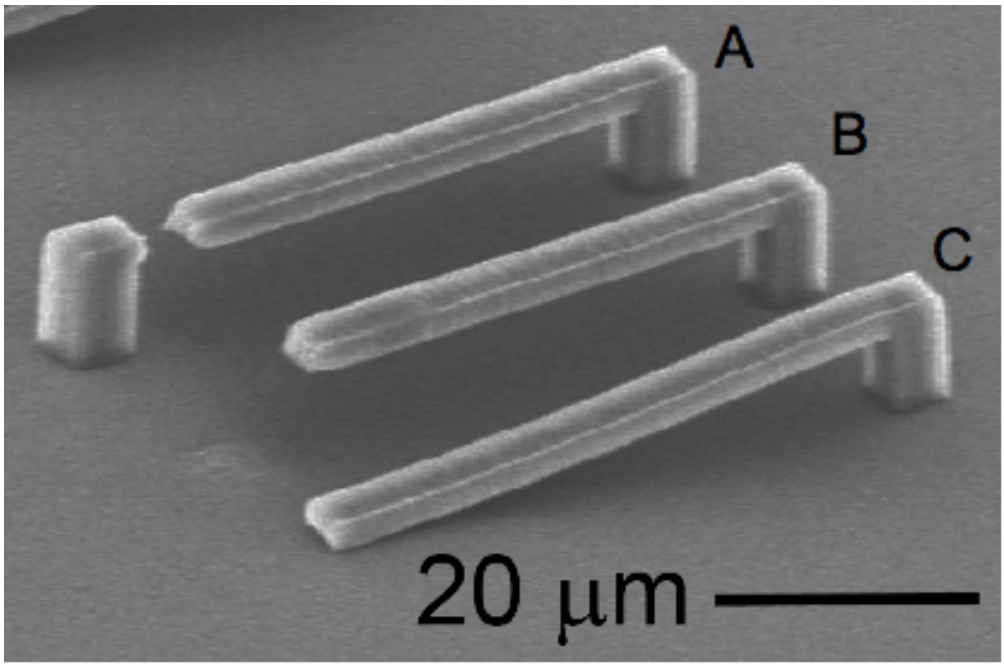

Figure 4.3 A series of microfabricated cantilevers illustrating that ablation can be used to overcome stiction effects. A) Cantilever with a support tower for which ablation has been used to remove a portion of the cantilever arm. B) A free standing cantilever where the support tower has been removed with ablation. C) A cantilever created without a support tower and that has attached to the substrate surface. Scale bar equal to 10 μm.

Two of these cantilevers (A and B) had support towers at the end of the cantilever arms. The third cantilever (C) had no support tower. After development, cantilever C became attached to the substrate while the cantilever with the support towers remained upright. Ablation was then used to remove one of the support towers completely in cantilever B, while only partially removing a section of the cantilever arm from cantilever A. After ablation both cantilevers A and B remained upright. Although cantilevers A and B are slightly shorter than cantilever C, it is presumed that cantilever C would have still attached to the substrate had it been of the same length given the previously reported work.[15]

Stiction is responsible for the behavior of cantilever C. Stiction is a common problem in MEMS devices because there is no easy way to repair a device once it has become stuck.[5, 6] By fabricating support towers at the ends of the cantilever arms on structures A and B, stiction effects were avoided and the cantilevers remained upright and functional. Using ablation, to avoid stiction effects could potentially provide a way to consistently create functional microstructures.

4.3.2 Fluorinated Microstructures

Another way to reduce stiction effects is the application of a coating to prevent adhesion. A fluorinated solution based on the work of Ha et. al. consisting of perfluorostearic acid (PFS) and pentafluorobenzene in methyl alcohol and ethyl alcohol was developed and tested for its adhesion prevention.[16] The hydrophobicity of the surface was tracked by measuring changes in the contact angle of water on acrylate treated glass and polymer surfaces and also by coating a series of microwalls.

Since the reactive site for PFS is a carboxylic acid, surfaces to be coated need to contain a complementary reactive site. However, the surfaces used in our studies are coated with acrylates, which are not directly compatible with carboxylic acid and therefore need to be functionalized. Amine groups are attached to these acrylate surfaces through a Michael addition. These newly functionalized amine groups are treated with the PFS to form an amide linkage. This reaction yields the desired fluorinated surfaces.

Water on hydrophobic surfaces, such as those with coated with fluorinated species, beads up to form droplets. The angle these droplets form with the substrate

can be measured and is known as the contact angle. On hydrophobic surfaces these angles can be 70° or larger. Contact angles of larger than 90° can be seen on superhydrophobic surfaces. Contact angles on hydrophilic surfaces tend to be smaller, typically less than 30°. Therefore, the coating of the acrylate surfaces with PFS can be tracked using contact angle measurements (Figure 4.4). The higher the contact angle measured the more fluorine groups are attached to the surface.

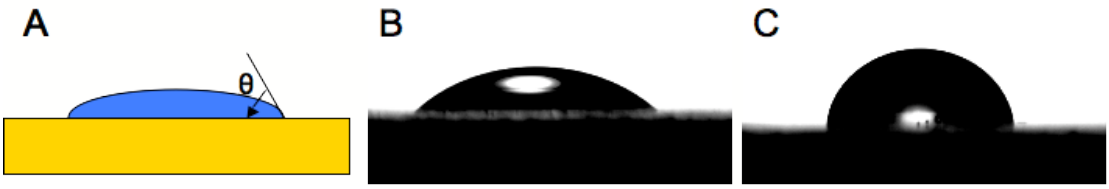

Figure 4.4 A) An illustration of the angle measured between a liquid and a surface. **B)** The contact angle of water on acrylate glass, the angle shown is 43°. **C)** The contact angle of water on a fluorinated surface, the angle shown in 94°.

Acrylate coated glass slides were used for initial testing and have an average baseline contact angle of 45°. These acrylate slides were then amine treated followed by functionalization with PFS. Prior to fluorine functionalization the average contact angle was 41° (Figure 4.5). After treatment with PFS the average contact angle increased to 86°, which indicates that the fluorinated molecules attached to the surface (Figure 4.5). To confirm that the amines are needed for the attachment of the fluorine groups, a piece of acrylate glass was treated with fluorine groups, which resulted in a contact angle of 46°, which is comparable to the angles measured on acrylate and amine functionalized glass (Figure 4.5).

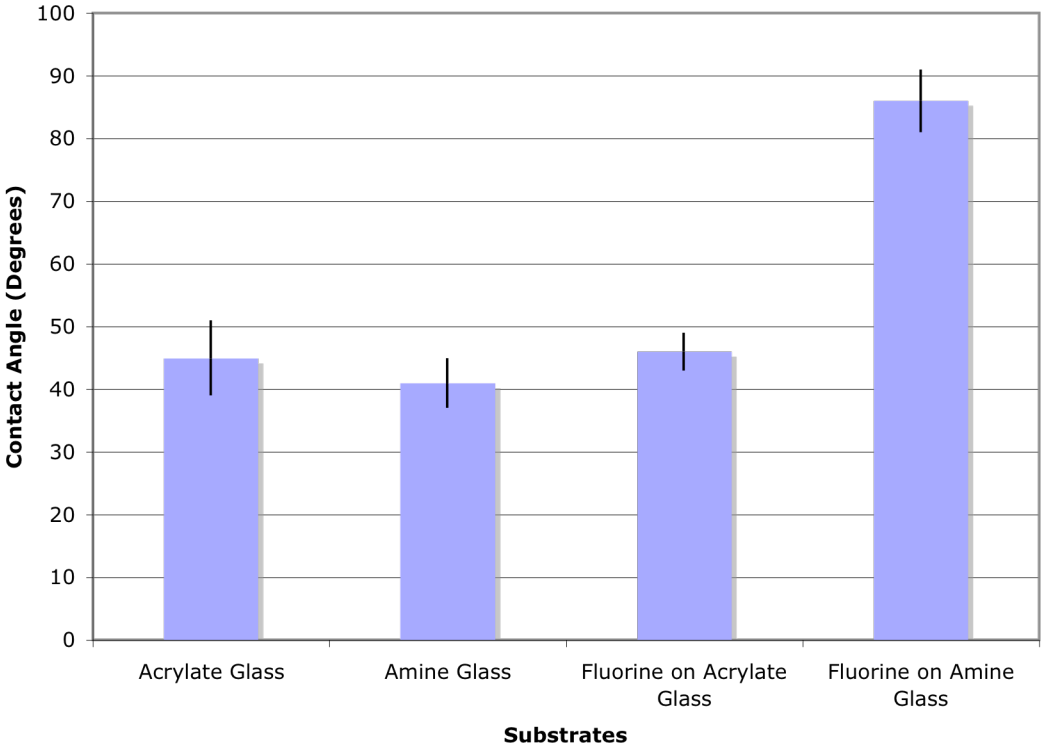

Figure 4.5 Averaged contact angles for glass, surfaces. Acrylate glass, 45° (±6°), amine glass 41° (±4°), fluorinated amine glass, 86° (±5°), and fluorinated alkanes on acrylated glass 46° (±3°).

These experiments were repeated on acrylate polymer surfaces using photoresist II, and results were consistent with those found on glass (Figure 4.6). Contact angles of 98° were found for surfaces treated with fluorinated species and angles of 40° were found for those with amines. These results confirm that the applying the fluorine treatment to acrylate groups increases the hydrophobicity of the surface. Hydrophobic surfaces are less prone to surface adhesion, which suggests that by treating a microstructure with PFS one would be able to decrease the adhesion seen on that structure.

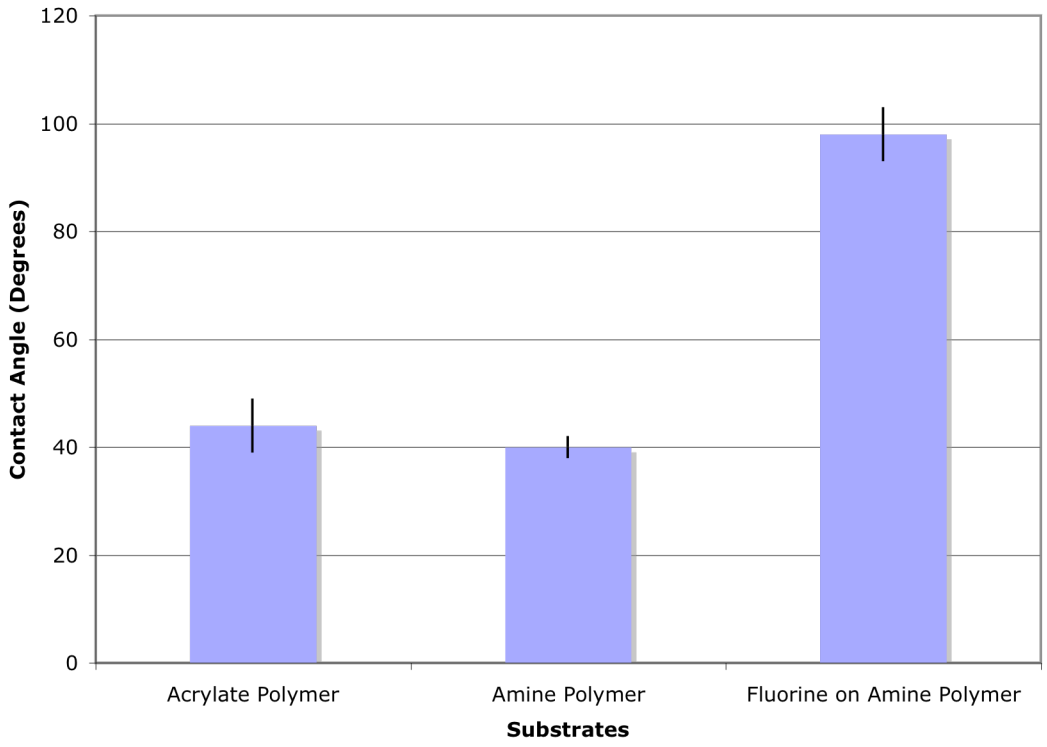

Figure 4.6 Averaged contact angles for polymer surfaces. Acrylate polymer, 44° (±5°), amine treated polymer, 40° (±2°), and fluorine treated polymer 98° (±5°).

Microwalls created using MAP were chosen as the test structure for the fluorinated coating. The microwalls were designed so that they were flexible, to allow for bending of the structure, and far enough apart that during development the top edges would touch if no coatings were added. Sets of walls are shown in Figure 4.7A and B. The walls are all the same length, width and height, 10 × 1.5 × 40 microns respectively, but vary in spacing. Walls in set 1 were created with a spacing of 4 microns, while in set 2 the spacing is 5 microns. Spacings were varied to ensure that some walls would stick during washing without the fluorine treatment.

By fabricating two sets of these walls and rinsing one set in the fluorine solution, with the other set used as a control, it was revealed that the addition of the

fluorinated solution significantly reduces the stiction effects seen on the microwalls (Figure 4.7B). In the control sample, Figure 4.7A, all the walls in set 1 stuck together

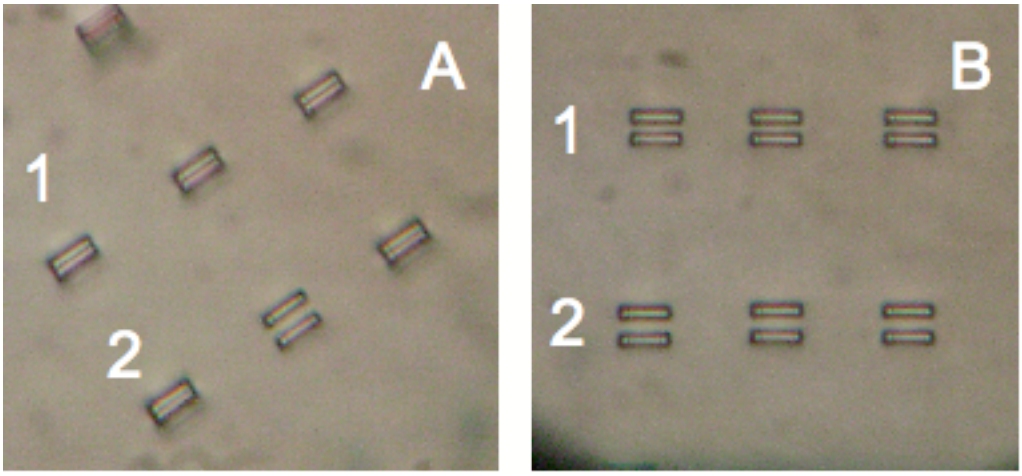

Figure 4.7 Two samples both fabricated with the same series of microwalls. A) Developed without the fluorinated solution. B) Developed with the fluorinated solution.

while in set 2 only one wall pair remained apart after washing. On the sample treated with the fluorine solution all of the walls remained apart.

Finally, this fluorinated solution was also applied to another structure that has previously demonstrated stiction effects after ablation. MAP was used to create a post with a ring attached at 4 points to the top of the post. The goal of this fabrication project was to cause the ring to fall down the post using ablation to remove the 4 connecting points (Figure 4.8). MAP could not be used to fabricate a free ring-and-post structure because the detached ring would wash away during development. Initial attempts to remove the ring from the post using ablation yield a ring that would stick to the post once freed as seen in Figure 4.8 A and B.

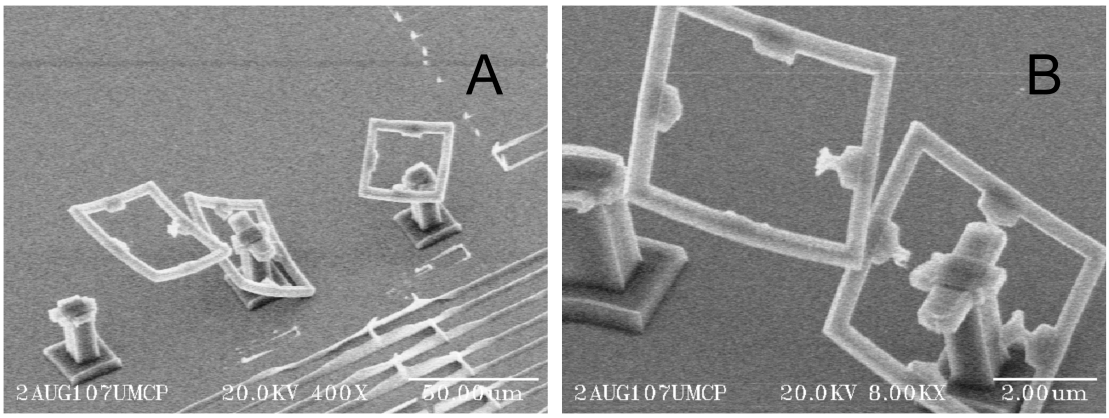

Figure 4.8 Demonstrations of stiction effects on a ring and post structure. A) Rings detached from their posts. B) Close up of two attached rings.

The sticking seen in these microstructures can be enhanced due to the thin ring size, resulting in less electrostatic force needed to cause stiction. To prevent sticking, the fluorinated coating was applied to a similar ring and post structure after development.

When ablation was used to remove the connecting points the ring no longer stuck to the post or neighboring rings, as seen in Figure 4.9A. The fluorinated solution appeared to prevent the ring from sticking to the post on one structure. Unfortunately, there was still sticking of the ring on another structure in Figure 4.9B, although it appears that stiction occurred only where the laser was used to ablate the connection points, where no fluorinated coating is present.

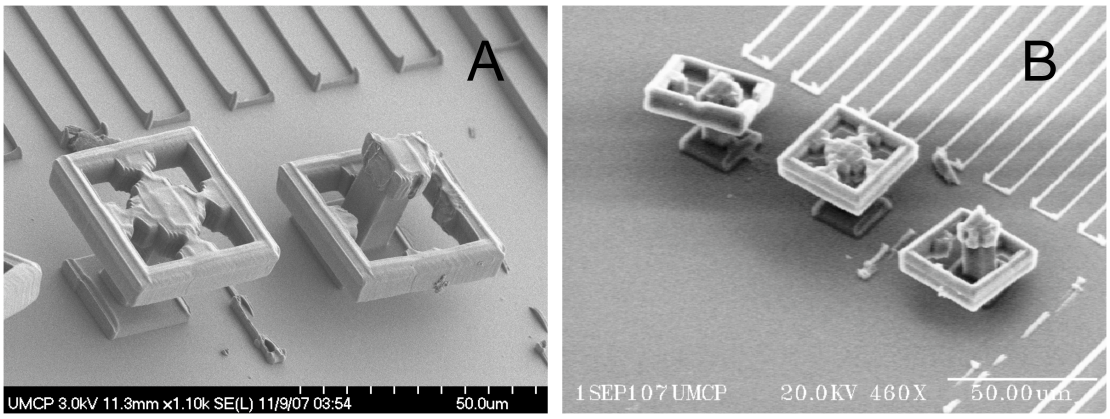

Figure 4.9 SEM images of ring and post structures created using MAP, functionalized with fluorine groups and ablated. A) A structure with no ablation, left and a structure where ablation has been used to attach the ring causing it to fall down the post, right. B) A zoomed out image of A showing that even with the fluorinated coating there are still sticky points where ablation was performed that can lead to sticking.

4.4 Conclusions

Ablation was demonstrated as a means to prevent stiction on microcantilevers fabricated with MAP. By using ablation to remove support towers at the end of microcantilevers, collapse of the cantilever due to stiction was prevented. By specifically designing these cantilevers with towers for removal with laser ablation a free standing cantilever structure could be created.

The development of a fluorinated solution was also described to help overcome stiction effects, and experiments showed that this solution is able to create hydrophobic surfaces by functionalizing amine glass and polymer surfaces with fluorine groups. Microwalls were created using MAP and tested to confirm the ability of the above solution to decrease adhesion on microstructures. This solution also showed some success when applied to a microstructure prior to ablation.

Ablation was also shown to be able to free a ring from a post structure created using MAP, providing a way to create microstructures with unsecured parts.

References

1. LaFratta, C. N.; Fourkas, J. T.; Baldacchini, T.; Farrer, R. A., Multiphoton fabrication. *Angew. Chem.-Int. Edit.* **2007,** *46* (33), 6238-6258.

2. Sun, H. B.; Kawata, S., Two-photon photopolymerization and 3D lithographic microfabrication. In *Nmr - 3d Analysis - Photopolymerization*, Springer-Verlag Berlin: Berlin, 2004; Vol. 170, pp 169-273.

3. Kawata, S.; Sun, H. B.; Tanaka, T.; Takada, K., Finer features for functional microdevices - Micromachines can be created with higher resolution using two-photon absorption. *Nature* **2001,** *412* (6848), 697-698.

4. Bustillo, J. M.; Howe, R. T.; Muller, R. S., Surface micromachining for microelectromechanical systems. *Proceedings of the IEEE* **1998,** *86* (8), 1552-1574.

5. Zhao, Y. P.; Wang, L. S.; Yu, T. X., Mechanics of adhesion in MEMS - a review. *J. Adhes. Sci. Technol.* **2003,** *17* (4), 519-546.

6. Bhushan, B., Adhesion and stiction: Mechanisms, measurement techniques, and methods for reduction. *J. Vac. Sci. Technol. B* **2003,** *21* (6), 2262-2296.

7. Tanaka, T.; Morigami, M.; Oizumi, H.; Ogawa, T., Freeze-drying process to avoid resist pattern collapse *Jpn. J. Appl. Phys. Part 1 - Regul. Pap. Short Notes Rev. Pap.* **1993,** *32* (12A), 5813-5814.

8. Shi, Y. Solvent study on micro towers fabricated via MAP. The University of Maryland, College Park, 2008.

9. BASF, Lucirin TPO-L. In *Technical Information, Coatings Raw Materials* BASF, Ed. 1999.

10. Li, L.; Fourkas, J. T., Multiphoton polymerization. *Materials Today* **2007,** *10* (6), 30-37.

11. Kumi, G.; Yanez, C. O.; Belfield, K. D.; Fourkas, J. T., High-speed multiphoton absorption polymerization: fabrication of microfluidic channels with arbitrary cross-sections and high aspect ratios. *Lab Chip* **2010,** *10* (8), 1057-1060.

12. Williams, R.; Goodman, A. M., Wetting of Thin-Layers of SiO2 by Water. *Appl. Phys. Lett.* **1974,** *25* (10), 531-532.

13. Goeders, K. M.; Colton, J. S.; Bottomley, L. A., Microcantilevers: Sensing chemical interactions via mechanical motion. *Chem. Rev.* **2008,** *108* (2), 522-542.

14. Meyer, E., Atomic Force Microscopy. *Prog. Surf. Sci.* **1992,** *41* (1), 3-49.

15. LaFratta, C. Multiphoton Absorption Polymerization: Issues and Solutions University of Maryland, College Park, MD, 2006.

16. Ha, K.; Kim, J.-M.; Rabolt, J. F., Monolayer studies of perfluorostearic acid at air/water interface. *Thin Solid Films* **1999,** *347* (1-2), 272-277.

Chapter 5: Investigations of PerMX as a Transferable Photoresist

5.1 Introduction

The use of light to pattern surfaces (photolithography) is well studied and commonly used in microelectronics and microelectromechanical systems (MEMS), and other techniques.[1, 2] There are many variations of photolithography, one of which (multiphoton absorption polymerization), was discussed in Chapters 1 and 4. All variations of photolithography have three essential components, a light source, a photoresist, and a way to create a pattern in the photoresist.[3] After creating a pattern in a photoresist, a series of development steps are used to reveal the final pattern.

As mentioned in Chapter 1, photoresists are light-sensitive materials. For MAP experiments, photoresists are typically liquids that contain a blend of monomers with a photoinitiator. These liquid photoresists are usually applied using a spin coater.[4, 5] A spin coater creates a layer of photoresist on a rotating substrate. Photoresist thickness can be controlled by adjusting the rate at which the substrate is spinning.

Photoresists are also available in solid films that can be laminated directly onto a substrate.[5, 6] During lamination, the photoresist is applied to a clean substrate using a heated roller.[6] Soft-baking (heating of the photoresist prior to exposure), is also necessary. Typical substrates used are glass and silicon wafers, which are pretreated with an acid etch or oxygen plasma to ensure they are free of contamiants.[4]

Glass and silicon are commonly used substrates because of they are chemically inert, have planar and well-ordered surfaces, and are easily functionalized through reactions with silane groups.[4] Gold substrates are also used because of their unique interactions with thiol groups.[7]

In traditional photolithography, a UV light source is used to transfer a pattern to a photoresist.[4] Patterns are created by placing a mask between the light source and photoresist. A mask is a material, typically glass, that has been patterned to contain light and dark regions.[4] The shapes created with these masks are called features. Features can range in size from tens of nanometers to centimeters. High quality masks are patterned with chrome and can be very costly due to the precision required to create each feature.

As with photoresists, masks come in two varieties: positive and negative. Examples of each type are shown in Figure 5.1. In positive masks, the features are

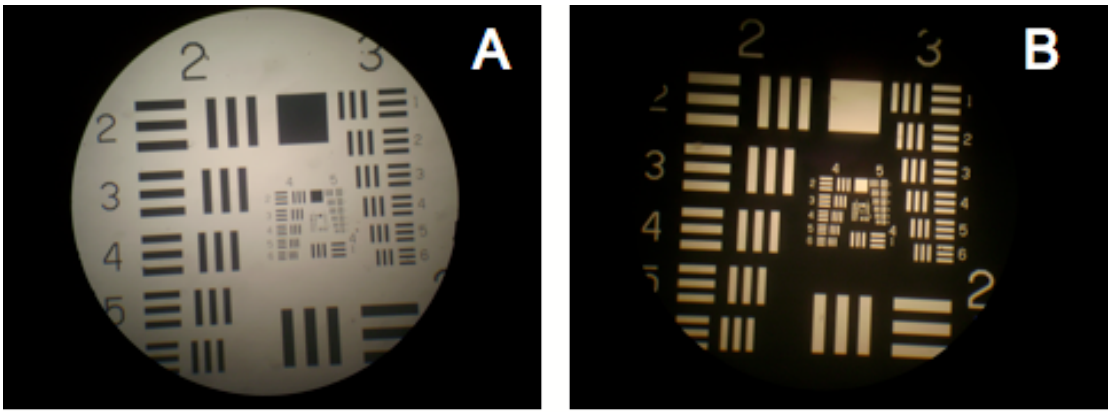

Figure 5.1, A) The USAF 1951 positive mask. The size of the largest stripes shown, lower right, are 125 microns for one stripe. In the smallest set, not visible, one stripe is 2.2 microns. B) The USAF 1951 negative mask, The size of the largest stripes shown is 125 microns for one stripe. In the smallest set, not visible, one stripe is 0.78 microns.

created in chrome while the surrounding areas are transparent. This scheme creates a pattern in the photoresist in which the features are not exposed to the light source but the surrounding areas are exposed. In negative masks the features are transparent while the surrounding areas are opaque. This scheme creates a pattern in the photoresist where the features are exposed to the light source and the surrounding areas are not exposed. The kind of mask chosen for an application depends on the photoresist being used.

The type of photolithography described above is a single-photon process meaning that photon absorption and subsequent polymerization will occur throughout an entire exposed region. This type of photolithography is useful for patterning large areas in a short amount of time. Photolithographic patterning also requires that the light source be aligned above the substrate so that the light is distributed evenly. Additionally, the distance between the mask and substrate should be uniform across the substrate.[8] If misalignment occurs, features will be underexposed and can appear slanted.[8] The creation of complex structures can be challenging and expensive due to the careful alignment required of the mask and the need to create and employ multiple masks.

Photolithography involving multiple photons, or MAP, has been thoroughly discussed in the literature.[9-12] MAP has advantages over traditional single-photon photolithography, in that complex 3D structures can be easily created without the use of an expensive set of masks.[12] Additionally, although not described in this work, alterations of a structure can be easily performed with MAP by making changes to a computer program.[12] With traditional photolithography, a different mask would be

required for each needed change. Additionally, MAP can create undercut and curved structures that would be challenging using traditional photolithography techniques.

However, there are several drawbacks to using MAP. Since MAP is a serial process, each structure needs to be created individually, which can lead to long processing times.[12] Progress of structure creation is tracked visually, thus ideal substrates are transparent to allow light to reach the sample. Translucent and opaque substrate, such as gold or silicon, present challenges for fabricating structures using MAP because alternative methods for finding the substrate surface are needed. One approach could be the use of reflection imaging in an optical microscope.[13]

In this chapter, the use of light to pattern an epoxy photoresist is presented. This epoxy-based photoresist is a dry solid film that is intended for use with lamination and exposure to traditional UV light sources. It is commercially available, from Dupont, which has been making dry-film photoresists since 1968.[5 6]

The photoresist used in this study, PerMX, is a solid, translucent, negative-tone photoresist that comes in sheets with three layers: a polyolefin separator sheet, the photoresist, and a mylar backing. Currently PerMX can be ordered in three film thicknesses: 10, 20, and 50 μm. These films can be layered to create greater thicknesses. Pieces of the film can be cut from the larger sheet and exposed as needed. PerMX is designed to be laminated onto a substrate prior to exposure.

Aside from its intended use, these studies show that PerMX sheets are used without lamination to a substrate prior to exposure. This scheme is made possible because, as mentioned above, PerMX has three layers. By leaving the mylar backing layer attached to the photoresist, this layer acts as a temporary substrate that can later

be removed and transferred to the desired substrate. This ability to pattern first and transfer later can present new opportunities for photolithography by being able to use curved substrates. In this study, we investigate PerMX for use as a transferable pattern onto different substrates using traditional, single-photon photolithographic techniques for creating 2D structures.

In addition to investigating PerMX as a transferable, patternable resist, PerMX is also explored for use with MAP by creating 3D arches. PerMX is designed for use with a 365 nm i-line exposure lamp and traditional single-photon photolithographic processes for the creation of simple, straight-edged structures. Arches highlight MAP's ability to easily create complex curved 3D structures, and the ability to perform MAP on PerMX samples would allow for the creation of transferable, complex 3D structures. This transferability opens up the possibility of using many materials as substrates for MAP structures. Being able to use opaque substrates would allow conductive materials such as silicon or gold to be used with considerably greater ease. Although transferability and adhesion of arches created in PerMX with MAP was studied on glass surfaces here, extension to other surfaces should be relatively straightforward.

5.2 Experimental Setup

5.2.1 Commercial Procedure

PerMX 3000 (Dupont) processing begins with removal of the polyolefin separator sheet and lamination of the photoresist to a substrate at 65-85 ºC. The resist is soft-baked between 95-115 ºC for 2-5 min. The mylar backing is removed from the

adhered photoresist and exposed to a UV light source. The peak absorption for PerMX films is 365 nm. After exposure, films are post-baked at 95 ºC for 2-4 min. The sample is then developed in propylene glycol monomethyl ether acetate (PGMEA) for 4-6 min to remove any non-cross-linked photoresist. An optional hard-bake at 150-200 ºC for 30 min can be included to improve adhesion.[6]

5.2.2 Adapted Procedure

Since PerMX is designed for use with automated lamination systems, the commercial procedure was adjusted for manual application of the photoresist and was improved as experiments progressed. The general procedure is described here and will be expanded throughout this chapter. Removal of the polyolefin separator sheet is followed by a soft-bake of the PerMX film, photoresist-side-up, for a total of 15 minutes (5 minutes each at 65, 95, and 65 ºC). After soft-baking, the PerMX films are exposed to a light source, either a UV lamp (Black Ray, Model B 100) for single-photon work or an 800 nm laser (Coherent MIRA 900-F) for MAP work. After exposure, the sample is placed resist-side-down on a substrate and baked for a total of 15 minutes (5 minutes each at 65, 95, and 65 ºC). Finally, the mylar layer is removed and the photoresist is developed in SU-8 developer (Microchem) for 6 minutes, isopropyl alcohol (99% Reagent Grade, Pharmco-Aapar) for 30 seconds, and hexanes (Fisher) for 1 minute. The SU-8 development step consists of two separate rinses of 4 and 2 minutes.

5.2.3 Single-Photon Curing

Single-photon curing of PerMX photoresists was preformed with a UV light (Black Ray, UV lamp Model B 100) or a UV spot source (Lighting Cure 200 UV spot source, Hamamatsu photonics K. K. Model L7212-01). A piece of PerMX (less than 1 inch^2) with the polyolefin layer removed was placed on a 3 in. glass slide, resist-side-up. A mask (Negative, 1951 USAF Hi-Resolution, Edmund Optics) was used to pattern the photoresist during UV exposure. To prevent the mask from coming into contact with the photoresist, a spacer (typically glass slides or coverslips) was placed between the mask and photoresist. The spacers are placed on either side of the glass slide and the patterned mask is placed on top of the spacers. The setup is exposed to UV with exposure times of 2 min. or less. The sample setup was the same for both UV sources, and is shown in Figure 5.2.

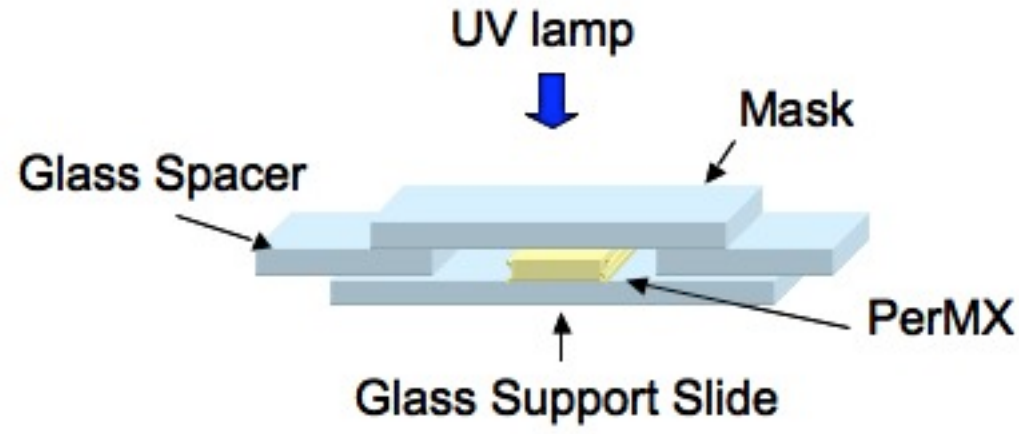

Figure 5.2 Setup for single-photon curing of PerMX films. Coverslips or cut glass slides are used as spacers, and the PerMX film is placed photoresist side up.

5.2.4 Substrate Preparation

To prepare glass substrates for pattern transfer, slides were sonicated three times, once each for 3 min. in acetone (Production Grade, BDH), isopropyl alcohol,

and distilled water, followed by oxygen plasma cleaning (Harrick plasma cleaner/sterilizer, Model PDC-32G). The slides were exposed to an oxygen plasma for 4 min. at 300 mtorr resulting in a hydroxylated, hydrophilic surface.

5.2.5 Sputter-Coated Surfaces

Plasma cleaned glass substrates were coated with gold or silver using a sputter coater (Cressington sputter coater, Model 108). These silver and gold substrates were used for pattern transfer tests from single-photon cured samples only. The substrates are sputtered in an argon plasma for at least 150 sec at 0.1 mbar. Improved gold slides were made using a 10 nm chromium adhesion layer with 100 nm of gold deposited on top. This coating process was done at the Maryland Nanocenter fabrication laboratory on the AJA sputtering unit (AJA International ATC 1800-V).

5.2.6 PDMS Creation

Polydimethylsiloxane (PDMS) was also used as a substrate for pattern transfer testing with single-photon cured PerMX films. PDMS was made from a commercially available polymer kit (Dow Corning) that consists of a base and a curing agent that when mixed, create a flexible polymer. The two liquids were combined in a 10:1 ratio of base to curing agent, mixed by hand, centrifuged at 3400 rpm for 5 min, then mixed and centrifuged again to blend. The blended PDMS was poured over a square mold (to create a flat surface) and placed in a vacuum desiccator to remove air bubbles. The molds were then cured at 95 ºC for 30 min. After curing, the PDMS stamp was peeled away from the mold and plasma cleaned prior to use.

5.2.7 Amine Coating

To improve adhesion of the PerMX film to a substrate, glass substrates were treated with amino silanes. Starting with plasma cleaned glass, amine groups can be attached by submerging substrates in a solution of 100 mL methyl alcohol (Reagent Grade, Pharmco-Aapar) and 5 mL aminopropyltrimethoxysilane (99%, Sigma Aldrich) for 4 hours. Samples are then rinsed with methyl alcohol and dried at 95 ºC for 1 hour.

5.2.8 Adhesion Tests

Adhesion tests were preformed to evaluate how well patterns attach to substrates. After development of a sample, the patterns were scratched with the edge of a pair of forceps to see if the feature could be remove. If the features moved, the sample was considered to have poor adhesion. If the features did not move, adhesion was deemed good. Sample movement could be tracked by eye due to the large feature sizes (on the order of 1000 microns).

5.2.9 Multiphoton Absorption Polymerization

For the MAP samples, an 800 nm laser beam from an approximately 200 femtosecond Ti:Sapphire laser source (Coherent MIRA 900-F) was focused into the photoresist through an objective (either a 40× or 100× oil immersion objective) of an inverted microscope (Zeiss Axiovert 135). The photoresist was placed on a programmable *xyz* piezoelectric stage (Physik Instrumente, P-563 3CD) that was

mounted on the inverted microscope. The position of this stage, and hence the position of the focal point of the beam within the photoresist, was controlled using Labview software. 3D structures were fabricated by translating the focus of the beam within the resist, which selectively exposed the chosen regions. A mechanical shutter was used to control access of the laser beam to the sample, thereby providing a means of abruptly starting or ending exposure.

Sample preparation for MAP involves cutting an approximately 0.5 inch × 0.5 inch piece of PerMX. The PerMX is placed mylar-side-down onto a coverslip that is taped to a glass slide. The PerMX is then covered by a second coverslip that is secured by tape on either side, prior to mounting the sample on the microscope.

In order to ensure that structures can be transferred to a substrate, structures need to be fabricated at a specific photoresist interface. For PerMX samples, the structures should be fabricated on the photoresist side opposite that of the mylar backing layer. Fabricating at this film face ensures that the fabricated structure will be in contact with the substrate during development. Fabricating structures within the photoresist, rather than at the interface, results in structures that wash away, or move during development steps (Figure 5.3).

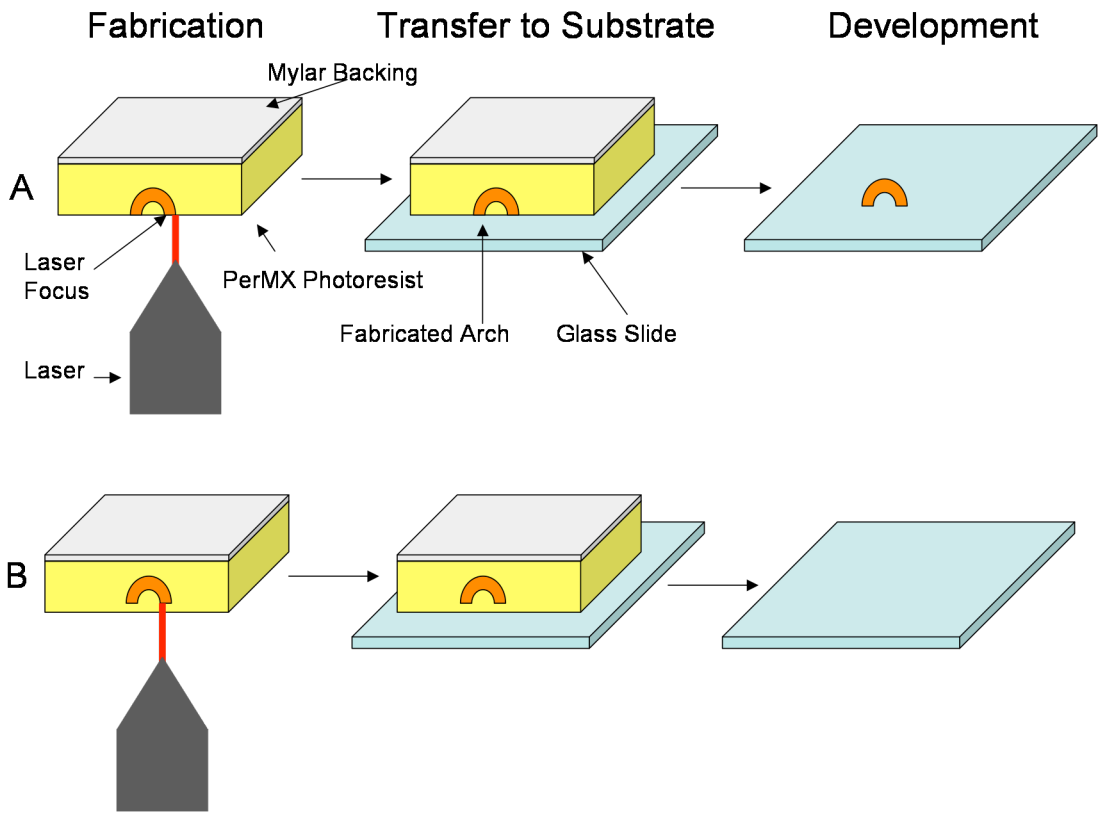

Figure 5.3 An illustration of how fabrication with contact at the incorrect photoresist interface will lead to decreased adhesion of the final structure. A) An arch fabricated at the face of a PerMX film. B) An arch fabricated in the bulk of a film. Notice that during transfer that the arch does not make contact with the substrate. With no anchor for the arch during development, the arch will wash away.

To ensure fabrication begins from the correct interface of the PerMX film, once the surface is first found visually, the stage is adjusted by a few microns to begin fabrication just outside of this photoresist surface. This will allow the fabrication to start just outside the edge of the photoresist and move through the photoresist interface, working in towards the bulk. Another technique used to ensure fabrication at the surface was to add a drop of gold nanobeads to the PerMX film prior to fabrication. The nanobeads can be easily seen on the microscope, and when in focus these beads indicate where the surface of the PerMX lies.

An additional cause of structures not being attached to a surface is the presence of gaps between the photoresist film and the substrate. Good contact between the PerMX film and the substrate needs to be made in order for structures to transfer successfully. Any air gaps between these two surfaces can cause these patterns to remain on the mylar backing.

In order to prevent the above scenario, PerMX films were placed on substrates for transfer by making contact with the substrate at one edge of the film and slowly lowering the PerMX until complete contact is made with the substrate. This process is similar to how coverslips are placed over wet mount microscope slides to prevent the formation of air bubbles. Experiments using a roller to simulate lamination were pursued to improve adhesion, but results were consistent with those from samples adhered without the use of a roller.

5.3 Results

5.3.1 Transfer to Planar Surfaces

Single-photon curing was used for initial studies of pattern transfer. After exposure the patterned photoresist was transferred to a silicon substrate and developed. After development the transferred pattern could be clearly seen by eye on the substrate and was well attached, as confirmed by adhesion testing. This initial test confirms that transferring the patterned photoresist to a substrate after exposure is possible.

To further explore potential substrates, patterns were then transferred to gold, silver, copper, PDMS and glass substrates. The copper was conductive copper tape

attached to a glass slide. Well-adhered patterns could be seen on glass, gold and silver substrates. The patterns on the copper and PDMS substrates were incomplete and poorly attached, as scratching easily removed them. Examples of patterns transferred to various substrates can be seen in Figure 5.4.

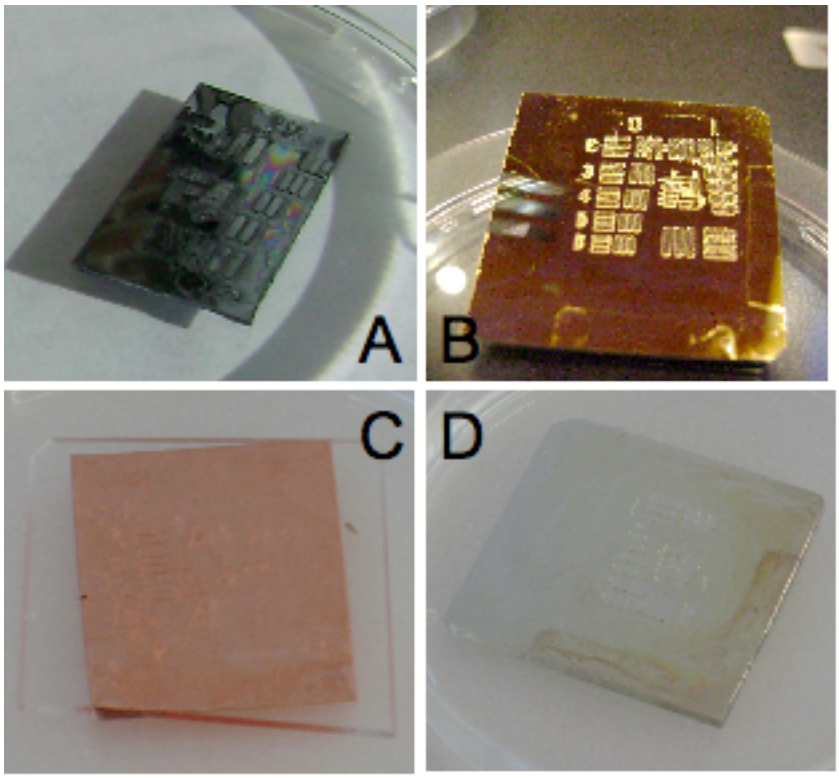

Figure 5.4 Examples of single-photon cured, patterned PerMX films that have been transferred to various substrates: (A) silicon (B) gold (C) copper (D) silver. The substrates were 1 × 1 in or less with individual sections of the pattern being no larger than 1000 microns.

The copper tape had a surface texture that was macroscopically different from the gold, silver and glass surfaces prior to transfer. This rougher appearing surface was visible by eye, and could interfere with the contact between the PerMX and this substrate, leading to the incomplete pattern transfer. Transferring a pattern to a

copper sputtered substrate would help determine if the tape texture was interfering with the adhesion as a sputtered copper surface would have much less texture.

The flexibility of the PDMS substrate may also be a cause for pattern transfer failures in these samples. The PDMS sample may have been too flexible to keep the photoresist pattern attached. PerMX is not an extremely flexible photoresist prior to being heated, and if care is not taken it will crack and flake at room temperature. The tensile property differences between the two materials could make the PDMS incompatible for use with PerMX. Additional tests could introduce a clamp or some other device to keep constant pressure and contact between the substrate and the photoresist film during development. Also, the ratio of components used to create the PDMS could be altered to decrease flexibility in the polymer or H-PDMS could be used. H-PDMS is a variation of PDMS that uses additional catalysts to produce a more rigid form of PMDS.

The patterns transferred to glass, gold, silicon and silver all showed complete transfer of the features. Adhesion of these features to the substrate was good, with the structures remaining attached during development as well as during adhesion testing. The experiments described in this chapter will continue to use glass for its low cost and these promising pattern transfer results.

5.3.2 Curved Surfaces

Room temperature PerMX films, which requiring care to prevent cracking, do become flexible when warmed. This flexibility was investigated for use on a cylindrical surface by transferring a patterned PerMX film to the curved surface of a glass rod. It was discovered that the film can bend but does not remain bent.

Bending prevents the PerMX film from making complete contact with the substrate. Without complete contact features within a pattern will not transfer to the substrate. To assist in keeping the film flush against the substrate, rubber bands were used on the edges of the PerMX film to keep the film in contact with a glass rod. Using this method, a complete pattern was transferred to a glass rod (Figure 5.5).

Figure 5.5 A glass rod with a transferred PerMX patterned adhered to it.

5.3.3 Soft-Baking

PerMX polymer films were examined under the optical microscope. The samples appear to have an evenly distributed pitted surface (Figure 5.6A). The

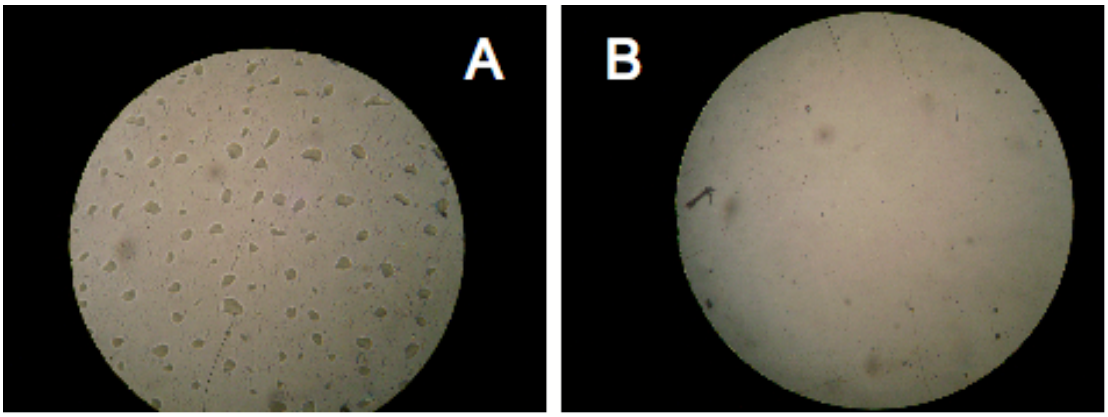

Figure 5.6 Optical images of PerMX 3050 films. A) An unbaked PerMX film. B) A soft-baked PerMX film.

commercial procedure suggests soft-baking the PerMX, and after a ten second soft-bake at 95 °C the appearance of the pits was diminished. After twenty seconds the pits disappeared completely (Figure 5.6B).

Comparing patterns created in soft-baked and pristine samples reveals a difference that is distinct. The soft-baked sample is smooth and clear while the pristine PerMX is textured and less transparent (Figure 5.7). The texture that appears

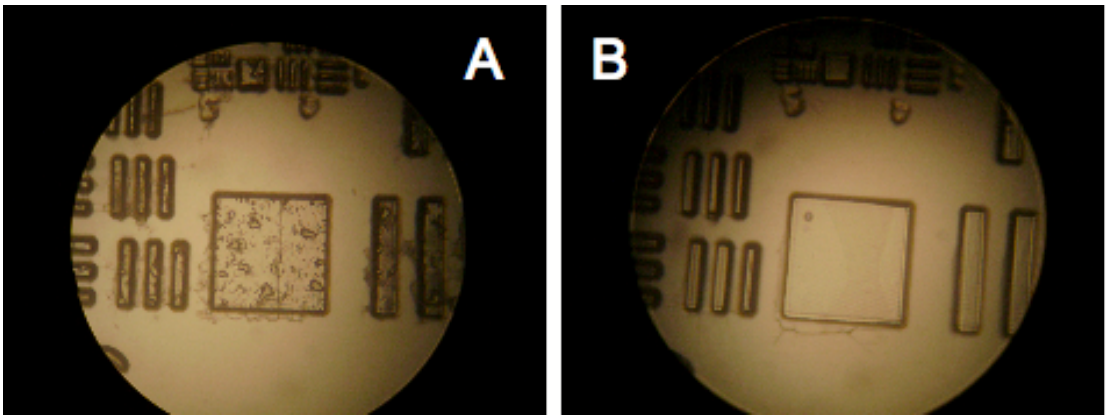

Figure 5.7 Optical images of a lithographically-patterned piece of pristine PerMX transferred to a glass slide **(A)** and compared to PerMX that was soft-baked prior to exposure **(B)**. The largest stripes, on right of both images have a size of 112 microns.

on the PerMX could come from the application of the polyolefin separator sheet during manufacture. It is likely that this texture diminishes upon heating due to solvent evaporation in the photoresist. Differences in soft-baked and pristine samples will be explored in the next section.

5.3.3 Multiphoton Absorption Polymerization

The above section discussed the ability to pattern PerMX via single-photon curing and then to transfer the pattern to a final substrate. To expand these curing possibilities, both soft-baked and unbaked films of PerMX were examined to see if

they would serve as suitable photoresists for use with MAP. Initial characterization studies were performed using unbaked PerMX films. To highlight MAP's ability to create curved 3D structures, an arch shape was chosen for fabrication. An array of arches was created in the PerMX photoresist and developed against the rounded portion of a glass rod. The arch transfer was successful, with 67% of the arches remaining upright and 33% having fallen down (Figure 5.8). This result illustrates that PerMX can be used as a photoresist with MAP.

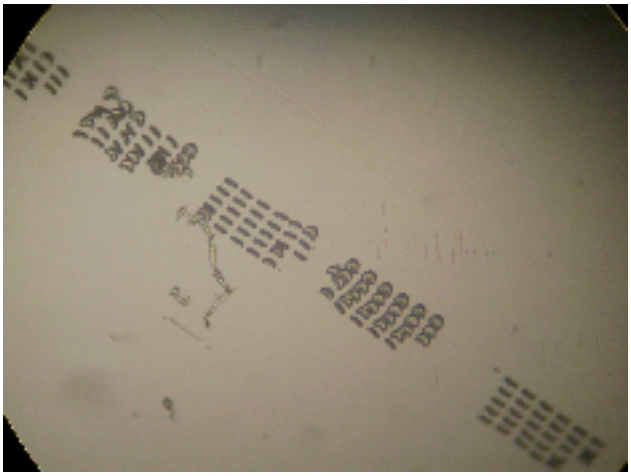

Figure 5.8 Optical image of arches created using MAP in PerMX 3050 transferred to a plasma cleaned glass rod. Arches have an outer diameter of 30 microns and are no taller than 50 microns.

These fallen arches indicate that the two feet at the ends of the arches are not attached to the substrate in their intended way. Larger and taller feet were created for the arches to test if an increase in contact area would decrease the fraction of fallen arches (Figure 5.9). Additionally, to promote adhesion and assist the arches in

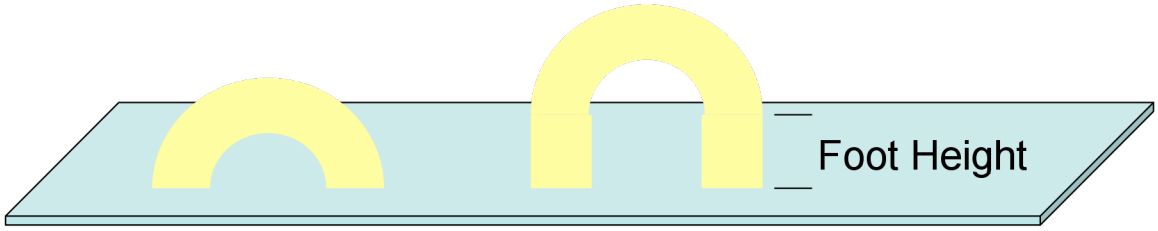

Figure 5.9 Illustration of how the addition of a foot changes the arch shape.

remaining upright, these arches were transferred to an amine functionalized glass rod. Amine groups can form bonds with epoxy resins. Thus, using an amine functionalized substrate should promote adhesion between the PerMX photoresist and the substrate. The improved arches, again transferred, confirming the creation of structures using MAP in PerMX, with 40% of structures moving out of place (Figure 5.10). It should also be noted that, during fabrication of improved arches, the

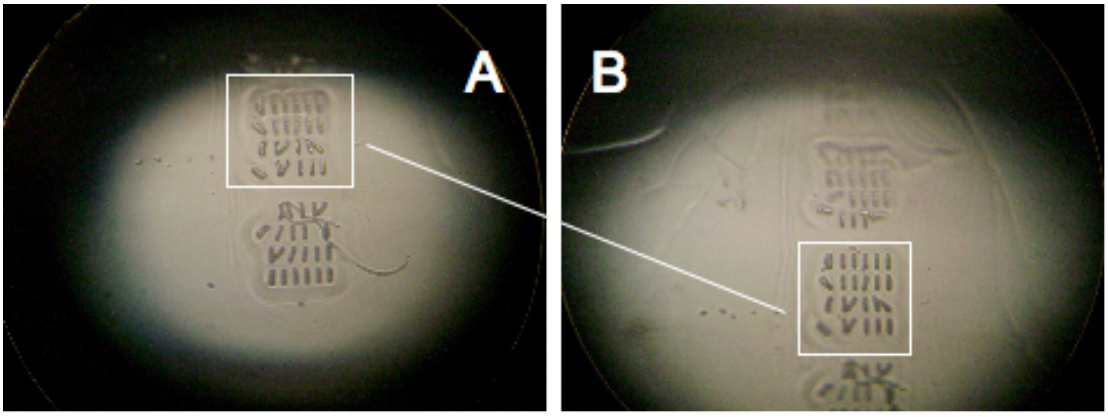

Figure 5.10 Optical images of arches created using MAP in PerMX 3050 photoresist and transferred to an amine coated glass rod. Arches have a 6 × 6 × 10 micron foot with an outer diameter of 47 microns. Arches are no taller than 50 microns. A and B are the same rod rotated to highlight two regions of arches.

structures were made unintentionally smaller. These shorter arches may have a higher surface affinity resulting in a lower number of fallen structures. This result suggests that a shorter arch could be more stable because of a decreased aspect ratio.

To improve the stability of arches upon transfer of a PerMX film to a substrate planar substrates were used to investigate how arch shape contributes to adhesion. Comparing the arches with a 6 × 6 × 10 micron foot and a line spacing of 1.5 microns (Figure 5.11A) with those made with a 10 × 10 × 5 micron tall foot and a line spacing of 0.5 microns (Figure 5.11B) shows no improvement in adhesion, but the arch shape appears much rounder. Line spacing controls the space between two scanned lines. The smaller the line spacing, the more lines that are created within a structure. Increasing the number of lines leads to a smoother structure, but it also leads to longer fabrication times. It is surprising that adhesion is not improved despite being transferred to an amine functionalized glass substrate (Figure 5.11). Further improvements were found in the arch shape by decreasing the line spacing to 0.25 microns (Figure 5.11 C), but no improvements in adhesion were observed.

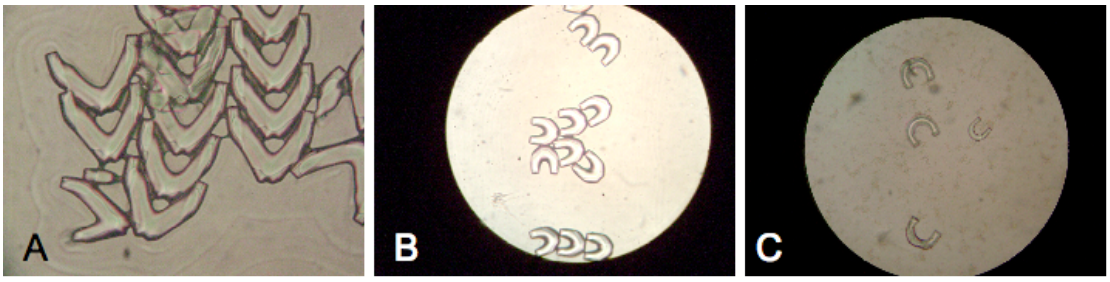

Figure 5.11 Optical images of arches created using MAP and transferred to amine functionalized glass slides. Notice the more rounded shape seen is C vs. A. A) Arches that have a 6 × 6 × 10 micron foot with a line spacing of 1.5 microns and an outer diameter (OD) of 47 microns. B) Arches that have a 10x10x5 micron foot with a line spacing of 0.5 microns and an OD of 40 microns. C) Large arches that have an outer diameter of 50 with a 10 × 10 × 15 foot and a spacing of 0.25. The small arch has an OD of 30 microns and a 5 × 5 × 15 foot with a spacing of 0.25 microns.

The addition of a platform below the arches was used to stabilize and increase upright adhesion when transferring arches to substrates (Figure 5.12A). The samples were imaged using a SEM, and as seen in Figure 5.12B, all of the arches are present with only one platform appearing slightly lower than the rest. Repeating the process revealed that while in some cases structures fell over (Figure 5.12D), in others all four remained attached (Figure 5.12C). The process resulted in about 75% adhesion in most cases. Figure 5.13 highlights one arch that had a defect on the underside of the platform. It is likely this defect is responsible for the structure not being properly adhered due to a decreased amount of surface area that is in contact with the substrate.

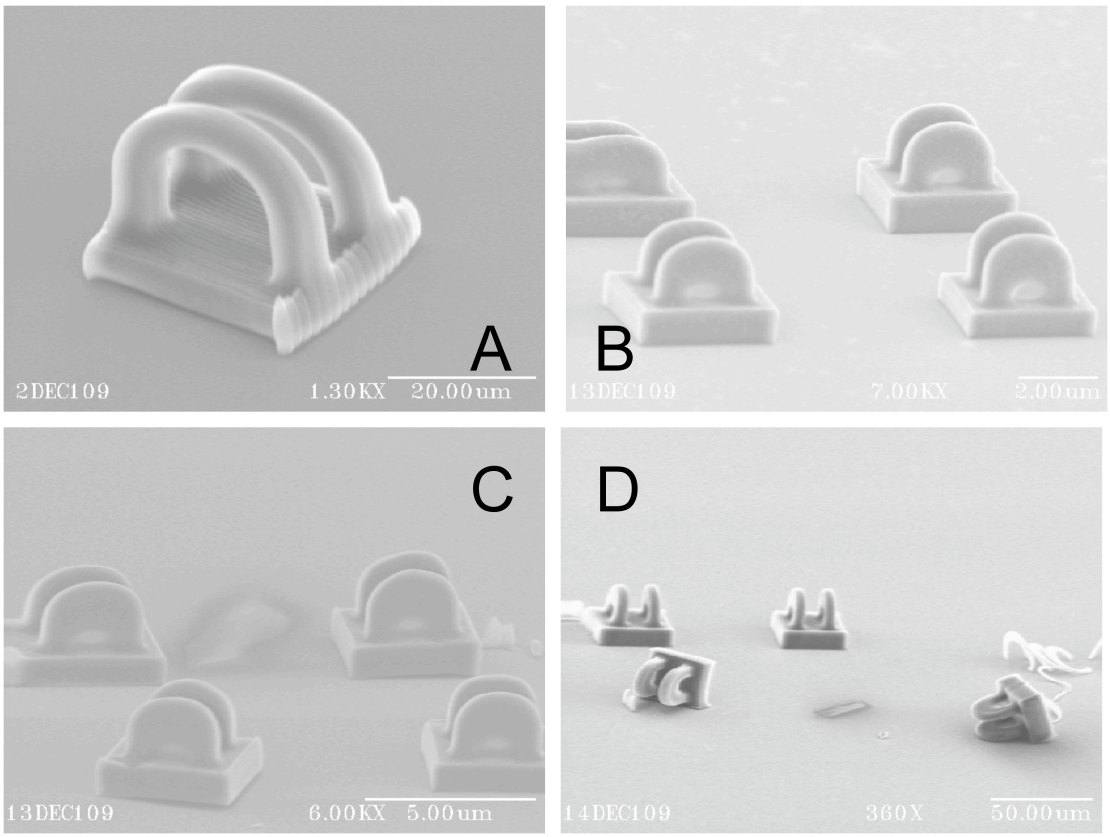

Figure 5.12 SEM images of arches created using MAP in PerMX 3050. All bases are 30 × 30 × 10 microns. A) The Arches created with a 20× air objective at a power of 17.8 mW. Arches have an OD of 30 microns and a foot size of 5 × 5 × 10 microns. B) These arches have an OD of 20 microns and a foot size of 5 × 5 × 6 microns. Arches created with a 100× oil-immersion objective at a power of 18.4 mW. C) Arches created with a 100× oil-immersion objective at a power of 18.4 mW. The arches have an OD of 20 microns and a foot size of 5 × 5 × 6 microns. D) Arches that have an OD of 20 microns and a foot size of 5 × 5 × 6 microns. Both samples are created with the 100× oil-immersion objective using 16.3 mW of power.

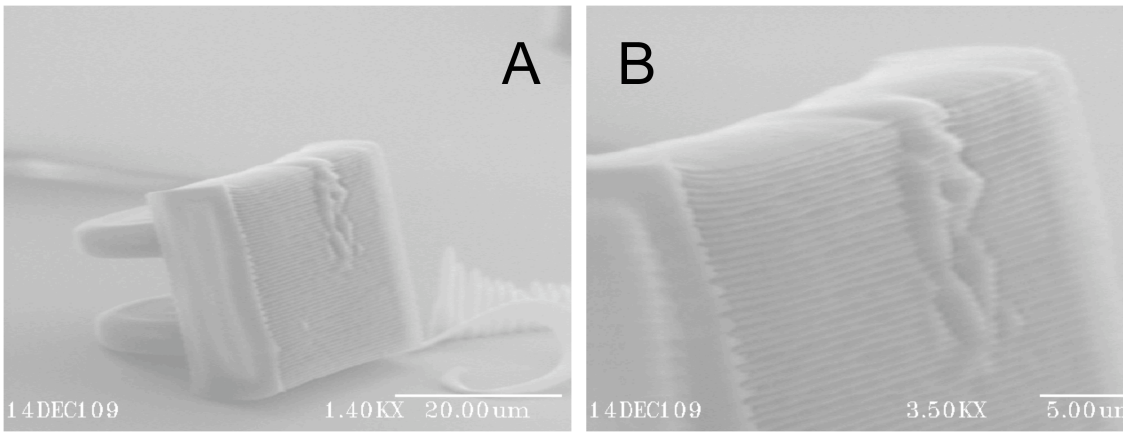

Figure 5.13 SEM images of underside of a fallen arch seen in sample 5.12D in the lower right. A) Arches have an OD of 20 microns and a foot size of 5 × 5 × 6 microns and were created using the 100× oil-immersion objective with a power of 16.3 mW. B) Close up of the defect in the underside of the arch platform.

As seen when examining the PerMX film in the single-photon polymerization experiments, the PerMX films exposed with MAP also have a pitted appearance when not preheated (Figure 5.6). There were no previous indications that this pitted surface was affecting the structures. However, if the pitted areas contain no photoresist, then when structures are fabricated within that region, no polymerization will occur. This effect may lead to weak or weakened structures. This weakness could explain why only some fabricated structures have defects. Typically, defect free regions were chosen for fabrication, but it was not always possible to find a completely clear area that was large enough for the desired structure. All samples presented in the next section were soft-baked.

5.3.4 Soft-baking

To investigate the effects of baked vs. pristine PerMX, samples of soft-baked PerMX were used to create arches with MAP. Arches fabricated in the soft-baked

photoresist and then transferred to glass slides showed similar behavior to unbaked PerMX samples. This observation reaffirms that the unbaked PerMX does not significantly affect the adhesion statistics, but may occasionally lead to structures with defects. As seen in Figure 5.14A four arches are present but one appeared to have no platform.

We also examined effects from the addition of a cooling period prior to fabrication, which allows the less viscous photoresist that formed during the baking to solidify. The cooling period ranged from as little as ten minutes to as long as a few hours. The arches fabricated in the cooled samples had similar results to those without a cooling period, with one arch appearing weaker and occasionally falling over.

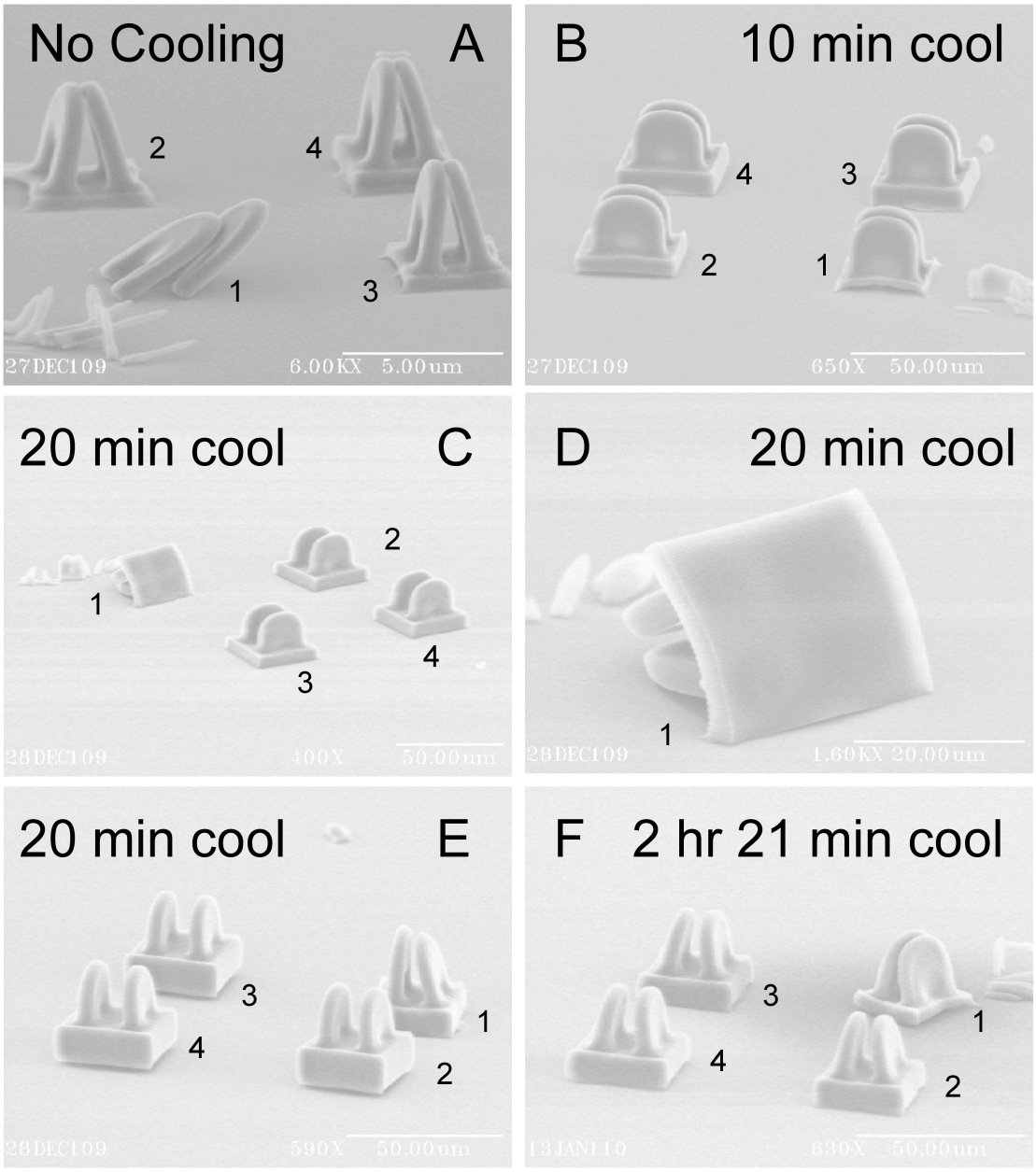

Figure 5.14 SEM images of arches fabricated with soft-baked PerMX at 95 °C. Number indicates the order in which fabrication occurred. All arches were made using the 100 × oil-immersion objective with 30 mW of power and have an OD of 20 microns and foot size of 5 × 5 × 10 microns. **A)** No cooling time after soft-baking. **B)** Soft-baked for 20 seconds and let cool for 10 minutes. **C)** Soft-baked for 20 minutes and let cool for 20 minutes. **D)** Close up of the underside of a platform on sample C. Soft-baked for 20 and let cool for 20 minutes. **E)** Soft-baked for 30 seconds and let cool 20 minutes. **F)** Soft-baked 30 seconds and let cool for 2 hours and 21 minutes.

Examining the underside of one of these soft-baked, fallen arches shows no visible defects (Figure 5.14D), although these results suggest that the soft-baking does not provide improved adhesion of the structures to the substrate. Additionally, in each set of 4 arches, the arch with the most defects and least adhesion appears to be the first one fabricated. The arches fabricated in unbaked PerMX films also showed this weakened first arch, suggesting that there is some systematic error in the fabrication process leading to the defective arches.

The addition of a system warm-up period during the fabrication process was investigated as a possible cause of the initial arch weaknesses. This warm-up period occurs when the photoresist is interacting with light during the fabrication of the first structure. It is possible that the light, either from laser scatter or the external light from the microscope, causes local heating or cross-linking of the polymer. The possibility that the defect is due to a warm-up of the sample is supported by the fact that the weakness occurs in structures fabricated in both unbaked and soft-baked samples. Additionally, the three structures created after the warm-up period appear similar in both baked and pristine of samples.

Initial testing was performed to investigate these effects by adjusting the times that the microscope light was on during fabrication. Structures were created with the microscope light on only at the beginning of fabrication, only at the end of fabrication, for the entire time, and never. The amount of time needed for setup was kept to a minimum for all samples. The surface of the PerMX films is typically found via fluorescence from the photoresist. This process can be time consuming, since the fluorescence can be hard to detect. For these experiments, to minimize the amount of

time the light is on, the gold nanoparticle method was used prior to soft-baking. In this case, the solvent from the nanoparticles evaporates off during soft-baking, leaving behind the nanoparticles to serve as markers for the surface.

Results from these light experiments are preliminary due to the lack of complete structure transfer, but it can be noted that the sample fabricated with the light on only at the beginning has all three structures present (Figure 5.15C). Only

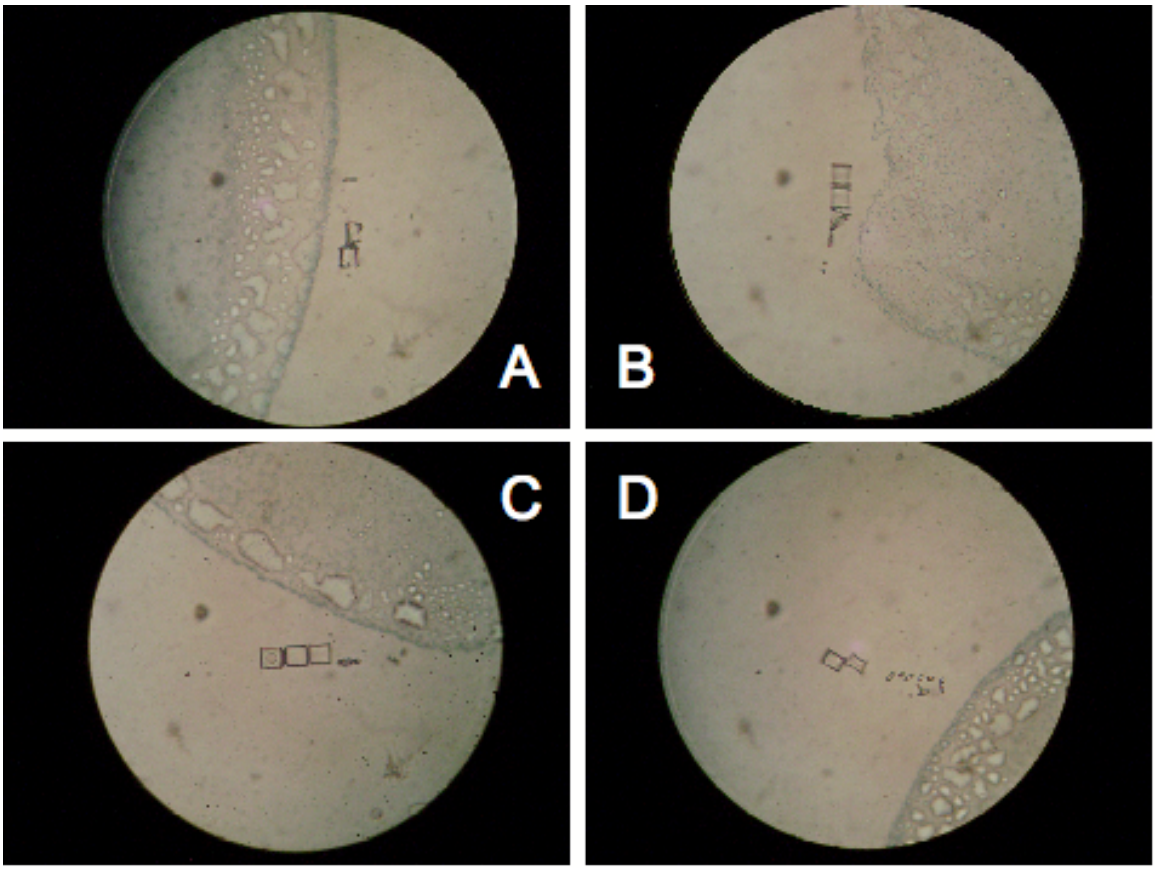

Figure 5.15 Lighting study done by creating identical structures but changing the amount of time they are exposed to light from the microscope. Structures are 3 squares 20 × 20 microns with heights of 5, 10, and 15 microns. Fabricated all samples with the 100 × oil-immersion objective and a power of 25.5 mW. **A)** Light on during fabrication. **B)** Light off during fabrication. **C)** Light on at the beginning of fabrication. **D)** Light on after fabrication.

two structures transferred when the light was on the entire time (Figure 5.15A) and light on only at the end (Figure 5.15D), and one appears weak in each case. The light off sample has three structures present with only one appearing weak (Figure 5.15B). Of the samples with weaker structures, as seen previously it is the first structure that exhibits defects. A more complete study that includes fabrication of arches will help conclusively determine if warm-up time is an important factor.

5.4 Conclusions

The above experiments show that PerMX is able to transfer a pattern to a substrate. This pattern transfer was demonstrated using both single-photon and multiphoton absorption. The single-photon samples showed excellent transfer to gold, silver, silicon and glass substrates. Pattern transfer to PDMS and copper tape showed limited or no adhesion of the PerMX. Arches were created in PerMX films using MAP, and they showed promising success when transferred to glass substrates, although amine functionalization did not seen to improve adhesion.

In MAP experiments, sample adhesion between the arch and the substrate was investigated by changing the arch shape to decrease the aspect ratio and increase the surface area. The addition of soft-baking was also examined to improve adhesion by decreasing the number of defects on the surface of the photoresist. The best arches were created on platforms in soft-baked PerMX and transferred to amine-functionalized glass slides.

It seems that a systematic error is responsible for a weakened first structure fabricated in PerMX. If adhesion between the substrate and the structures can be

improved, this will assist in studying this systematic error. A system warm-up period needs further investigation, but may be the cause of this problem.

The above experiments lead to the conclusion that PerMX is a compatible photoresist for use with MAP and can easily be used as a transferable photoresist using simple modifications to the manufacturer's procedure. Further work needs to be done to improve adhesion during transfer as well as to examine why the weaknesses occur in the fabricated structure, but the ability to pattern first and transfer later using PerMX makes it a powerful photolithographic tool. Patterning curved and flexible surfaces makes transfer possible to an infinite variety of substrates and will provide for the transfer of MAP structures to opaque substrates.

References

1. Bratton, D.; Yang, D.; Dai, J. Y.; Ober, C. K., Recent progress in high resolution lithography. *Polym. Adv. Technol.* **2006,** *17* (2), 94-103.

2. Geissler, M.; Xia, Y. N., Patterning: Principles and some new developments. *Adv. Mater.* **2004,** *16* (15), 1249-1269.

3. Chiu, G. L.-T.; Shaw, J. M., Optical lithography: introduction. *IBM J. Res. Dev.* **1997,** *41* (1-2), 3-6.

4. Adams, T. M.; Layton, R. A., *Introductory MEMS: Fabrication and Applications*. Springer: 2010.

5. Shaw, J. M.; Gelorme, J. D.; LaBianca, N. C.; Conley, W. E.; Holmes, S. J., Negative photoresists for optical lithography. *Ibm Journal of Research and Development* **1997,** *41* (1-2), 81-94.

6. DuPont, DuPont PerMX 3000 Photodielectric dry film adhesive technical data sheet. DuPont, Ed. DuPont: 2010.

7. Nuzzo, R. G.; Allara, D. L., Adsorption of bifunctional organic disulfides on gold surfaces *J. Am. Chem. Soc.* **1983,** *105* (13), 4481-4483.

8. Ronse, K., Optical lithography - a historical perspective. *C. R. Phys.* **2006,** *7* (8), 844-857.

9. Maruo, S.; Fourkas, J. T., Recent progress in multiphoton microfabrication. *Laser Photon. Rev.* **2008,** *2* (1-2), 100-111.

10. LaFratta, C. N.; Fourkas, J. T.; Baldacchini, T.; Farrer, R. A., Multiphoton fabrication. *Angew. Chem.-Int. Edit.* **2007,** *46* (33), 6238-6258.

11. Kawata, S.; Sun, H. B.; Tanaka, T.; Takada, K., Finer features for functional microdevices - Micromachines can be created with higher resolution using two-photon absorption. *Nature* **2001,** *412* (6848), 697-698.

12. Sun, H. B.; Kawata, S., Two-photon photopolymerization and 3D lithographic microfabrication. In *Nmr - 3d Analysis - Photopolymerization*, Springer-Verlag Berlin: Berlin, 2004; Vol. 170, pp 169-273.

13. LaFratta, C. Multiphoton absorption polymerization: issues and solutions. University of Maryland, College Park, 2006.

Chapter 6: Efforts Towards the Creation of a DNA Microarray

6.1 Introduction

6.1.1 Microarray Background

Understanding the expression of genes is of critical importance for the study of diseases and drug interactions with cells.[1] Genes are specific sequences of deoxyribonucleic acid (DNA) or ribonucleic acid (RNA) with a specific trait associated with them. Microarrays are an important technology for monitoring gene expression.[2] These arrays have been around since the early 1990s, and have revolutionized the way in which genomic studies are carried out by providing the ability to study expression in parallel.[3, 4]

Microarrays are small chips, typically three inches or less per side, that are patterned with multiple analysis sites. These sites are also known as features, and the number of sites varies based on the array size and feature spacing.[3] Each site is covered by biomolecular strands that are capable of selectively pairing with a complementary biomolecule. For biomolecules such as DNA (and RNA) this selective pairing is hybridization (which follows Watson-Crick base-pairing guidelines). The biomolecules tethered to the surface are known as probes, while their complementary counterparts are known as targets.[5]

Microarray substrates are typically made of glass, due to its low cost and durability.[5] To facilitate attachment of DNA to these substrates, functionalization is

performed to allow covalent binding with the probe DNA strand, thus ensuring that the strand does not detach from the surface during analysis.[3, 5] There are many chemical functionalizations that can facilitate the binding of DNA to glass. Amines and aldehydes are the most commonly used functionalizations.[3]

For DNA microarrays, probe molecules can range in size from long, single-stranded DNA (300-800 bases) to oligonucleotides (~25 bases).[6] Most DNA microarray experiments use a fluorescent tag to detect hybridization by attachment to the target DNA.[3, 4, 7] Typically, commercial dyes used in microarray experiments are Cy3 and Cy5, because of their high solubility and ability to be attached to phosphoramidite.[3]

Figure 6.1 details how a fluorescence-based microarray experiment is performed for determining the presence of an unknown DNA sequence.[7] The experiment involves a mixture of unknown DNA targets that have been fluorescently labeled (red circles). The known probe DNA is patterned on the substrate in four features. Each feature contains probes of a different sequence of DNA (A, B, C and D). The target DNA hybridizes with the probe DNA. The microarray is then scanned to excite each target, which causes light emission that is collected and analyzed. When no target molecules hybridize to the probes in a specific feature (Figure 1, Sequence C), no fluorescence should be observed.

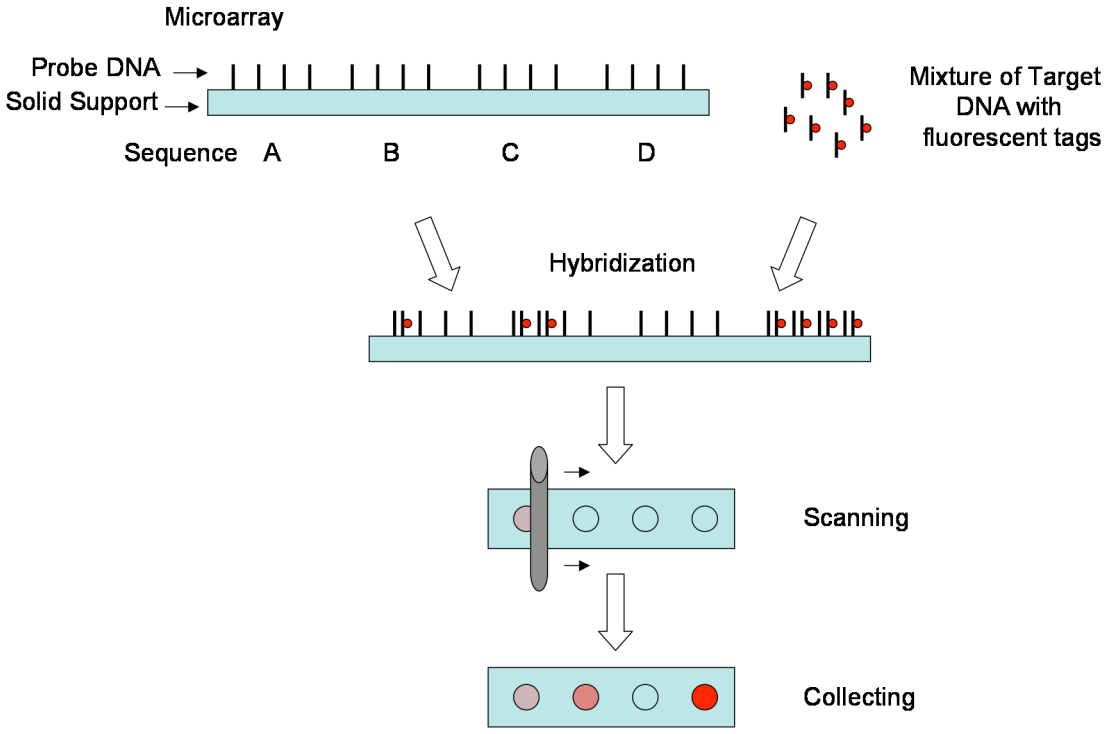

Figure 6.1 A typical microarray experiment, consisting of fluorescently labeled targets (red circles) and a solid support containing probes (straight lines) arranged by feature. Each feature contains a different sequence of DNA (A, B, C, and D). Hybridization occurs and then the sample is scanned to excite each dye, which causes emission that is collected and analyzed. The presence of fluorescence indicates that a positive match has been made between target and probe and the absence of fluorescence (sequence C) indicates that no target molecules hybridized the probes in that feature. The intensity of fluorescence observed is proportional to the amount of hybridization in that feature. Image adapted from a reference.[7]

6.1.2 Diffraction Based DNA Microarrays: Label Free Methods

Label-free-DNA microarrays can provide more reliable and reproducible results due to more true-to-life samples and minimal variation in emission signals. Fluorescence-based techniques rely on attachment of a label to a target to analyze a sample. These labels are not naturally found on DNA, and therefore DNA properties, including hybridization, can be compromised.[8, 9] Attachment of the label to the target

DNA can provide variable results due to photobleaching and non-specific binding.[3, 8]

Photobleaching is the destruction of a dye as a result of repeated excitation and emission cycles.[3] This photobleaching rate is related to the sample exposure time and the light source intensity.[3] Photobleaching causes a decrease in the signal because as the dye becomes damaged, the release of photons is diminished.

Non-specific binding occurs when fluorescently-labeled target DNA adheres to the surface of a microarray substrate without actually hybridizing with a probe molecule.[8] When scanned, the stray target will produce a signal that is not associated with a probe DNA, thus creating a false positive.[8] A label-free detection system is desirable to reduce, and ideally avoid, these effects.

6.1.3 Diffraction Based Investigations

The concept of using a patterned surface to create diffraction for biomolecule detection is not new.[10] In 1991, Y. G. Tsay proposed the idea as a way to examine fluids in the human body for analytes, and the technique was called an optical biosensor assay (OBA).[10] An OBA employs antibodies as probes on an amine treated silicon wafer to detect the presence of an antigen, also known as the target, in a sample.

The antibody-coated wafer is exposed to UV light (254 nm) through a patterned mask. Masks have translucent and opaque regions that control the amount of light that reach various areas of a sample. The wavelength is chosen so that the probes that received UV exposure are incapable of binding with the target. These damaged probe regions can create a diffraction pattern, as a result of refractive index

changes, when the intact probes are bound with targets. If no target molecules are bound to the probes on the surface, diffraction will not occur. Targets are then introduced, and the sample is illuminated. Reflection is used because silicon wafers do not transmit visible light. Diffraction is detected with a photodiode.

The ultimate goal of the work presented in this chapter is to create a DNA microarray that uses label-free targets and a diffraction based detection method. Instead of fluorescence, changes in a diffraction pattern would be detected. The diffraction will be based on differences in height and refractive index of single-versus double-stranded DNA. Using a diffraction-based technique could potentially lead to more accurate results. Attempts to create a DNA microarray in-house will be discussed in detail. This novel microarray utilizes amine groups as the linkers to bind DNA and fluorine groups or long chain alkyl groups to create a hydrophobic surface. To create this amine and hydrophobic-patterned surface many paths were explored. One path, photolithography, will be discussed below. In addition to creating patterns on substrates, a resolution study was performed to determine the smallest feature size that could be made.

An alternative approach to creating a patterned substrate using PDMS also showed promise, and amines were visualized using a selective metallization technique. Although DNA was never used in these experiments, the hydrophobic surfaces were tested for their stability in solvents used during DNA synthesis. Contact-angle measurements of water droplets on the microarray surfaces provided an indication of the surface compatibility for use as a DNA microarray. The following is a description of two photolithographic pathways used to create patterned surfaces.

6.1.4 Photolithography

6.1.4.1 Method 1

One method for creating an amine-functionalized / hydrophobic patterned surface involves the use photolithography (patterning photosensitive materials with light) which was discussed in Chapter 1. Two multistep approaches using photolithography were proposed, one using a positive mask, and the other a negative mask to create a patterned surface. In the positive-mask method (referred to as method 1), photolithography is used to create a polymerized layer atop of a fluorinated glass slide. Plasma cleaning removes the fluorination on the unprotected regions, allowing them to be functionalized with amines. The polymer is then removed to reveal an amine/fluorinated patterned substrate (Figure 6.2).

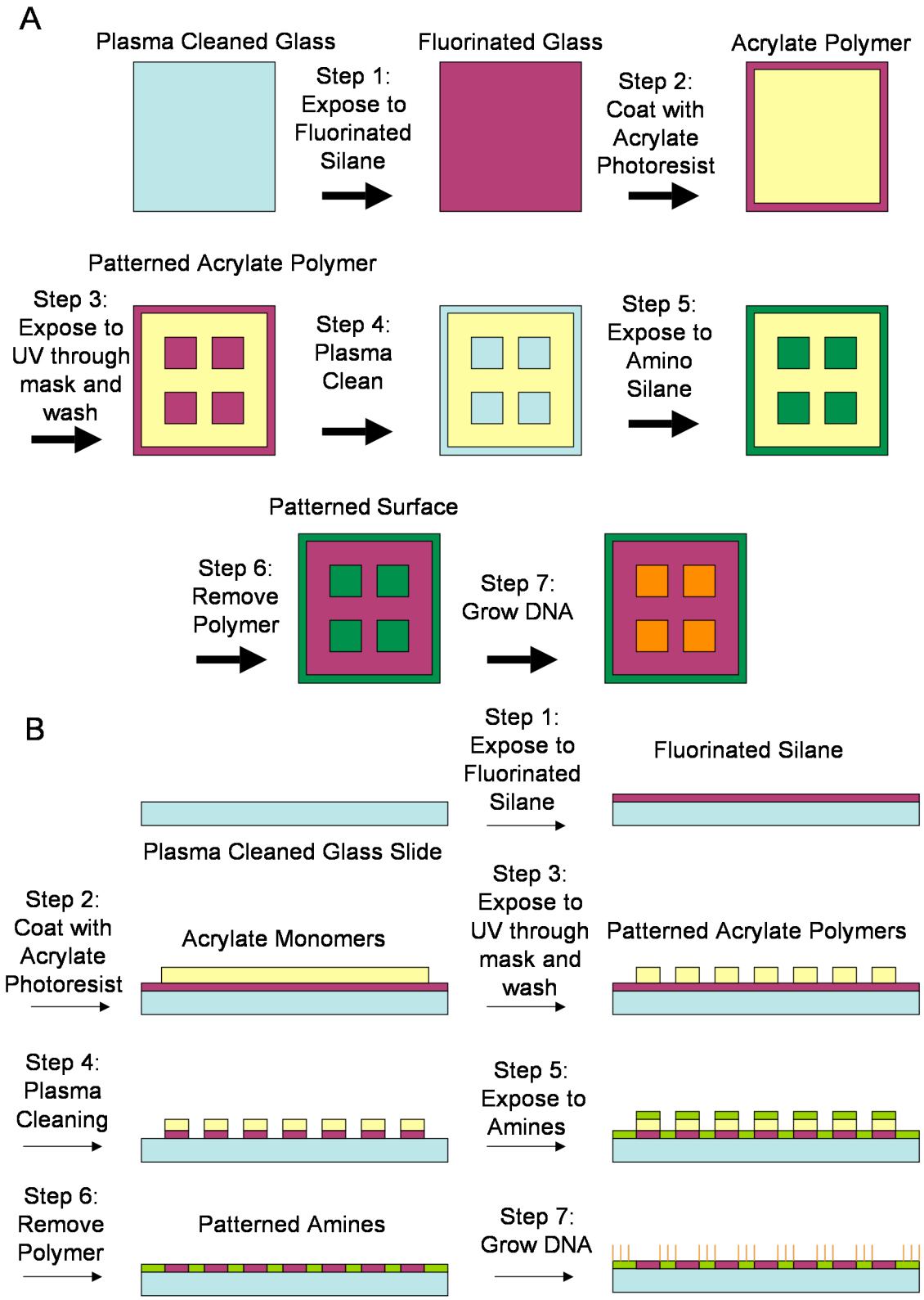

Figure 6.2 A) A top-down view of method one using a positive mask. **B)** A cross sectional view of method 1.

6.1.4.2 Method 2

In the negative-mask method referred to as method 2, photolithography is used to create polymerized features on the surface of an acrylate-functionalized glass slide, Figure 6.3. The polymer features shield the underlying acrylate functionalization. The unshielded areas can be cleaned and functionalized with a hydrophobic molecule containing fluorine. The polymer can then be removed to reveal the underlying functionalization that can then go on to be reacted with amines.

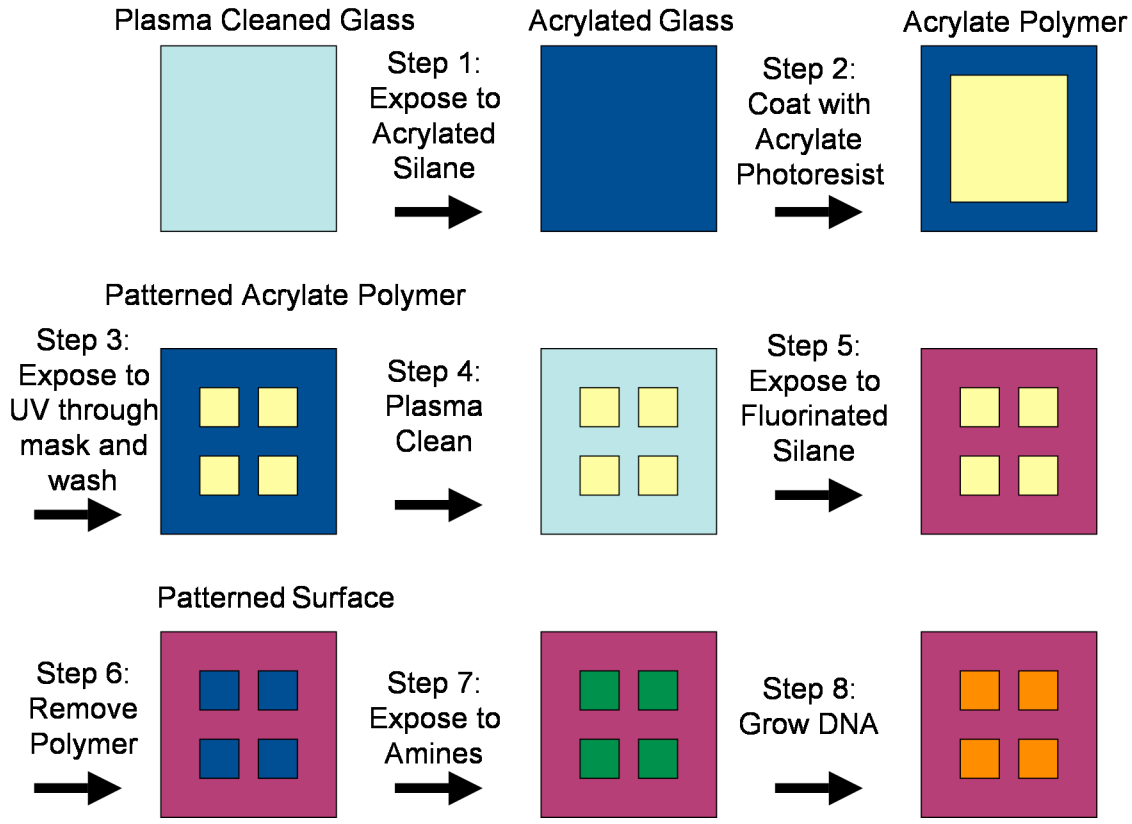

Figure 6.3 A top-down view of method 2, which uses a positive mask to create an amine and fluorinated surface.

The work presented in this chapter lays the foundation for a diffraction-based, label-free microarray. Although visualization of a completed patterned substrate was not achieved, various steps along each pathway were characterized. Recalling individual steps along these original pathways throughout the chapter provides the rationale for the experiments presented.

6.2 Experimental Setup

6.2.1 Polymer Removal and Creation of Duel Functionalized Slides

6.2.1.1 Plasma Cleaning

Prior to coating, substrates were cleaned in an oxygen plasma cleaner (Harrick plasma cleaner/sterilizer, Model PDC-32G) for 2 minutes at 200 mtorr. This cleaning results in a hydroxylated surface that is ideal for functionalization with silanes (method 1 and 2, step 0).

6.2.1.2 Acrylated Glass

Substrates were functionalized with acrylate groups to promote adhesion of the photoresist (method 2, step 1). Plasma cleaned substrates were immersed directly into an acrylate silane solution for at least 12 hours, rinsed in ethyl alcohol (200 proof, Pharmco-Aapar), and then dried at 95 °C. The acrylate solution consisted of 93 vol% ethyl alcohol, 5 vol% distilled water, and 2 vol% (3-acryloxypropyl) trimethoxysilane (95%, Gelest, Inc.).

6.2.1.3 Fluorinated Glass - Silanes

Vapor deposition was used to create a layer of tridecafluoro -1,1,2,2-tetrahydrooctyl dimethylchlorosilane (Gelest) onto a plasma-cleaned substrate (method 1, step 1). Substrates were placed vertically in a slotted holder so that both sides of the substrates were coated, and the holder was placed in a desiccator dedicated to coating a specific silane. A few drops of one of these silanes was placed in a clean watch glass. The watch glass and cleaned glass substrates were placed into the desiccator. The desiccator was evacuated and left for 24 hours.

6.2.1.4 Amine Glass – Ethlyenediamine

Acrylated glass coverslips (#1 and #2 Corning) were submerged in a solution of 1:4 ethlyenediamine (≥99.9% Sigma Aldrich):ethyl alcohol. Samples were in solution for no longer than 1 hour but no less than 30 minutes. After exposure samples were rinsed in 2-3 ethyl alcohol rinses for 2-3 minute each.

6.2.1.5 Metallization

Metallization was used as a means of visualizing amine groups once attached to a substrate. This procedure is based on the work described by Charbonnier et al.[11] The metallization procedure is used to deposit copper metal only onto amine surfaces, leaving other surfaces unmetallized. An amine-coated substrate was submerged for 15 minutes in a solution of 0.01g $PdCl_2$ (99.9+%, Sigma Aldrich), 100 mL of distilled water and 10 μL of hydrochloric acid (37% Sigma Aldrich). The $PdCl_2$ solution was prepared in advance to allow the $PdCl_2$ to dissolve. Prior to use, the solution was

filtered with a 0.65 μm nylon filter (Magna, Whatman), followed by three ethyl alcohol dips and a distilled water dip.

A solution consisting of 0.28 M copper II sulfate (98% ACS, Sigma Aldrich), 0.60 M $KNaC_4H_4O_6$ (99% ACS, Sigma Aldrich), and 0.03 M EDTA (ACS, Fisher) was made in distilled water. Slow addition of sodium hydroxide pellets (ACS, Fisher) was performed until a pH of 12 was reached. Immediately prior to use a 5:1 solution of the copper solution and formaldehyde (37% w/w ACS Grade, Fisher) was filtered through a 0.2 μm nylon filter (Fisherbrand).

The substrate was then placed in a 0.1 M sodium hypophosphite hydrate (Sigma Aldrich) solution at 85 °C for 10 minutes, followed by a water rinse. The sample was then placed on a level surface and a few drops of a copper solution were placed on top of it. The amount of time the copper solution remained in contact with the substrate varied with each sample, and was tracked by eye. Generally, copper started forming on the surface within ten minutes of exposure.

6.2.1.6 Photoresist

Photoresists were used to create the protecting polymer. In this section they are made using an acrylate monomer blend of dipentaerythritol pentaacrylate (SR399 Sartomer)/tris (2-hydroxy ethyl) isocyanurate triacrylate (SR368 Sartomer). The monomer blend was mixed with 3 percent by weight of a commercial photoinitiator, Lucirin TPO-L (BASF).

6.2.1.7 Contact Angle Measurements

The sessile drop method was used to measure contact angles at room temperature between distilled water droplets and treated surfaces.[12] A contact-angle goniometer (Ramé-Hart Instrument Co., 250-000) was used to deliver a drop of distilled water from a syringe onto a treated surface. The drop was imaged using a drop-shape analysis program (DROPIMage, Ramé-Hart Instrument Co.) and the contact angle was measured between the solid-liquid interface and the line tangent to the drop shape at the liquid-vapor interface.

6.2.2 Feature Size Optimization

6.2.2.1 Methacrylate Glass

Methacrylate-functionalized substrates were used in place of acrylate-functionalized substrates because methacrylates do not react in the metallization solutions, allowing the substrate to remain unmetallized. Substrates, #2 and #1 coverslips (Corning) or #0 coverslips, were oxygen plasma treated prior to functionalization, resulting in a hydroxylated, hydrophilic surface. The substrates were then immersed directly in a methacrylate silane solution for at least 12 hours, rinsed in ethyl alcohol, and then dried at 95 °C. The methacrylate solution consisted of 93 vol% ethyl alcohol, 5 vol% distilled water, and 2 vol% (3-methacryloxypropyl) trimethoxysilane (95%, Gelest, Inc.).

6.2.2.2 Photoresists

In this case photoresists were created using two acrylate monomer blends: ethoxylated (6) trimethylolpropane triacrylate (SR499 Sartomer)/tris (2-hydroxy ethyl) isocyanurate triacrylate (SR368 Sartomer) or dipentaerythritol pentaacrylate (SR399 Sartomer) / tris (2-hydroxy ethyl) isocyanurate triacrylate (SR368 Sartomer). Both blends were created using 50 wt% of both monomers. The prepolymer resin blends were mixed with 3 wt% of a commercial photoinitiator, Lucirin TPO-L (BASF).

6.2.2.3 UV Lamp Setup

The initial feature size studies were performed using a UV lamp (Black Ray, UV lamp Model B 100) to cure the photoresists. The wavelength of the UV lamp was 365 nm and the power was measured at 33 mW. The acrylate photoresist was sandwiched between a methacrylate functionalized coverslip and a fluorinated glass coverslip. This combination is used to keep the resulting pattern on only one glass surface. The fluorinated substrate also serves as a way to keep the mask clean. To prevent the glass slides from coming into contact with one another and displacing the photoresist, Scotch tape is placed on either side of the coverslip as a spacer (Figure 6.4). A negative patterned mask (USAF 1951 1 × Hi-Resolution, Edmund Optics) is placed atop the fluorinated slide and exposed to UV.

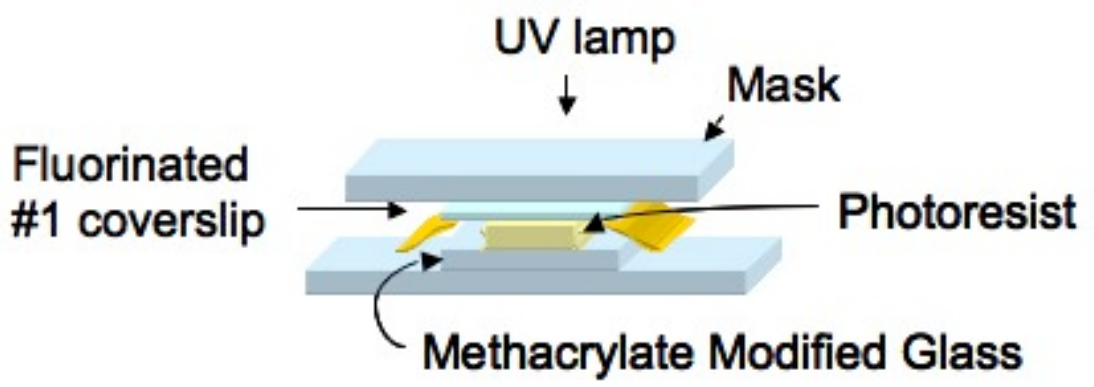

Figure 6.4 Sample setup for UV lamp.

6.2.2.4 UV Spot Source Setup

A UV spot source (Lighting Cure 200, Hamamatsu, Model L7217-01) with a wavelength of 365 nm was also used to cure photoresists. The spot source is an adjustable light source, with a measured maximum power of 9 mW, that focuses UV light through a fiber optic cable, allowing the light to be positioned directly above the photoresist. The curing of photoresists using a UV spot source used the same sandwich technique described above, only with the addition of using spin casting (Headway Research Inc.) to apply the photoresist. In this process a drop of photoresist was applied to a methacrylate-functionalized coverslip and spin cast at 2000 rpm for 2 minutes. Spin casting provides an evenly distributed layer of photoresist onto a substrate.

6.2.2.5 UV laser Setup

The final technique used to expose photoresists consisted of a tripled, λ=355 nm, ND:YAG laser (Continum 8010 powerlight series, 10 Hz). The same sample setup was used as in the UV lamp exposure, except the setup was positioned vertically along the beam path, and therefore required an additional piece of tape to secure the fluorinated coverslip to the glass slide that holds the methacrylate glass and photoresist (Figure 6.5). One laser pulse was used to pattern the photoresist.

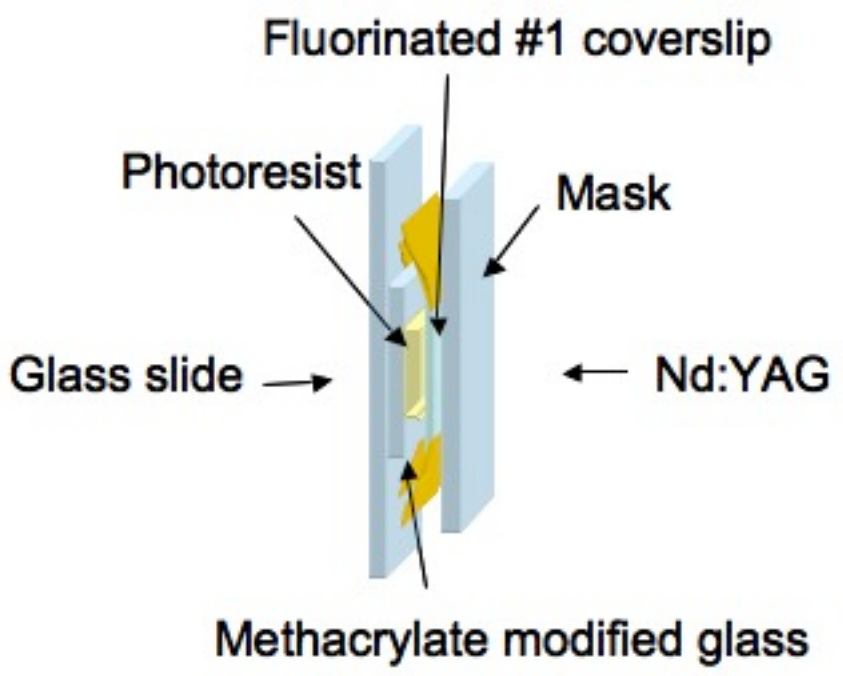

Figure 6.5 Initial sample setup for the Nd:YAG laser.

In later samples the setup was adjusted to minimize the distance between the mask and the photoresist. In addition to spin casting the resin onto a #0 coverslip at 4000 rpm for 1 minute, the coated methacrylate slide was placed against the target with the glass slide touching the target (Figure 6.6). Using this method the light only

travels through the target and methacrylate substrate before patterning the photoresist. Later work with the Nd:YAG laser also used a positive mask (USAF 1951 1 ×, Hi-Resolution Edmund Optics).

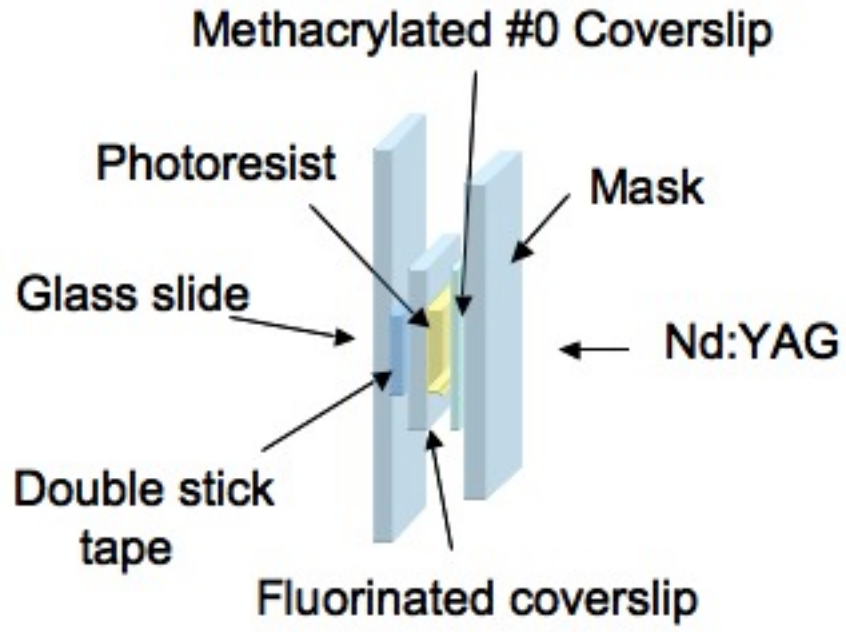

Figure 6.6 Improved sample setup for Nd:YAG laser.

6.2.2.6 Development

After exposure photoresists were developed in a series of solvent rinses. For photoresists created with SR399 the exposed sample was subjected to two dimethylformamide rinses followed by two ethyl alcohol rinses for 2-3 minute each. This procedure removes any unpolymerized photoresist and reveals the polymerized pattern. Photoresists created with SR499 are developed only in two ethyl alcohol rinses. After development samples are air dried at room temperature.

6.2.2.7 Mask Resolution

To create patterns in photoresists, negative and positive resolution masks were used. These masks are designed with a series of decreasing lines of known resolution. When the mask is used to create a pattern in a photoresist the resolution of the features created can be measured and is determined using line-pair (lp) per millimeter. The smallest line-pair that can be created with this mask is 645 lp/mm, but without special equipment creation of features with this size cannot be seen.

To measure the resolution, the mask contains groups of 6 bars, 3 horizontal and 3 vertical. These bars are equally spaced from one another resulting in various line-pairs. The lp/mm values for each element within a group is provided by the company. The resolution can be determined by finding the element within a group for which the features are merged together. The element prior to that one establishes the resolution.

6.2.3 Patterning with a PDMS Mold

6.2.3.1 Amine Glass - Silane

Plasma-cleaned glass coverslips (#1 and #2 Corning) were submerged in a solution of 100 mL methyl alcohol (Reagent Grade, Pharmco-Aapar) and 5 mL aminopropyltriethoxysilane (99%, Sigma Aldrich) for 4 hours. Slides were then rinsed and sonicated with methyl alcohol and dried at 100 °C for 1 hour.

6.2.3.2 Making Masters

The creation of master structures, to be molded with PDMS, was carried out on a setup described previously.[13] Briefly, a circularly polarized, ~200 femtosecond Ti:Sapphire laser (Coherent MIRA 900-F), tuned to 800 nm, was focused through an objective of an upright microscope. The laser was focused onto the sample, which was mounted onto a programmable stage (LEP MAC5000) controlled using Labview. A CCD camera (COHU 4915-2000/0000) attached to the microscope allowed observation of the fabrication process.

The sample setup for fabrication begins with applying an acrylate photoresist, (399/368 for these studies) to an acrylate-functionalized glass slide (Figure 6.7) in a

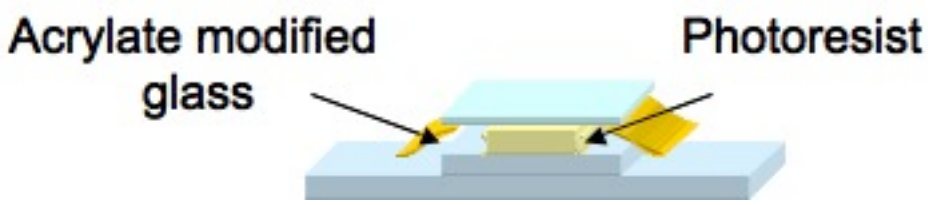

Figure 6.7 Setup for master fabrication. An acrylate photoresist is dropped onto an acrylate-functionalized slide. A piece of Scotch tape is used as a spacer and a coverslip is lowered onto the photoresist and taped into place.

similar fashion as in previous experiments. No mask is needed because a programmable shutter controls when exposure of the acrylate will occur. After fabrication the sample is developed, resulting in polymerized structures adhered to the glass substrate.

Immediately after development, samples were functionalized with a layer of amines for subsequent fluorine attachment. The specific fluorine species does not directly react with acrylates, but does react with amines. The addition of fluorinated

species to the surface of the acrylate polymer helps when the master structures are molded because it allows the completed mold to be removed from the master more easily.

The sample was immersed to a 1:4 ethlyenediamine:ethyl alcohol solution for 30 minutes. Samples were rinsed in three ethyl alcohol washes. Samples were then exposed to a solution made up of 0.0043g perfluorostearic acid (97% Alfa Aesar), 4.4604 g of hexafluorobenzene (99%, SynQuest Labs), 0.01g methyl alcohol and 16 mL of ethyl alcohol for 1 hour. Fluorinated samples were rinsed in ethyl alcohol for 1 minute and air dried.

6.2.3.3 PDMS Molding

The master structures, which contained a fabricated grid pattern, were subsequently molded in PDMS. The mold generates an inverse of the master, and has 30 × 30 microns squares which will later shield amine-functionalized surfaces. Polydimethylsiloxane (PDMS) (Dow Corning) is a commercially-available elastomer kit that comes in two parts, base and curing agent. The two liquids were combined in a 10:1 base to curing agent, mixed and centrifuged at 3400 rpm for 10 minutes to blend. The PDMS was poured into a premade 20 × 20 mm square mold and degassed. The fluorinated master structure was gently lowered at an angle, structure side down into the PDMS, being careful to avoid creating air bubbles. The sample was cured for 30 minutes at 110 °C. After curing, the mold was peeled away from the master.

6.2.3.4 Patterning with a PDMS Stamp

After the molds were created they were placed, pattern side down onto an amine functionalized substrate and then plasma cleaned. A clamp was used to keep the mold flush with the substrate during cleaning.

6.2.4 Functionalization Compatibility with DNA Synthesis Solvents

6.2.4.1 Silane Application for the Creation of Hydrophobic Surfaces

6.2.4.1.1 Vapor Deposition of Fluorinated Silanes

Vapor deposition was used to create a layer of tridecafluoro-1,1,2,2-tetrahydrooctyldimethylchlorosilane (Gelest), or tridecafluoro-1,1,2,2-tetrahydrooctylmethyldichlorosilane (Gelest) onto a plasma-cleaned substrate. Substrates were placed vertically in a slotted holder so that both sides of the substrates were coated, and the holder was placed in a desiccator dedicated to coating a specific silane. A few drops of one of these silanes was placed in a clean watch glass. The watch glass and cleaned glass substrates were placed into the desiccator. The desiccator was evacuated and left for 24 hours.

6.2.4.1.2 Reflux Application of Alkyl Silane

An additional method of creating a hydrophobic surface was tested using alkyl chains. n-octadecyldimethylchlorosilane (Gelest) was applied to surfaces in a reflux setup. The coverslips, originally 25 × 25 mm, were cut in half so they could be placed in a round-bottom flask with 0.5 g of n-octadecyldimethylchlorosilane. Nitrogen gas was flowed through the reflux setup that contained 50 mL of dry

toluene. The flask was heated to 130 °C with stirring. The solvent was refluxed overnight, ~ 16 hours. After coating, slides were sonicated in toluene (Sigma), for 3 minutes followed by an additional 3 minutes rinse in toluene, and two more 3 minutes rinses in methyl alcohol. Slides were air dried and kept in a desiccator prior to use.

6.2.4.2 DNA Synthesis Solvents used to Test the Stability of Hydrophobic Substrates

6.2.4.2.1 Trichloroacetic Acid/Dichloromethane

Tridecafluoro-1,1,2,2-tetrahydrooctyl dimethylchlorosilane-coated silicon slides were submerged in a 5% trichloroacetic acid (Fisher) in dichloromethane (HPLC Grade, JT Baker) solution for 24 hours at room temperature. Samples were removed and air dried at room temperature. Adapted procedure from Zaramella et al. and Ellington et al[14, 15]

6.2.4.2.2 Ammonium Hydroxide

Silane coated slides were submerged in concentrated ammonium hydroxide (28% in water, Fluka) at 60 °C for 16 hours. Unless otherwise noted, samples were rinsed in distilled water for 10 minutes and air dried at room temperature. Adapted procedure from Ellington et al.[15]

6.2.4.2.3 Ammonium Hydroxide/Methyl Amine

Silane coated slides were submerged in a 50/50 solution of concentrated (28-30%) ammonium hydroxide and methyl amine at 65 °C for 10 minutes. Samples

were rinsed with distilled water for 10 minutes and air dried at room temperature. Adapted procedure from Ellington et al.[15]

6.2.4.2.4 Ethylenediamine/Ethyl Alcohol

Silane coated slides were submerged in a 50/50 solution of ethylenediamine (En) and ethyl alcohol for 4 hours at room temperature. Samples were rinsed in two, 3 minute distilled water rinses and dried under a stream of nitrogen. Adapted procedure from McGall et al.[16]

6.3 Results and Discussion

6.3.1 Polymer Removal and Creation of Dual-Functionalized Slides

Protection using a polymer coating on a functionalized surface requires the ability to remove the polymer from a substrate without consequence (method 1 and 2, step 6). The ability to remove cured polymer using sonication was investigated by creating dots of acrylate photoresist on an acrylate-functionalized glass substrate. The dots varied in size from a few millimeters to a centimeter. Sonication in water showed no effect on the removal of the dots, while sonication in ethyl alcohol and dimethylformamide (DMF) softened the dots so they could be removed by hand. Thus, it was found that DMF and ethyl alcohol can be used to soften the polymer dots, making them easier to remove. For removal, a slide functionalized with a fluorinated silane underwent the same procedure, and during sonication in DMF the small dots fell off in solution and the larger ones were easily removed by hand. This observation may make method 1 slightly more favorable than method 2. Sonication

in ethyl alcohol provided for easy removal of dots by hand, but no independent removal during sonication was observed.

Once it was demonstrated that polymer coatings could be removed, further testing was performed to demonstrate the possibility of having two functionalizations on the same substrate, as needed in step 6, method 1 and step 7 for method 2. Half of a fluorinated substrate was covered with a layer of acrylate photoresist that was UV cured. The sample was then plasma cleaned to remove the fluorination on the unshielded side. Sonication in DMF then softened the polymer for removal. Contact-angle measurements were performed on both sides of the substrate and revealed a difference of 66° between the region shielded by the acrylate polymer (measuring an angle of 98°) and the plasma-cleaned area (measuring 32°) (Figure 6.8). These results indicate that using acrylate

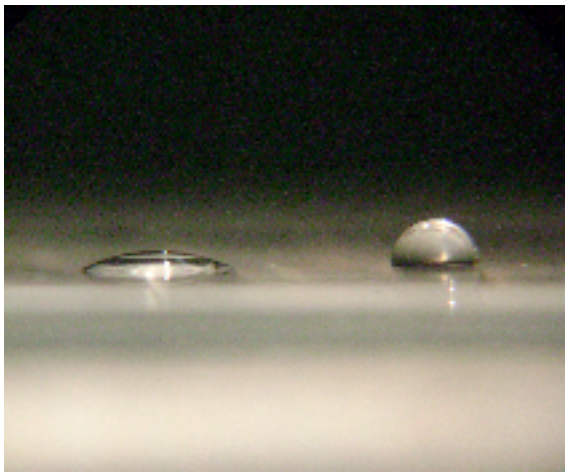

Figure 6.8 Drops of water placed on the same slide. The drop on the left is placed on the oxygen-plasma-cleaned side of the substrate. The drop on the right is placed on the shielded fluorinated side after removal of the polymer.

polymer to shield a fluorinated surface during plasma cleaning leaves the protected functionalization intact. On a separately prepared sample the freshly cleaned slide was then treated with an amino silane to create an amine-functionalized surface. The polymer was then removed and a metallization solution was applied. This experiment revealed that indeed, half of the surface had been amine-functionalized and no metal deposition occurred on the fluorinated region. This encouraging result indicates that it is possible to protect a functionalized surface using UV cured polymer to create multi-functional surfaces.

6.3.2 Feature Size Optimization

The purpose of this study was to determine how small a feature size could be created using in-house equipment (method 1 and 2, step 3). Three UV light sources were tested to minimize features sizes. Feature size is important to determine the number of reactive sites, for DNA, that can be placed on a microarray.

Initial attempts at creating features in a photoresist made of SR499/SR368 resulted in over-exposed UV patterns (Figure 6.9B). The over exposure of a photoresist results in merging of the features. Even with short (5 second) exposure times the features were not well resolved. The SR399/SR368 blend was also tested, and the features created showed better separation although the resolution was still only 7.13 line-pair (lp)/mm (Figure 6.9A). As seen in upcoming studies, the mask used is meant to have higher resolution features in the center of Figure 6.9A but these features failed to form.

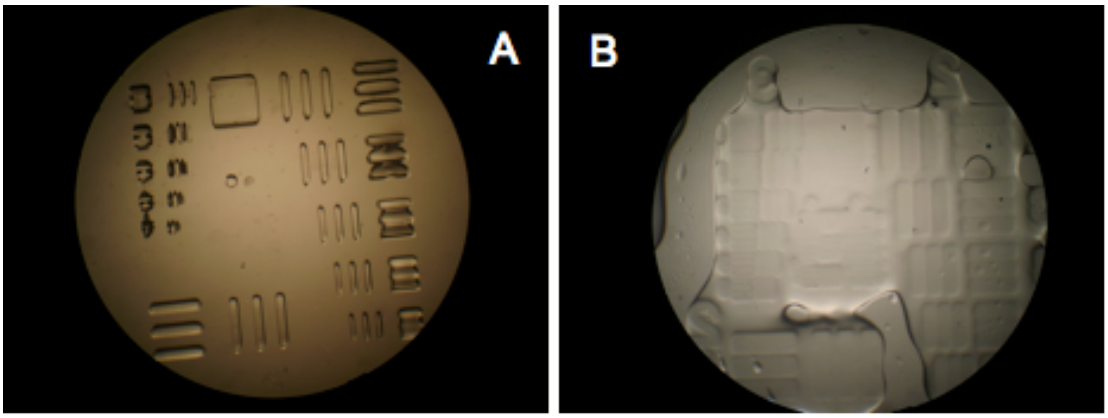

Figure 6.9 Patterns created with the UV lamp. **A)** 30 sec UV exposure of SR399/SR368 resin; notice the center has no pattern. Resolution is 7.13 lp/mm **B)** 30 sec UV exposure of SR499/SR368 resin; notice the blending of the features.

The feature definition observed in the SR399/SR368 samples (rather than in the SR499/SR368 samples) could be a result of the viscosity difference between the two resins. The SR499/SR368 blend is much less viscous than the SR399/SR368 blend; therefore when sandwiched between two substrates and immediately exposed to UV, the former photoresist could be still moving. Such movement could lead to the observed feature merging.

To further improve the definition of the features created in SR399/SR368, the exposure source was changed from a UV lamp to a UV spot source, and the photoresist films were prepared by spin casting. Spin casting the photoresist (rather than pressing the photoresist between two coverslips) allows for the creation of a thin, even surface and thus thin, even features.

Using the spot source rather than the UV lamp provided a more focused beam of light to use for patterning. Rather than exposing the sample under a light bulb, as was done with the UV lamp, the spot source employs a fiber optic cable that provides

a focused spot of UV light that can be positioned directly above the sample. Centering the UV light directly above the mask leads to straight vertical sidewalls on the features created, and therefore better feature definition.

The features seen on photoresists exposed using the UV spot source all have much better definition. In the smallest feature sizes near the middle of Figure 6.10,

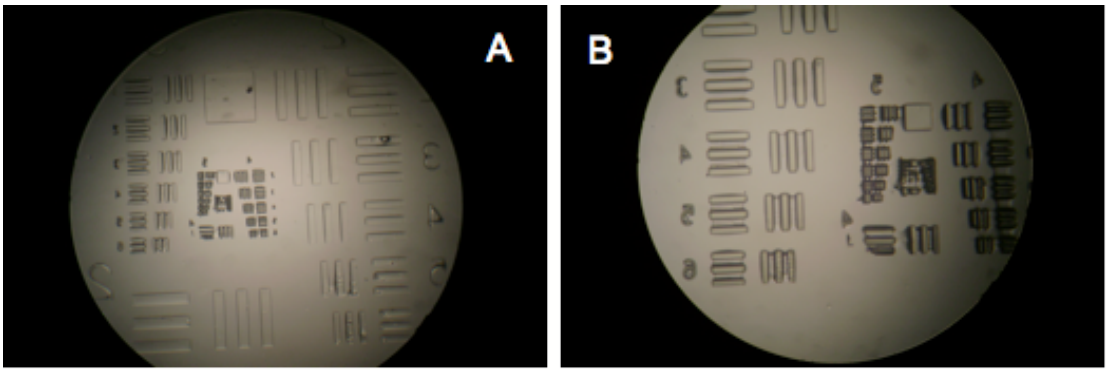

Figure 6.10 Patterns created on SR399/SR368 photoresist by exposing to UV from UV spot source for 1 minute. **A)** Optical image magnified with 5× objective **B)** Optical image of the same sample magnified with 10× objective. The line-pair resolution is 8.00 lp/mm.

Some blending can bee seen, but with a best resolution of 8.00 lp/mm we see improvement verses the UV lamp test.

Using the same rationale, it was hoped that even better resolution could be obtained from a tripled Nd:YAG laser for sample exposure. For this study, SR399 resin was used. By exposing the samples to only one laser pulse, a feature resolution of 25.40 lp/mm was attained (Figure 6.11). Smaller features were present and appeared separated, but also had moved or fallen over (Figure 6.11B) It is quite possible that the thickness of the photoresist created by sandwiching it between two slides produces features too large for the width, causing the samples to collapse.

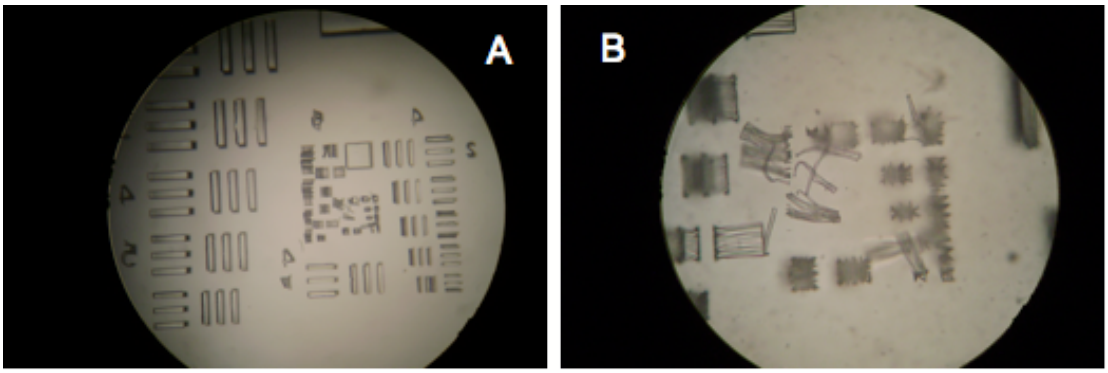

Figure 6.11 Patterns created on SR399/SR368 photoresist by exposing to UV from an ND:YAG laser for 1 pulse. Line-pair size is 39 microns. A) Optical image magnified with 10× objective. B) Optical image of same sample magnified with 45× objective.

To circumvent this problem photoresists were spin cast, and a thinner coverslip (# 0) was used. Decreasing the size of the coverslip from #2 to #0 decreased the amount of glass the light had to travel through before it reaches the photoresist. The more materials light has to travel through before it reaches the photoresist, the more diffraction occurs, effectively dispersing the light. Minimizing the distance between the light and the photoresist, as well as decreasing the photoresist thickness, resulted in better feature definition. Using this improved method, a line-pair resolution of 45.25 lp/mm was achieved (Figure 6.12).

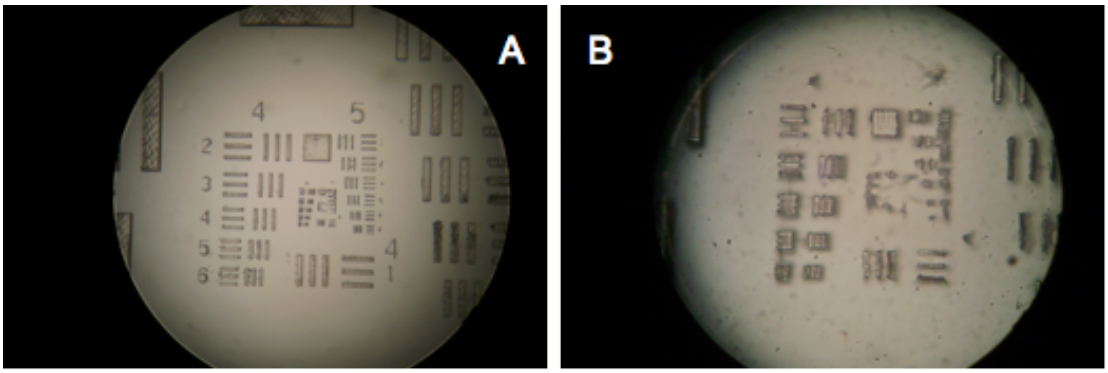

Figure 6.12 Patterns created on SR399/SR368 photoresist by exposing to UV from an ND:YAG laser for 1 pulse. Photoresist was prepared by spin casting on a #0 coverslip. Line-pair resolution is 45.25 lp/mm. **A)** Optical image magnified with 10× objective. **B)** Optical image magnified with 45× objective.

As demonstrated above, using a laser as the exposure source for patterning of a photoresist creates well-defined features. Compared to the other sources, the laser has a significantly higher intensity, 300 mW. The intensity of the UV lamp was measured at 33 mW and the spot source has a maximum intensity of 9 mW. This increased intensity allows for samples to be polymerized in a much shorter amount of time, one pulse of the laser (< 1 second) compared to the 30 seconds and 1 minute used for the UV lamp and spot source, respectively.

An additional advantage to the use of a laser is that it is a collimated source of light for which all of the rays are parallel. The creation of straight edges in features greatly improves with collimated sources. If the light enters a mask at many angles, then those angles are transferred to the photoresist, producing features with angled edges. By collimating the light, the light goes through the mask and reaches the photoresist at only one angle, allowing the formation of a straight edge that is normal

to the substrate. The combination of collimation and high intensity allows for the creation of such small features in acrylate photoresists.

6.3.3 Polymer Removal of Smaller Features

In this section it is the creation of features with a resolution of 45.25 lp/mm is demonstrated, but recalling step 6 in both methods, these small features will later have to be removed. To remove these smaller features, Nd:YAG patterned samples were placed in methyl alcohol and sonicated to soften the polymer. Samples were transferred to DMF and sonicated. Despite earlier results showing that DMF could be used to remove the polymer, these smaller features remained attached to the substrate. Exposure to acetone and methlyene chloride was also not effective in removing the polymer.

Unfunctionalized substrates were tested to see if features could be more easily removed after patterning. Unfortunately, the features detached from the substrate during development of the photoresist. A fluorinated substrate was also tested, and the results were identical with those of the unfunctionalized substrate. Increasing the aspect ratio of the features created by decreasing the angular velocity used when spin casting on a methacrylate-functionalized substrate was also tested, but the features remained attached.

As mentioned above, earlier results indicated that sonication in DMF for a short time would aid in the partial removal of UV-cured polymer from a substrate. The features created in the previous experiments were much larger and had a higher aspect ratio than the features created with the Nd:YAG laser. It is possible that these

smaller and thinner samples need to be removed using an alternative technique such as harsher solvents or much longer sonication times.

The features created with the Nd:YAG laser seem to be more strongly attached to the substrate than the initial features created with the UV lamp. This stronger adhesion could be due to the decreased size of the features or a more complete polymerization from the high intensity of the laser. The ideal combination of features and substrates would allow features to remain attached to the substrate through the development process and any further functionalization, but to detach after the functionalization is complete.

6.3.4 Positive Mask

The above experiments examined the procedure described in method 2. Switching to the positive mask and following method 1 allows for a larger percentage of the substrate to be covered with polymer, which presumably is more analogous to the large polymer dots described earlier. This increase in surface coverage may allow the balance of keeping features attached to a substrate through development but also allowing them to be removed after functionalization.

Following method 1, a positive mask was used to pattern a fluorinated glass slide with the Nd:YAG laser. Unfortunately, during development the photoresist detached from the substrate. Expanding the beam and increasing the number of laser pulses used from 1 to 10 also resulted in feature detachment during development.

Straying from the described methods, the positive mask was used to pattern methacrylate-functionalized slides to see if the photoresist could be developed

without detachment. The results were consistent with those obtained with the negative mask and features did remain attached for both a single pulse of the laser (Figure 6.13A) and 10 pulses (Figure 6.13B). To test if these, now-attached features

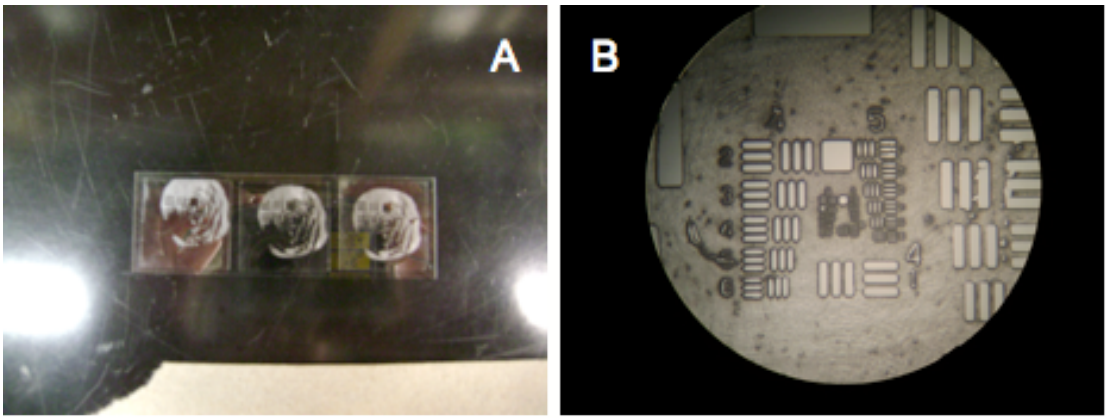

Figure 6.13 Positive mask results with the Nd:YAG laser. Panel A shows three samples created with only one pulse of the laser. Notice the missing sections in the center of the sample. Panel B is an optical microscope image of the center of a sample created with 10 pulses. A resolution of 16 lp/mm was achieved. Notice that the patchiness is gone.

could be removed, the sample was sonicated in DMSO, but showed no removal. A sonication for several hours in chloroform did show promise, with some of the polymer lifting off of the substrate.

A final attempt was made to develop a substrate, both retaining the polymer and allowing it to be removed after functionalization. By creating a substrate with a methacrylate-functionalization on the edges and a fluorinated center, there could be enough adhesion that the photoresist will remain attached to the substrate during development. Using a UV-cured acrylate polymer to shield the center of a fluorinated surface (the same procedure as in the earlier polymer dot experiment), a substrate was

plasma cleaned and placed in a methacrylate silane solution for functionalization. Upon completion of the methacrylate-functionalization the polymer was removed to reveal a substrate with a fluorinated center and methacrylate on the edges.

Applying a second round of photoresist to this substrate and exposing to UV revealed that the edges of the photoresist (in contact with the methacrylate-functionalization) remained stuck to the substrate, preventing the delamination seen with all of the fluorinated substrates, but there were some areas in the center of the film that lifted off the substrate. Refinement of this modified procedure with the second polymer film and the use of masks shows some promise, and this encouraging work provides a good basis for the future work that is required to perfect this step of microarray fabrication.

6.3.5 Patterning with a PDMS Mold

An alternative approach to patterning amines on a substrate involves the creation of a polydimethylsiloxane (PDMS) mold. PDMS is a two-part liquid that, when mixed creates a clear, flexible polymer which is ideal for making molds. The development of a grid pattern in a PDMS mold would, when placed against an amine-functionalized substrate, shield the amine areas and allow unshielded areas to be plasma-cleaned and later functionalized. Additionally, selective metallization was used to visualize amines, although other fluorescence-based visualization methods were also investigated.

This work hinges on the ability of PDMS to shield a functionalized area, in the same way that cured polymer was used in earlier photolithography experiments.

As a quick test, PDMS was placed on an amine-functionalized glass slide that was then subjected to an oxygen plasma. The areas not shielded by the PDMS should lose their amine functionality. After plasma cleaning the PDMS was removed and the slide was placed in a fluorinated solution that could only react with amines. After coating, the slide was rinsed in water. The water retreated from the area shielded by PDMS, indicating that it is possible to shield functionalized areas with PDMS.

To create a master with a grid pattern, a series of horizontal and vertical intersecting lines, 6,000 microns long, were created in SR499/SR368 photoresist (Figure 6.14). Once molded, these samples were cut to allow oxygen to flow into the

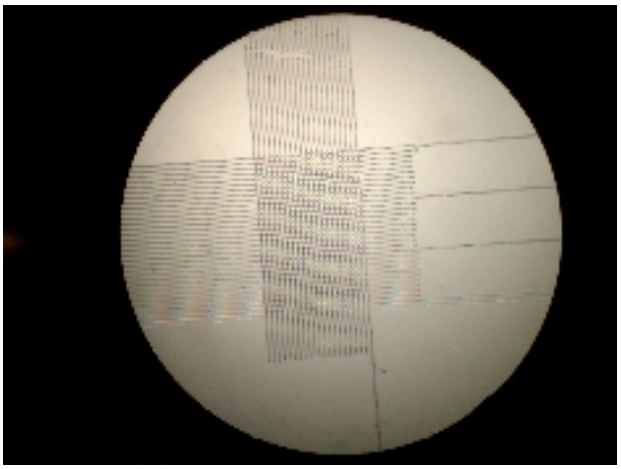

Figure 6.14. Master structure with a fabricated grid pattern and longer channels.

channels during plasma cleaning. The addition of longer, 12,000 microns, lines ensured that oxygen would reach the channels.

After fabrication, a mold was created and placed against an amine-functionalized substrate. To ensure that the PDMS stamp made good contact with the amine-functionalized substrate, a clamp was used to apply a slight pressure to the mold during plasma cleaning. If too much pressure was applied, channel collapse could occur.

After plasma cleaning, selective metallization was performed, and the amine blocks could clearly be seen with copper metal deposits on them. They were easily distinguished from the "streets" because they were transparent (Figure 6.15A and B).

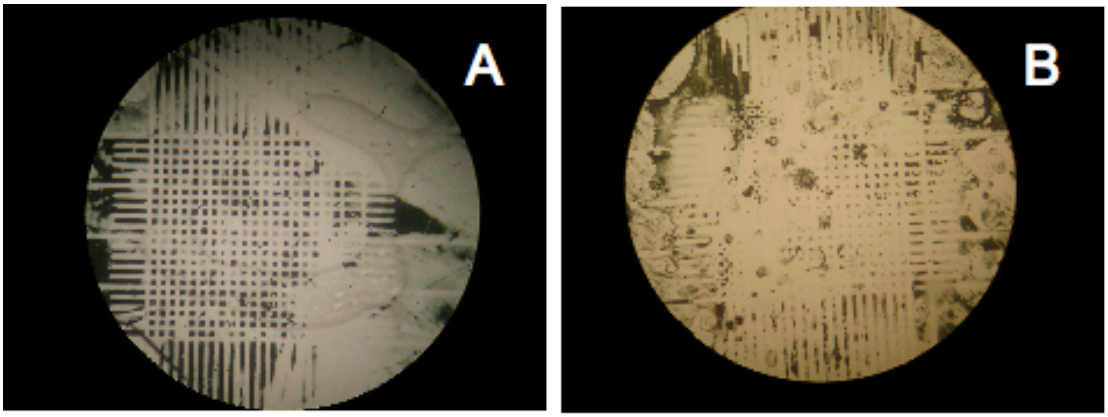

Figure 6.15 Optical images of metallized amine patterned substrates.

Areas with no patterns could be seen on both samples, and may arise from an incomplete reaction with the metallization solution or, conversely, overexposure to the metallization solution, which can lead to flaking of the deposited metal.

Fluorescence-based visualization methods were investigated as a means of confirming the presence of amines. Traditional fluorescent tags, such as dansyl chloride, tetramethylrhodamienisothiocyanate and coumarin 343 can react with the exposed patterned amines. Unfortunately, no fluorescence signal could be detected from these reactions, possibly due to a low concentration of amines on the substrate.

As seen in Figure 6.15, selective metal deposition can be used to visualize amines on a patterned substrate. The metallization solutions show the best deposition when solutions are made fresh. In the future, fluorination of these amine-patterned substrates could be attempted and it is likely that a fluorinated/amine-patterned

substrate could be created by exposing the clamped mold and substrate to a fluorinated silane.

6.3.6 Functionalization Compatibility with DNA Synthesis Solvents

The final part of this study investigates how well hydrophobic coatings retain their hydrophobic properties after exposure to solvents used in DNA synthesis (method 1, step 8, and method 2, step 7) . These solvents are generally weak acids and bases which are used to remove protecting groups from reactive sites on DNA bases. The harshest solvents used during DNA synthesis were selected to test the susceptibility of substrates to losing functionality. These solutions consisted of trichloroacetic acid (TCA) in dichloromethane (DCM), pure ammonium hydroxide (NH_4OH) and ammonium hydroxide in methyl amine (MA). In this section, three coatings are tested for compatibility with DNA synthesis solvents and tracked using contact-angle measurements.

6.3.7 Tridecafluoro-1,1,2,2-tetrahydrooctyldimethylchlorosilane

The vapor deposition of tridecafluoro-1,1,2,2-tetrahydrooctyldimethylchlorosilane, referred to as the fluorinated dimethylchlorosilane, was studied to see how long samples need to be exposed to the vapor before having a contact angle of 70° or higher (indicating that a hydrophobic surface is present). Substrates began as plasma-cleaned glass slides that had a contact angle of less than 5°. They were exposed to the silane in a desiccator, and contact-

angle measurements were taken at 1, 4, 16, 24, and 48 hours (Figure 6.16). Contact angles taken after 1 hour

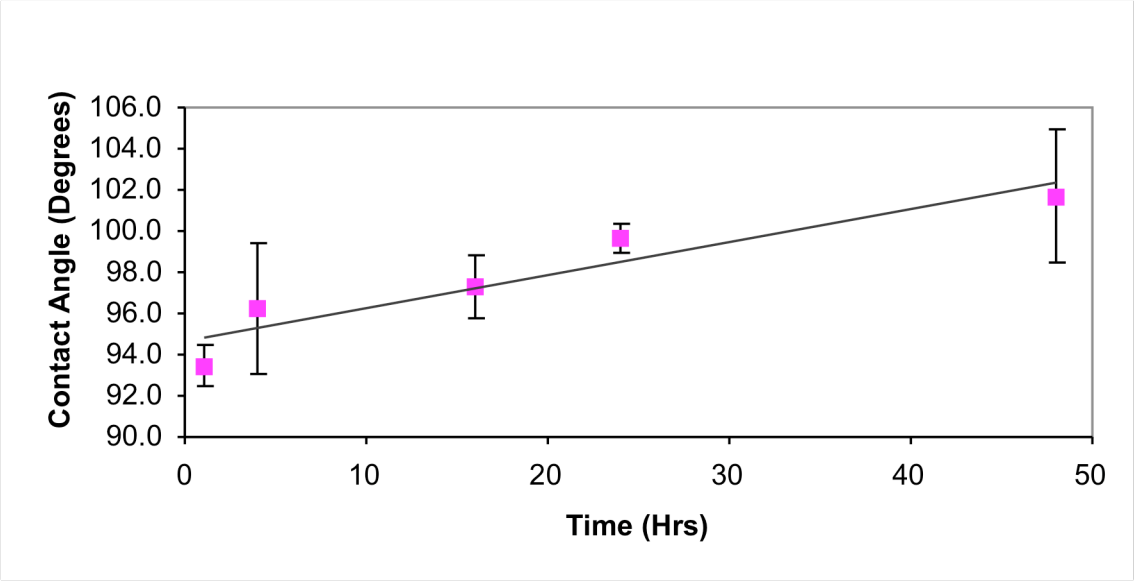

Figure 6.16 Time-dependent study of tridecafluoro-1,1,2,2-tetrahydrooctyldimethylchlorosilane deposited in vapor form on silicon wafers. Standard deviations were calculated from three separate samples that underwent the same procedure at the same time.

showed an angle of 93°, which is much higher than that of the original plasma-cleaned glass slide. Subsequent measurements indicated that as exposure time increases, the contact angle steadily increases. After the 1 hour mark, the contact angle reached 102°, indicating that 1 hour is clearly sufficient to produce a fluorinated surface.

To test if a fluorinated, dimethylchlorosilane-coated glass coverslips would remain hydrophobic after exposure to TCA/DCM, coated coverslips were submerged in a solution of TCA/DCM for 24 hours. Contact angles were measured before and after immersion in the acid and are shown in Figure 6.17. The TCA/DCM mixture

Treatments		Silanes		
		Fluorinated dimethylchloro silane[1]	**Fluorinated methyldichloro silane[2]**	**Alkyl dimethylchloro silane[3]**
TCA/DCM	Before	85 (±3)	-	-
	After	79 (±3)	-	-
NH_4OH	Before	80 (±3)	88 (±2)	81 (±4)
	After	17 (±7)	17 (±6)	47 (±8)
NH_4OH/MA	Before	82 (±1)	88 (±1)	79 (±4)
	After	52 (±10)	93 (±2)	80 (±2)
En/EtOH	Before	-	89 (±2)	81 (±3)
	After	-	84 (±3)	73 (±5)
[1] tridecafluoro-1,1,2,2-tetrahydrooctyldimethylchlorosilane				
[2] tridecafluoro-1,1,2,2-tetrahydrooctylmethyldichlorosilane				
[3]n- octadecyldimethylchlorosilane				

Table 6.1 Contact angles taken on three coatings applied to glass substrates in this section. Measurements were taken before and after treatments in 4 solvents that can be used during DNA synthesis. Measurements are calculated by taking the average of three angles collected on three samples for a total of 9 angles. For NH_4OH/MA on fluorinated dimethylchloro silane coated substrates only 6 angles were used.

appears to have little effect on the angle the water forms with the surface. The smallest contact angle was 76°, which is 11° less than the original angle of 87°. The

average difference in contact angle for before and after treatment was 6°. Indicating that the fluorinated dimethylchlorosilane remains stable after 24 hours.

Fluorinated dimethylchlorosilane coverslips were also treated in pure NH_4OH. Contact angles were measured before and after NH_4OH treatment and revealed that the NH_4OH removes the silane coating from the substrate (Figure 6.17). The contact angles measured prior to coating were all higher than 76°, while the highest angle after treatment was 25°. Another solution with less NH_4OH was also tested. This solution was 50/50 NH_4OH and MA, and samples treated with it showed contact angles no lower than 48°

6.3.8 Tridecafluoro-1,1,2,2-tetrahydrooctyl*methyldichloro*silane

The silane used in the above experiments is a fluorinated dimethylchlorosilane, which can only form one bond through the chlorine with the substrate. To double the amount of bonds that can form between the silane and the substrate, tridecafluoro-1,1,2,2- tetrahydrooctyl*methyldichloro*silane (fluorinated methyldichlorosilane) was used to test for improved performance in solutions containing NH_4OH. This fluorinated methyldichlorosilane is identical to the fluorinated dimethylchlorosilane, and is applied in the same manner using vapor deposition.

The sample was exposed to NH_4OH/MA solution, and experiments showed that the contact angle remained above 87° for all samples even after exposure, and that the contact angles increased slightly (Figure 6.17). This slight increase could be due to the removal of hydrochloric acid on the substrate. Hydrochloric acid is formed

when the fluorinated methyldichlorosilane attaches to the glass substrate. The samples are not rinsed prior to treatment in synthesis solvents, and therefore during the treatment in the synthesis solvents the hydrochloric acid is removed, which could lead to the observed increase in contact angle.

To see if fluorinated methyldichlorosilane would remain attached in harsher conditions, samples were treated with only NH_4OH. Contact angles of above 87° were obtained prior to exposure, while after exposure no angles larger than 22° were seen (Figure 6.17). As with the dimethylchlorosilane, the methyldichlorosilane is removed with the NH_4OH treatment.

A third solution that did not contain NH_4OH was also tested. Samples were exposed to En/EtOH, and contact angles of 84° were obtained. These are about 6% less than the original contact angles measurements of 89°, indicating that the fluorinated methyldichlorosilane is resistant to the En/EtOH solvent.

6.3.9 n-octadecyldimethylchlorosilane

A third non fluorinated coating was also tested for stability in DNA synthesis solvents. n-octadecyldimethylchlorosilane (alkyl dimethylchlorosilane) is a solid silane and was applied to slides in an overnight reflux setup. This silane creates a hydrophobic surface using a strand of 18 carbons. Being an alkyl dimethylchlorosilane, it only forms one bond with the substrate, but because the hydrophobic end does not contain fluorine groups it is less reactive and therefore potentially more resistant to the solvent rinses.

Exposure to NH_4OH revealed that, as with the other functionalizations, the contact angle dropped to below 50° for all samples (Figure 6.17). Exposure to the NH_4OH/MA solution revealed that alkyl dimethylchlorosilane is just as resistant to the solvent as the fluorinated methyldichlorosilane. All contact angles measured were larger than 76°. Exposure to EN/EtOH revealed similar results, with average angles after treatment being 73°.

6.3.10 Comparison

All samples treated in the pure NH_4OH showed significant loss of surface coatings. This loss was more pronounced (78% loss or higher) for the fluorinated silanes, regardless of the number of bonds attached to the substrate. The alkyl dimethylchlorosilane showed a loss of 42% after treatment in NH_4OH. The alkyl dimethylchlorosilane likely shows a higher contact angle compared to the fluorinated silanes due to the absence of fluorine.

Overall, the highest contact angles prior to treatment can be seen on surfaces coated with fluorinated methyldichlorosilane. This result is most likely due to a denser film formation due to an additional bonding site as well as the presence of fluorine on the molecule. The lowest contact angles observed prior to treatment were seen with the alkyl dimethylchlorosilane, which is likely due to the absence of fluorine species. The fluorinated dimethylchlorosilane showed promising results in TCA/DCM solution, and although not tested, similar results can be expected for the other silanes in this solvent. Of the tested silanes, the results discussed here indicate

that the fluorinated methyldichlorosilane provides the highest contact angles with the least loss of coverage in the tested solvents.

6.4 Conclusions

Steps in a photolithographic approach to create an amine and hydrophobic patterned substrate were examined for feasibility. One of these steps (step 3), the ability of cured polymer to protect an underlying functionalization, was demonstrated using fluorinated glass and plasma cleaning. This procedure results in the ability to have dual functionalities on the same surface.

For another step (step 6), the removal of polymer was demonstrated for larger features using sonication in DMF. However, when the feature size was decreased, the features could not easily be removed using sonication. Feature sizes as small as 11 microns could be achieved using an Nd:YAG laser. Alternative methods for polymer removal could be investigated such as longer exposure to solvents, or a more vigorous agitation.

In addition to photolithography, PDMS was investigated as a shield for amine-functionalized coated regions on a substrate. The creation of a grid of individual squares combined with plasma cleaning allowed for an amine-patterned substrate to be produced. Future work could investigate how small a feature size can be created using this method and the fluorination of the cleaned channels.

One method that did show success in visualizing amines is the use of a selective metallization solution that deposits copper only on amine areas. This solution demonstrates the best deposition when the solutions are made the day of use

but can still not deposit in areas that are amine-functionalized. Further work to investigate the appearance of metal in unfunctionalized areas needs to be done.

Final studies examined three hydrophobic coatings for compatibility with solvents used in DNA synthesis. The results indicate that washing in NH_4OH completely removes the silane and synthesis using this solvent would not be possible. Blending the NH_4OH with MA showed promise with the methyldichlorosilane and an alkyl silane remaining attached. Functionalizations were also tested in a EN/EtOH solution, with both of the above functionalizations remaining intact. The above results suggest that the potential to eventually attach DNA to these substrates is possible.

References

1. Lockhart, D. J.; Winzeler, E. A., Genomics, gene expression and DNA arrays. *Nature* **2000,** *405* (6788), 827-836.

2. Debouck, C.; Goodfellow, P. N., DNA microarrays in drug discovery and development. *Nature Genet.* **1999,** *21*, 48-50.

3. Schena, M., *Microarray Analysis*. John Wiley & Sons: Hooken, New Jersey, 2003.

4. Duggan, D. J.; Bittner, M.; Chen, Y. D.; Meltzer, P.; Trent, J. M., Expression profiling using cDNA microarrays. *Nature Genet.* **1999,** *21*, 10-14.

5. Cheung, V. G.; Morley, M.; Aguilar, F.; Massimi, A.; Kucherlapati, R.; Childs, G., Making and reading microarrays. *Nature Genet.* **1999,** *21*, 15-19.

6. Bryant, P. A.; Venter, D.; Robins-Browne, R.; Curtis, N., Chips with everything: DNA microarrays in infectious diseases. *Lancet Infect. Dis.* **2004,** *4* (2), 100-111.

7. Robertson, B. H.; Nicholson, J. K. A., New microbiology tools for public health and their implications. *Annu. Rev. Public Health* **2005,** *26*, 281-302.

8. Niu, S.; Singh, G.; Saraf, R. F., Label-less fluorescence-based method to detect hybridization with applications to DNA micro-array. *Biosens. Bioelectron.* **2007,** *23* (5), 714-720.

9. Fei, Y. Y.; Landry, J. P.; Sun, Y. S.; Zhu, X. D.; Luo, J. T.; Wang, X. B.; Lam, K. S., A novel high-throughput scanning microscope for label-free detection of protein and small-molecule chemical microarrays. *Rev. Sci. Instrum.* **2008,** *79* (1), 7.

10. Tsay, Y. G.; Lin, C. I.; Lee, J.; Gustafson, E. K.; Appelqvist, R.; Magginetti, P.; Norton, R.; Teng, N.; Charlton, D., Optical biosensor assay (OBA). *Clin. Chem.* **1991,** *37* (9), 1502-1505.

11. Charbonnier, M.; Romand, M.; Harry, E.; Alami, M., Surface plasma functionalization of polycarbonate: Application to electroless nickel and copper plating. *J. Appl. Electrochem.* **2001,** *31* (1), 57-63.

12. Williams, R.; Goodman, A. M., Wetting of Thin-Layers of SiO2 by Water. *Appl. Phys. Lett.* **1974,** *25* (10), 531-532.

13. Kumi, G.; Yanez, C. O.; Belfield, K. D.; Fourkas, J. T., High-speed multiphoton absorption polymerization: fabrication of microfluidic channels with arbitrary cross-sections and high aspect ratios. *Lab Chip 10* (8), 1057-1060.

14. Zaramella, S.; Yeheskiely, E.; Stromberg, R., A method for solid-phase synthesis of oligonucleotide 5 '-peptide-conjugates using acid-labile alpha-amino protections. *J. Am. Chem. Soc.* **2004,** *126* (43), 14029-14035.

15. Ellington, A.; Pollard, J. D., *Synthesis and Purification of Oligonucleotides*. John Wiley and Sons, Inc.: 2008.

16. McGall, G. H.; Barone, A. D.; Diggelmann, M.; Fodor, S. P. A.; Gentalen, E.; Ngo, N., The efficiency of light-directed synthesis of DNA arrays on glass substrates. *J. Am. Chem. Soc.* **1997,** *119* (22), 5081-5090.

Chapter 7: Investigations of Alkylphosphonate Coatings on Silicon Nitride

7.1 Introduction

Self-assembled monolayers (SAMs) are a subject of great scientific and technological interest due to their ability to modify surface properties such as wettability and adhesion.[1, 2] For example, SAMs have been employed to decrease adhesion within microfluidic channels.[3] The unintended adhesion of particles, within a channel can greatly hinder fluid flow.[3] Other areas where SAMs have also been used are in biology to immobilize biomolecules such as DNA and antibodies for use as a microarray and in lithography where SAMs can serve a photoresists to protect substrates subjected to acidic or basic rinses.[4-6]

We have examined alkylphosphonate coatings for their ability to reduce adhesion of quantum dots on silicon nitride surfaces. Phosphonate coatings were investigated because, unlike more typical coatings such as trichlorosilanes, they are not dependant on water to initiate cross-linking.[7] The presence of too much or not enough water in trichlorosilane systems can lead to polymerization in solution and incomplete monolayer formation, respectively.[8] By using a system that is not dependant on the amount of water present, more reproducible coatings could be created.[7] Phosphonate coatings have been studied previously on titanium, silicon, aluminum and zirconium oxide surfaces, as well as on planar mica.[7, 9-13]

Silicon nitride surfaces were selected for coating due to their ability, when applied to a silicon wafer, to easily create thin membranes.[14] Selectively etching away the silicon backing reveals a transparent silicon nitride film.[14-16] The created film can serve as a support for the fabrication of a photonic crystal that operates in the visible region of the spectrum due to its high refractive index ($n \approx 2.01$).[17-20] The membrane could also potentially be used in the optical trapping of particles in a microfluidic device. The trapping of quantum dots in a microfluidics device has already been demonstrated on glass surfaces.[21, 22]

To study these phosphonate surfaces, vibrational sum-frequency-generation (SFG) and X-ray photoelectron spectroscopy (XPS) were used. SFG is a non-linear, surface-sensitive optical technique that can provide information on the vibrational modes as well as the orientation of molecules at the interface of a material.[23] XPS is used to identify the presence of elements as well as their composition as the surface of a sample. XPS measures the number and kinetic energy of photoelectrons ejected from a material that has been irradiated with X-rays.[24]

Scanning electron microscopy (SEM) and atomic force microscopy (AFM) were used to image the sample surfaces to investigate alkylphosphonate multilayer formation. SEM scans the surface of a conductive sample with a beam of electrons. The secondary electrons that are generated by this scanning are collected and provide an image of sample surface. AFM uses a cantilever with a small probe at the end to examine a sample surface. When probe is brought close to the surface the deflection force is measured, providing images of the sample surface topography.

In the final section, an alternative coating, octadecyltrichlorosilane (OTS) was applied to the silicon nitride surfaces. OTS was chosen because it is identical to the alkylphosphonate with the exception of the headgroup being a silane rather than a phosphonate. Comparative SFG data for the OTS layer is presented.

7.2 Experimental Setup

7.2.1 Silicon nitride membranes

Low-stress, low-pressure chemical vapor deposition (LSLPCVD) of silicon nitride was performed on silicon wafers at the University of Maryland's FabLab. Silicon wafers were cleaned prior to deposition using a 3:1 sulfuric acid:hydrogen peroxide solution heated to 90-100 °C for 10 minutes. Wafers were then rinsed with distilled water and placed in a 6:1 ammonium hydroxide:hydrofluoric acid buffered oxide etch for 1 minute. Rinsing of wafers was performed in a spin rinse dryer under a nitrogen atmosphere.

For deposition, cleaned wafers were placed in a LPCVD furnace chamber (Tystar Tytan CVD furnace) and heated in a nitrogen atmosphere to 550 °C for 30 minutes. The temperature was then increased to 835 °C for deposition and 125 sccm of dichlorosilane and 25 sccm of ammonia were pumped into the chamber at a pressure of 250 mtorr. The standard growth rate for the silicon nitride films is 30 Å/min. After deposition, samples were cooled to 550 °C under a nitrogen atmosphere prior to being removed from the chamber. The silicon nitride layers grown were ~200 nm thick for the XPS measurements and AFM and SEM imaging. The SFG measurements were performed on a ~100 nm thick silicon nitride layer. Both wafers

contained a gradient of color, indicating there was inconsistent deposition of the silicon nitride layer. To avoid large inconsistencies, samples were cut from the same area on the wafer.

7.2.2 Phosphonate Coatings

In order to apply a layer of phosphonates to the silicon nitride layer, a solution of 40 μM octadecylphosphonic acid (ODPA) (Alfa Aesar) in dry tetrahydrafuran (THF) (Mallinckrodt Chemicals) was prepared. The THF was dried over sodium and kept in a nitrogen atmosphere until ready for use. The solution was stirred overnight for at least 10 hours.

Silicon wafers with a silicon nitride layer were prepared and coated with phosphonates following a procedure developed by Gouzman et. al.[25] Wafers were cut into 0.5 inch x 0.5 inch squares and sonicated in acetone (Production Grade, BDH) for 15 minutes followed by drying in a 95 °C oven for 30 minutes. After heating substrates were immersed in a 3:1 sulfuric acid (Technical Grade, Fisher):hydrogen peroxide (ACS Grade, Fisher) solution at 80 °C for 45 minutes. Substrates were rinsed in a series of distilled water rinses followed by immersion in a 50/50 hydrochloric acid (37% Aldrich)/hydrogen peroxide wash at 80 °C for 15 min. Samples were then rinsed in distilled water and dried under a stream dry nitrogen.

After drying, samples were immediately placed in a binder clip and held above a container with a rod (Figure 7.1).

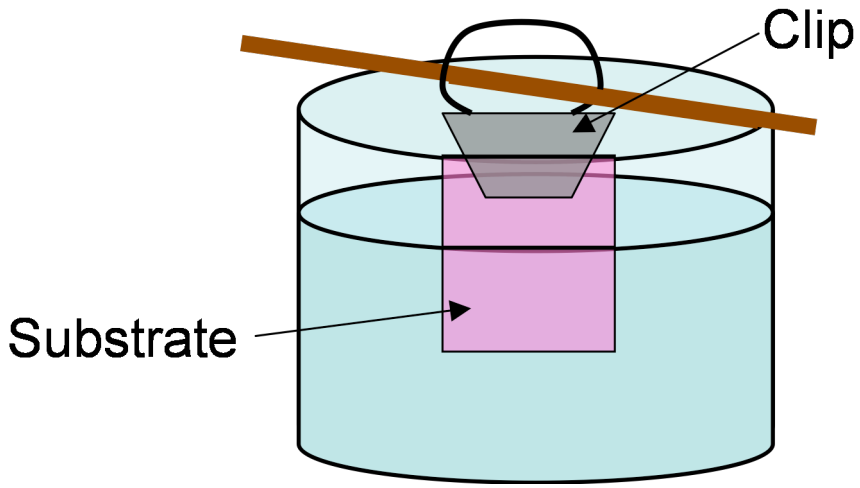

Figure 7.1 An illustration of the setup used to deposit ODPA onto silicon nitride coated wafers.

The prepared ODPA solution was added to the container until the exposed wafer was immersed. Over the course of 4 hours the solution evaporated, leaving a layer of phosphonates on the surface of the substrate. After evaporation substrates were removed and baked in a 140 °C oven for 40 hours.

After baking, substrates were sonicated in 3 THF rinses for 15 minutes each to remove any multilayers formed. The coating, baking and rinsing process was repeated twice more. After the final rinse, substrates were stored in a desiccator prior to use.

7.2.3 X-Ray Photoelectron Spectroscopy

Angle-resolved XPS data were collected on a Kratos Axis 165 X-ray photoelectron spectrometer operating in hybrid mode (using both electrostatic and magnetic lenses). The iris was set to 6 mm to reduce the angular acceptance of the

analyzer, thus increasing angular resolution. Samples were mounted onto the sample holder using electrically-conductive, double-sided copper tape. Charge neutralization was required to minimize surface charging. The charge neutralizer was set to 2 mA current, 2.5 V charge balance and 1 V filament bias. Survey spectra and high-resolution spectra were collected with pass energies of 160 eV and 20 eV, respectively. High-resolution spectra were collected for the Si 2p, N 1s, P 2p, P 2s, and C 1s at take-off-angles of 20^{o}, 40^{o} and 90^{o} relative to the sample surface. CASA XPS (Casa Software Ltd.) was used to calculate atomic percentage composition from peak areas after removal of a Shirley background using relative sensitivity factors from the Kratos Vision library.

Biased data were collected with the instrument running in electrostatic mode in an effort to prevent charge neutralization resulting from a combination of stray electrons in the chamber and the magnetic lens. The magnetic lens sits below the sample. Data were collected at 0 V bias (sample holder grounded), + 30 V and -30 V. Biases were applied using a variable DC power supply with the charge neutralizer turned off. Biased data were collected at a take-off angle of 40^{o} relative to the sample surface.

7.2.4 Sum-Frequency-Generation Spectroscopy

To determine if a well-ordered layer of phosphonate or silane was deposited onto a substrate, SFG spectroscopy was performed. A similar version of the SFG setup has been described previously in detail.[23] Briefly, a pulse shaped (FemtoJok, Biophotonic solutions) 130-fs, 800nm Ti:Sapphire laser (Coherent Legend Elite) is

divided, and 30 % is used to pump a optical parametric amplifier (TPOAS-C, Light Conversion) to generate tunable IR pulses while the other 30% is narrowed with an optical stretcher. The 800 nm and IR beams strike the surface of a sample at 64.5° and -54° from the surface normal respectively (Figure 7.2). The SFG signal is

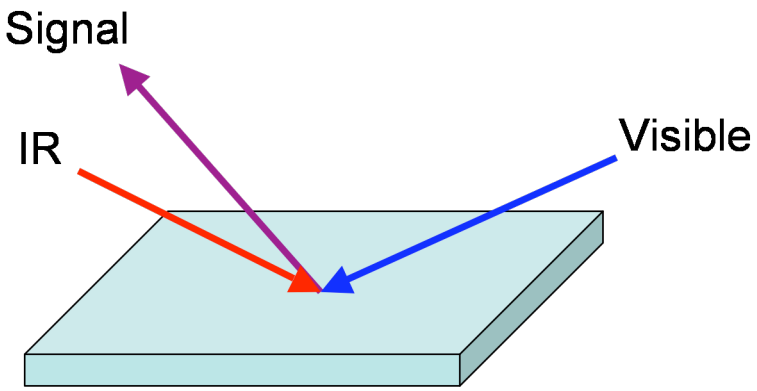

Figure 7.2 An illustration of the SFG sample geometry. Adapted from reference 23.[23]

detected by a spectrometer (Acton, SP2300i) and CCD array (Spec-10:100, Roper Science) at ~35° to the surface normal. The polarizations of the SFG signal, visible and IR beams can be varied to collect specific information about the molecular orientation at interfaces.[26] Polarizations used in these experiments were PPP and SSP.

SFG spectra was collected and processed as described in Ding et al.[27] Briefly, SFG data was collected for different IR wavelengths and averaged. Dividing the averaged SFG sample spectra by the average SFG spectra collected on gold provided a normalized spectra. Collecting additional spectra on gold where the IR beam passes

through a polystyrene film provides the frequency calibration with 4 or more IR absorption lines being used in the calibration.

7.2.5 Atomic Force Microscopy

Atomic force microscopy (AFM) images were taken on a Digital Instruments (Veeco) multimode AFM with a Nanoscope III controller and a 10 micron scanner. Cantilevers were gold-coated and had a < 10 nm tip radius. Substrates were mounted on a 15 mm specimen disc and AFM was performed in tapping mode. Images were captured with Nanoscope version 5.3 software and transferred to Gwyddion (Czech Metrology Institute) for image processing.

7.2.6 Silane Coating Procedure

Quartz (#1 coverslips, Electron Microscopy Sciences) and silicon nitride coated substrates were coated with octadecyltrichlorosilane following the procedure outlined by Liu et al.[28] Substrates were prepared for coating by soaking them in chloroform for 12 hours then rinsing in acetone, methyl alcohol (Reagent Grade, Pharmco-Aapar), and distilled water followed by drying under dry nitrogen. Substrates were submerged in a 3:1 mixture of sulfuric acid and hydrogen peroxide for 1 hour at ~110 °C. The substrates were rinsed with distilled water, dried with nitrogen and heated at 80 °C for ~30 minutes.

Substrates were then immersed in a 1 mM solution of octadecyltrichlorosilane (OTS) (95% Acros) in a 4:1 v/v solvent mixture of hexadecane (99% Acros) and carbon tetrachloride (99 +% Spectrophotometric Grade, Acros), for 1 hour.

Following coating, substrates were rinsed in the following order: chloroform, acetone, methyl alcohol, distilled water, methyl alcohol, acetone, and chloroform. Substrates were then sonicated in chloroform for 1 minute and rinsed again in acetone, methyl alcohol, and distilled water. A stream of nitrogen was used to dry the substrates prior to baking at 80 °C for 3 hours. Substrates were stored in a desiccator prior to use.

7.3 Results and Discussion

7.3.1 XPS Confirmation of Phosphonate Coating

XPS was used to determine if phosphonates were present on the substrate, and if sonication during washing had any noticeable effect on layer deposition. A survey scan of a sonicated sample (Figure 7.3A) vs. a non-sonicated (Figure 7.3B) sample confirms the presence of silicon, oxygen, nitrogen and carbon on both samples. The presence of phosphorus is also detected, but in very small quantities. The survey scan also shows a small amount of sodium contamination. The sodium contamination is not a concern, since it is a common contaminant due to its presence in tap water and is often found on glassware. In order to determine if sonication has an effect on phosphonate attachment, an angle-resolved study was performed to analyze the deposited phosphonate coating.

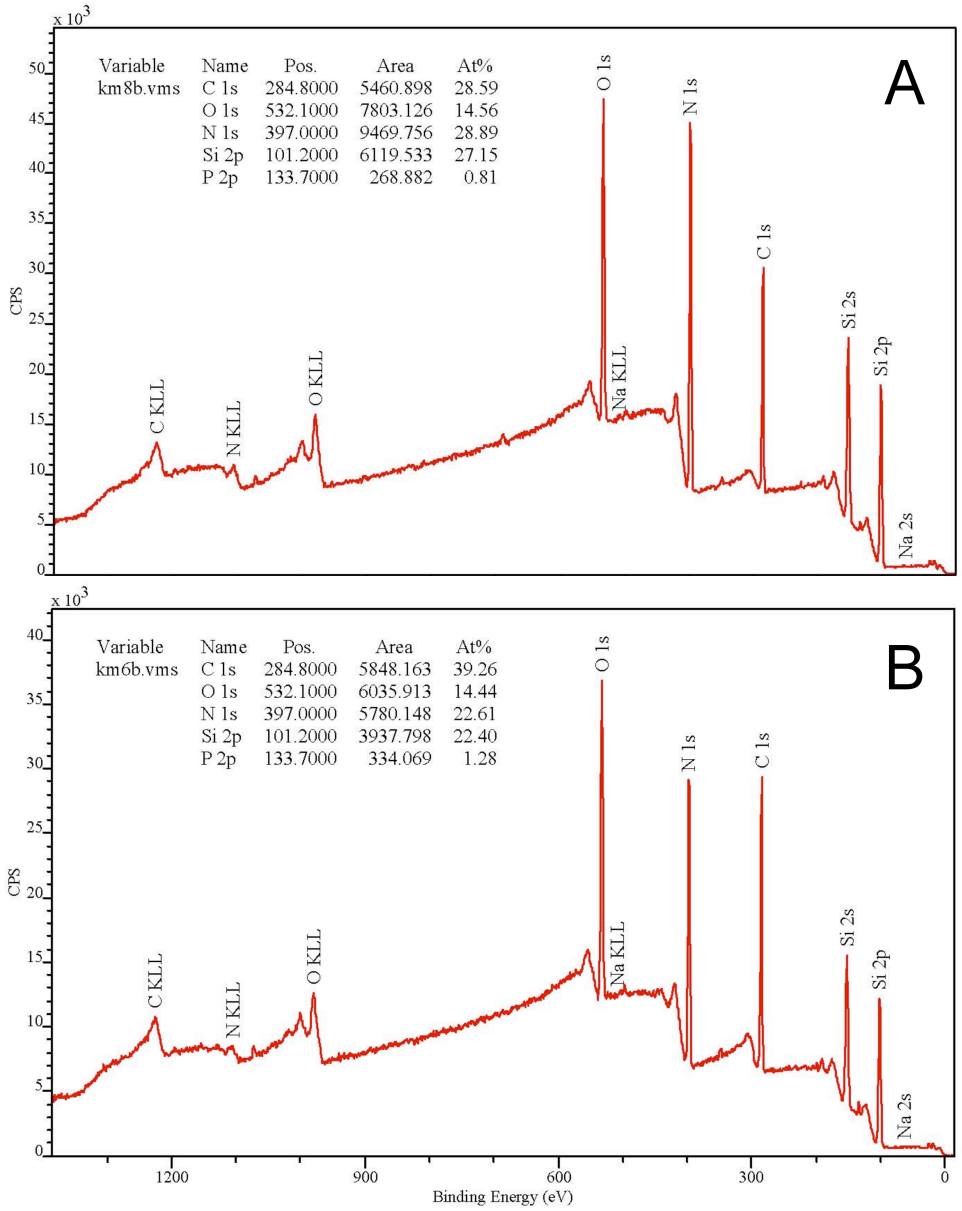

Figure 7.3 Survey scans of phosphonate-coated silicon nitride surfaces at a 90° take-off angle. A) Sample rinsed in THF with sonication. B) Sample rinsed in THF without sonication.

In an angle-resolved study, the take-off angle (the angle between the sample surface and the direction of the detected electrons) is adjusted. In these experiments, take-off angles of 20°, 40° and 90° were used to determine the amounts of carbon and phosphorus (via the 1s and 2p electrons respectively) present in the monolayer and

silicon and nitrogen (via the 2p and 1s electrons respectively) present in the silicon nitride layer (Table 7.1, Figure 7.4 And 7.5). Results show that amount of carbon

	Take-off ∠	Si 2p At%	N 1s At%	C 1s At%	P 2p At%	C/P
Not Sonicated	90°	22.4	22.6	39.3	1.3	30.2
	40°	17.5	14.9	49.4	1.3	38.0
	20°	12.17	6.4	65.6	1.3	50.5
Sonicated	90°	27.2	28.9	28.6	0.8	35.8
	40°	21.7	17.2	44.6	1.1	40.5
	20°	14.6	8.5	60.9	1.2	50.8

Table 7.1 Atomic percentages of the elements present in the silicon nitride layer, (silicon and nitrogen) as well as the coating, (phosphorus and carbon). Measurements were collected at take-off angles of 90°, 40° and 20°. The sum of atomic percentages is not equal to 100% due to the presence of other elements, such as oxygen.

and phosphorus present is less in the sonicated sample. This suggests that the layer of phosphonates on the surface is better attached on the sonicated sample as opposed to the not sonicated sample since sonication should remove any multilayers present.

As the take-off angle decreases, the detection becomes more surface sensitive. This trend is consistent with increasing amounts of carbon seen with both the sonicated and non-sonicated samples. At a 20° angle, the high concentration of carbon corresponds to the long carbon chain. The amount of phosphorus detected in the sample is near the noise limit for the XPS instrument and is therefore relatively consistent at all angles.

Comparing the atomic percentages of silicon and nitrogen there is a clear decrease with decreasing take-off angle, which is also consistent with the fact the silicon nitride layer lies below a phosphonate layer. Comparing the sonicated to non-sonicated samples, at 20° there is relatively less carbon and more nitrogen and silicon present in the sonicated samples, indicating that sonication leads to thinner phosphonate coatings. This picture is consistent at all take-off angles. These results confirm that a phosphonate coating can be added to sonicated silicon nitride substrates. The presence of a thinner layer on the sonicated samples suggests that sonication does remove any phosphonate molecules that are not attached directly to the substrate.

During the angle-resolved study it was also observed that the silicon detected comes from three sources on the sample: elemental silicon from the silicon wafer, silicon nitride from the deposited layer and silicon oxide that is formed on top of the silicon nitride layer during acid cleaning (Table 7.2, Figure 7.4). The elemental

	Take-off ∠	Silicon Nitride At %	Elemental Silicon At %	Silicon Oxide At %
Not Sonicated	90°	84.67	3.41	11.92
	20°	56.43	1.72	1.85
Sonicated	90°	82.68	7.00	10.32
	20°	65.88	1.64	3.48

Table 7.2 Atomic percentages of the silicon sources present on the sample. Measurements were collected at take-off angles of 90°, 40° and 20°.

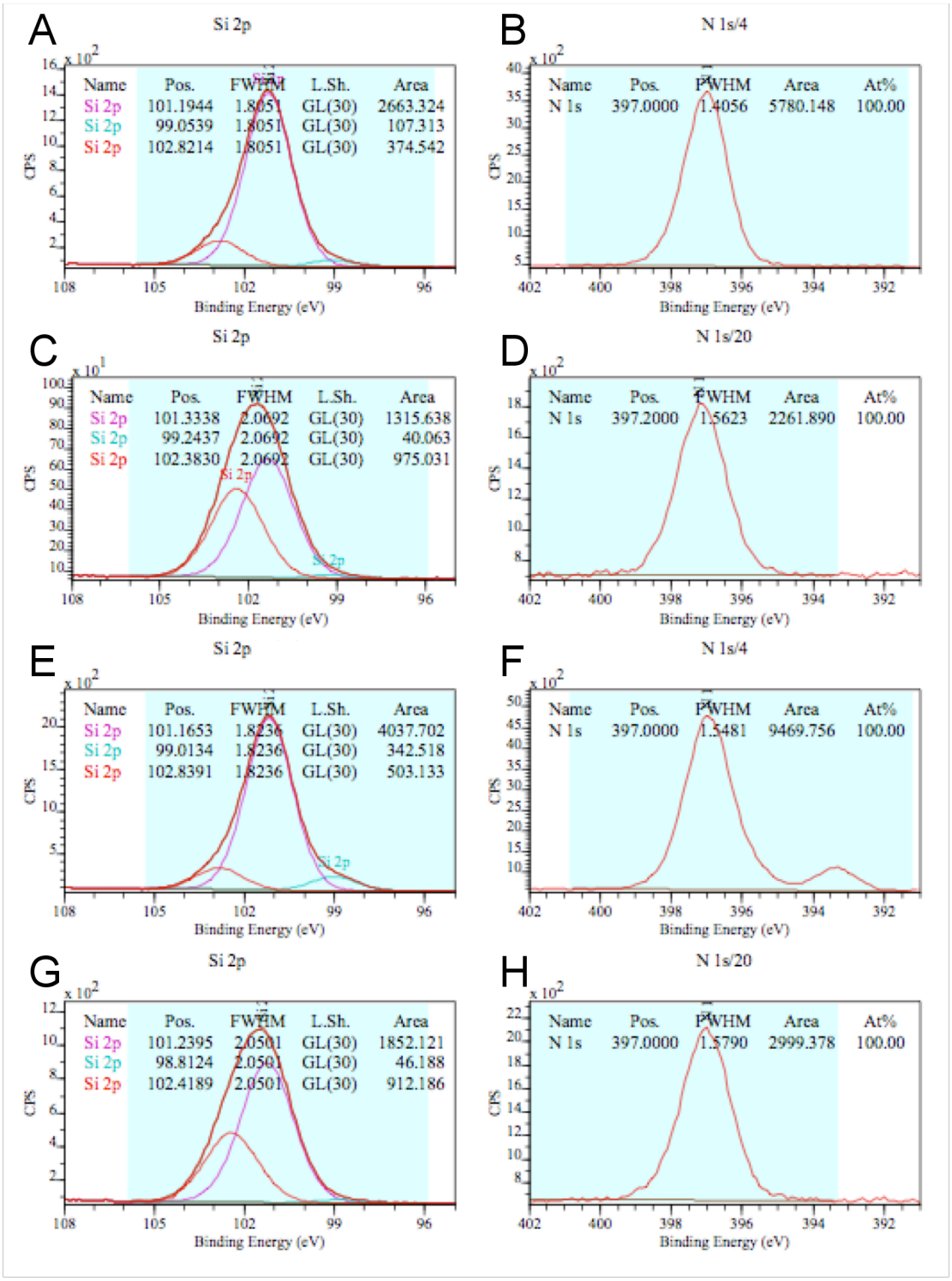

Figure 7.4 Angle-resolved studies of the Si 2p and N 1s peaks. **A)** Unsonicated Si 2p 90° **B)** Unsonicated N 1s 90° **C)** Unsonicated Si 2p 20° **D)** Unsonicated N 1s 20° **E)** Sonicated Si 2p 90° **F)** Sonicated N 1s 90 ° **G)** Sonicated Si 2p 20° **H)** Sonicated N 1s 20°. Silicon peak fitting was done with three separate curves of equal FWHM.

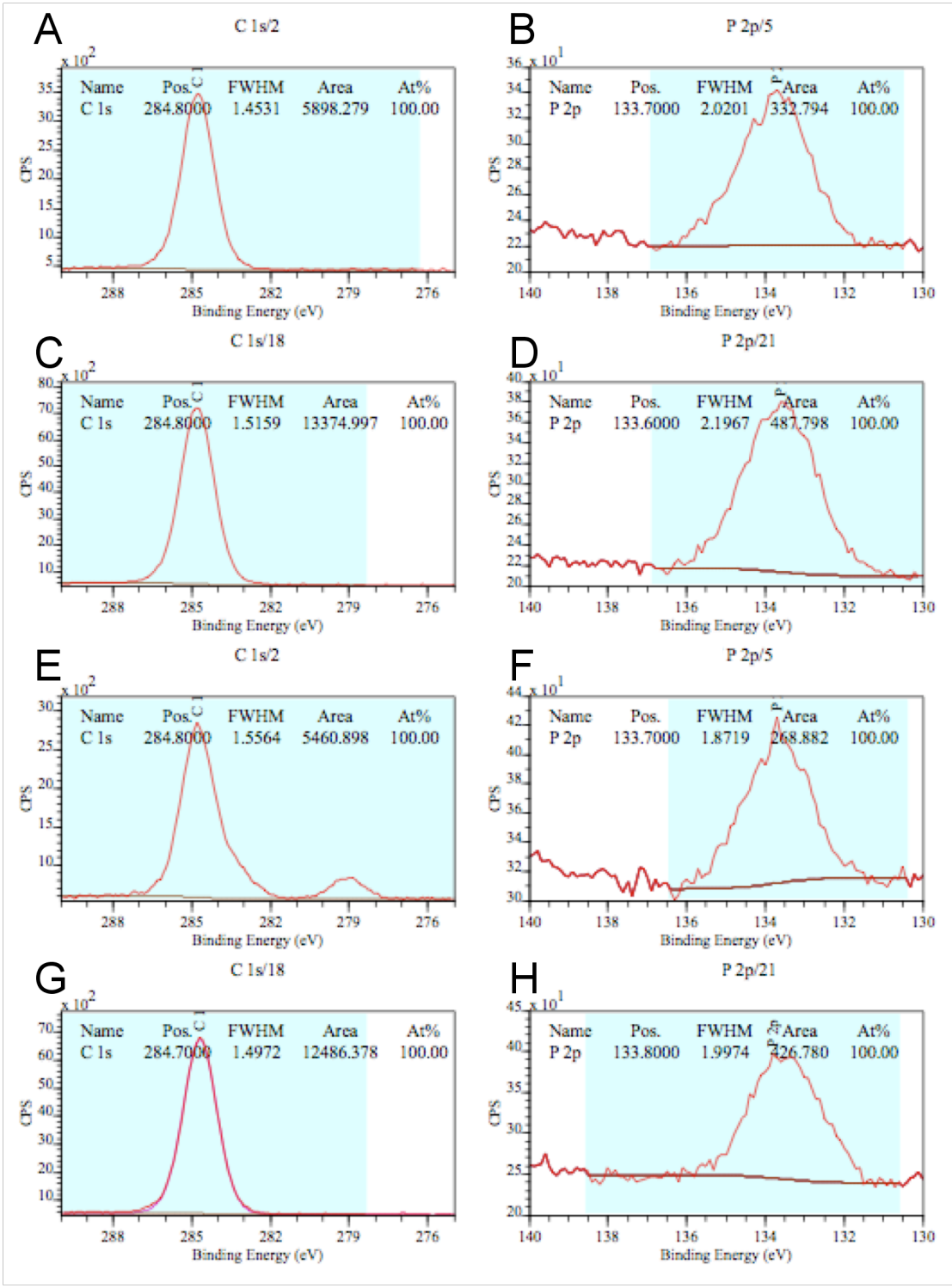

Figure 7.5 Angle resolved XPS studies on C 1s and P 2p **A)** Unsonicated C 1s 90° **B)** Unsonicated P 2p 90° **C)** Unsonicated C 1s 20° **D)** Unsonicated P 2p 20° **E)** Sonicated C 1s 90° **F)** Sonicated P 2p 90° **G)** Sonicated C 1s 20° **H)** Sonicated P 2p 20°

silicon makes up the least amount of the total silicon present in the sample, while the silicon nitride makes up the most. The trends seen for the individual sources of silicon are consistent with the silicon trend discussed above: as the take-off angle decreases the amount of silicon detected does as well. These findings indicate that the phosphonate layer is attaching to the oxidized silicon layer rather than directly to the silicon nitride.

7.3.2 Sum-Frequency-Generation Spectroscopy

To further characterize the phosphonate coatings on silicon nitride surfaces, SFG spectra were obtained to test for the presence of a monolayer. Based on the literature, the dominant SFG peak using PPP polarization should be present at 2965 cm^{-1}, corresponding to in-plane components of the antisymmetric methyl stretch.[29, 30] As shown in Figure 7.6, there is no indication of a distinct peak in the PPP spectra. Although XPS data confirms that a phosphonate layer is present, a well-ordered monolayer cannot be confirmed.

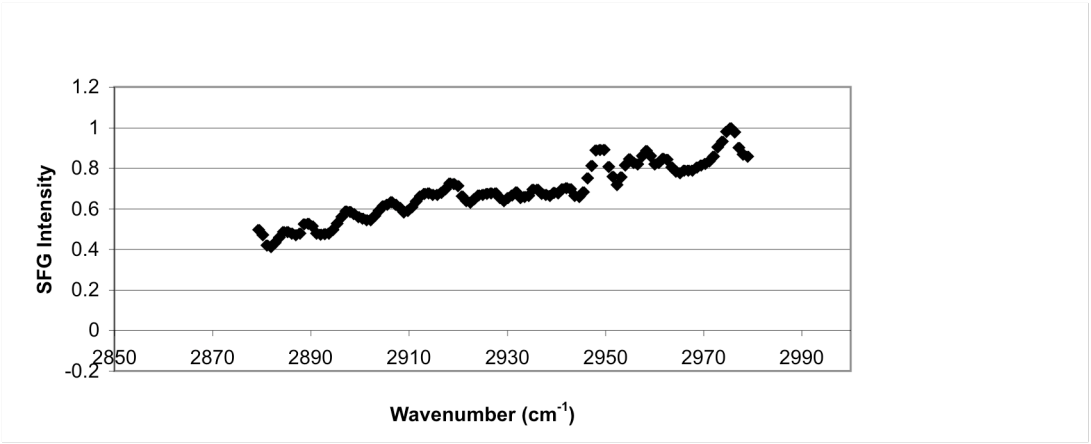

Figure 7.6 SFG spectra of a phosphonate coating on a silicon nitride coated silicon wafer collected with a PPP polarization.

The SSP spectra were also collected (Figure 7.7). The characteristic peaks at 2880 cm $^{-1}$ and 2940 cm^{-1} corresponding to the symmetric methyl stretch and the Fermi resonance of the same mode respectively are not present.[29] This result again conforms that the phosphonate layer is not well ordered on the silicon nitride surface.

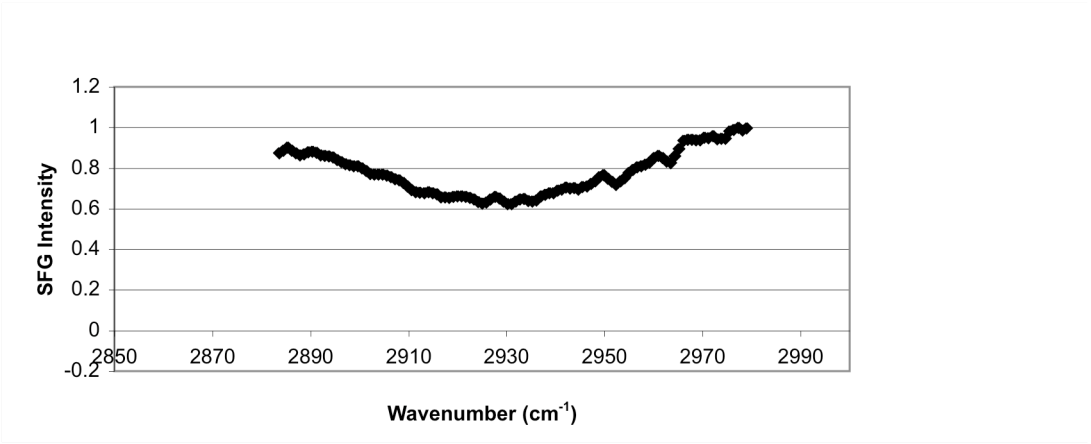

Figure 7.7 SFG spectra of a phosphonate coating on a silicon nitride coated silicon wafer collected in SSP polarization.

7.3.3 SEM and AFM studies of Phosphonate Coatings

The presence of a textured region in the middle of some of the phosphonate coated silicon nitrite samples was observed visually (Figure 7.8). This textured region was about 3.5 mm thick and was not noticeable on all samples. On either side of this textured region is a smooth region and a striated region. Figure 7.9 is a comparison of the textured verses smooth regions.

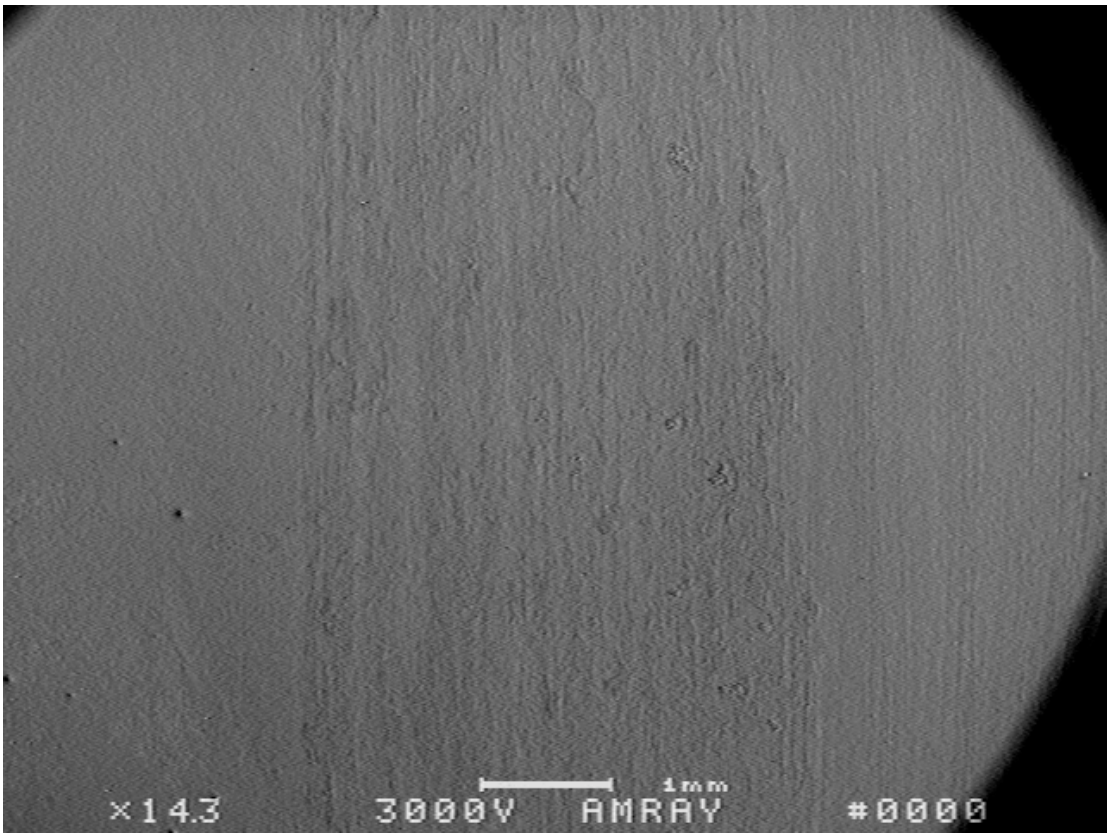

Figure 7.8 A SEM image of, from left to right, the smooth, textured, and striated regions of a phosphonate coated silicon nitride wafer.

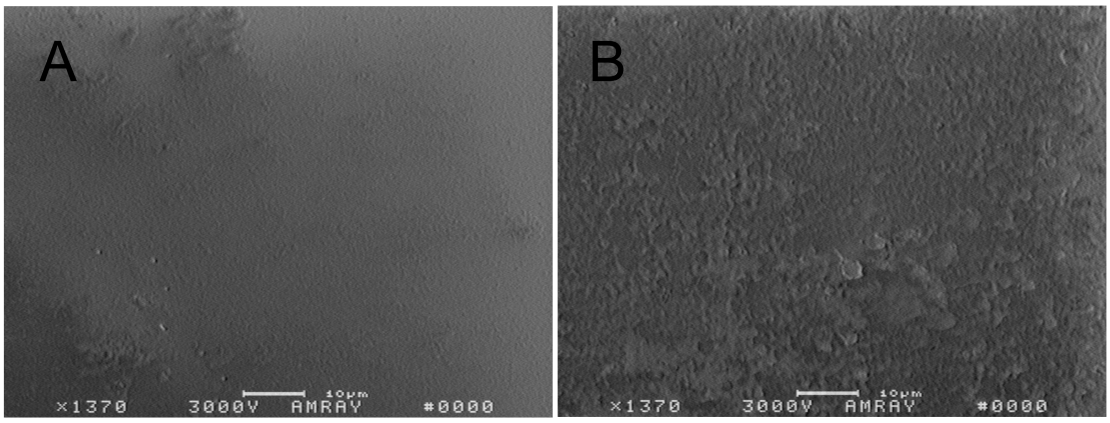

Figure 7.9 SEM images of a phosphonate coated silicon nitride wafer. **A)** Smooth region. **B)** Textured region.

To further investigate this surface, AFM measurements were made on the textured region and on an uncoated silicon nitride wafer (Figure 7.10). AFM results confirmed that the textured region was much more uneven, with peaks of 0.10 µm being detected. The uncoated samples have a much smaller and more evenly distributed peak heights none taller than 15 nm being detected.

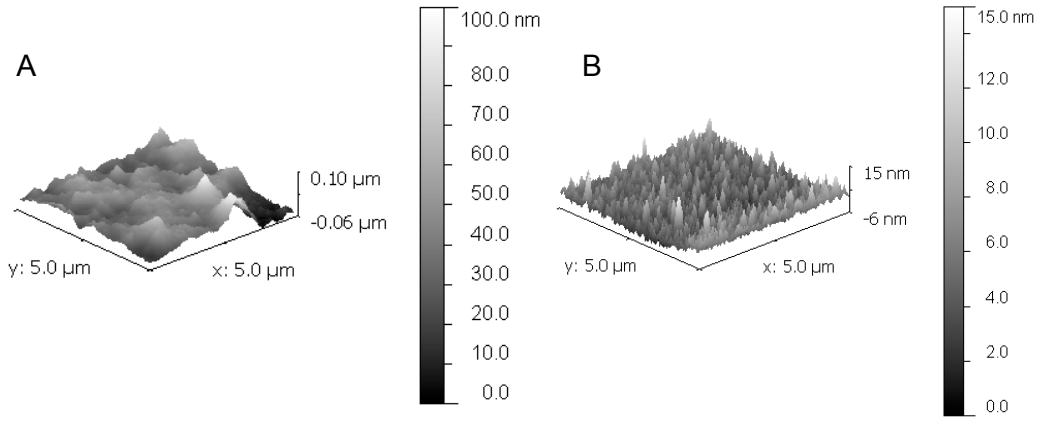

Figure 7.10 AFM images obtained on LSLPCVD silicon nitride. **A)** Textured region observed on a phosphonate coated silicon nitride layer. **B)** An uncoated silicon nitride layer.

The presence of these textured regions on coated samples is likely occurring during evaporation of phosphonates onto the surface of the silicon nitride. It is possible that the prepared solution of ODPA was not well dissolved, allowing large particulates to adhere to the surface of the silicon nitride. This textured region is not uniform across a sample, and is believed to deposit after the striated region that was seen in Figure 7.8. The appearance of the striated region prior to the textured region could be due to the surface tension of THF as it evaporates. If the THF clings to the substrate, as it evaporates, it could leave striations of undissolved ODPA crystals. As the THF evaporates, the concentration of undissolved crystals increases and could potentially deposit a thicker layer (textured region). The smooth region could be the portion of the substrate that was still submerged in ODPA solution at the end of coating. Despite sonication, this textured region was still present after the final rinsing.

7.3.4 Determination of Mono vs. Multi Layers using XPS

To determine if a multilayer or a monolayer is present on the silicon nitride substrates, a bias of +30 V and -30 V was applied to the sample.[25, 30] In theory, when a bias is applied to a conductive substrate the XPS signal observed will shift in the direction of and by the amount of the applied bias.[25, 30] The signal observed from a monolayer chemically bound to the substrate will also shift in response to the applied bias.[25, 30] The XPS shift observed for a biased multilayer that is not covalently bound to the substrate will exhibit only a weak shift in the direction of the applied bias.[25, 30]

Since the substrates used in these experiment consisted of a conductive silicon wafer with a layer of insulating silicon nitride on top and a phosphonate coating, when a bias was applied the shift observed in the XPS spectrum should be less than the applied bias. In the grounded sample (0 V) the C 1s peak is present at 287.9 eV with a FWHM of 2.1072, and when a bias of +30 V is applied the peak shifts by +27.6 eV to 317.3 eV and the FWHM narrows slightly to 2.0752 (Figure 7.11). This narrowing could be due to the attraction of stray electrons from the vacuum that neutralize any additional differential charging. When a bias of – 30 V was applied, the peak shifted – 28.2 eV to 261.5 eV and broadened with a FWHM of 3.0647.

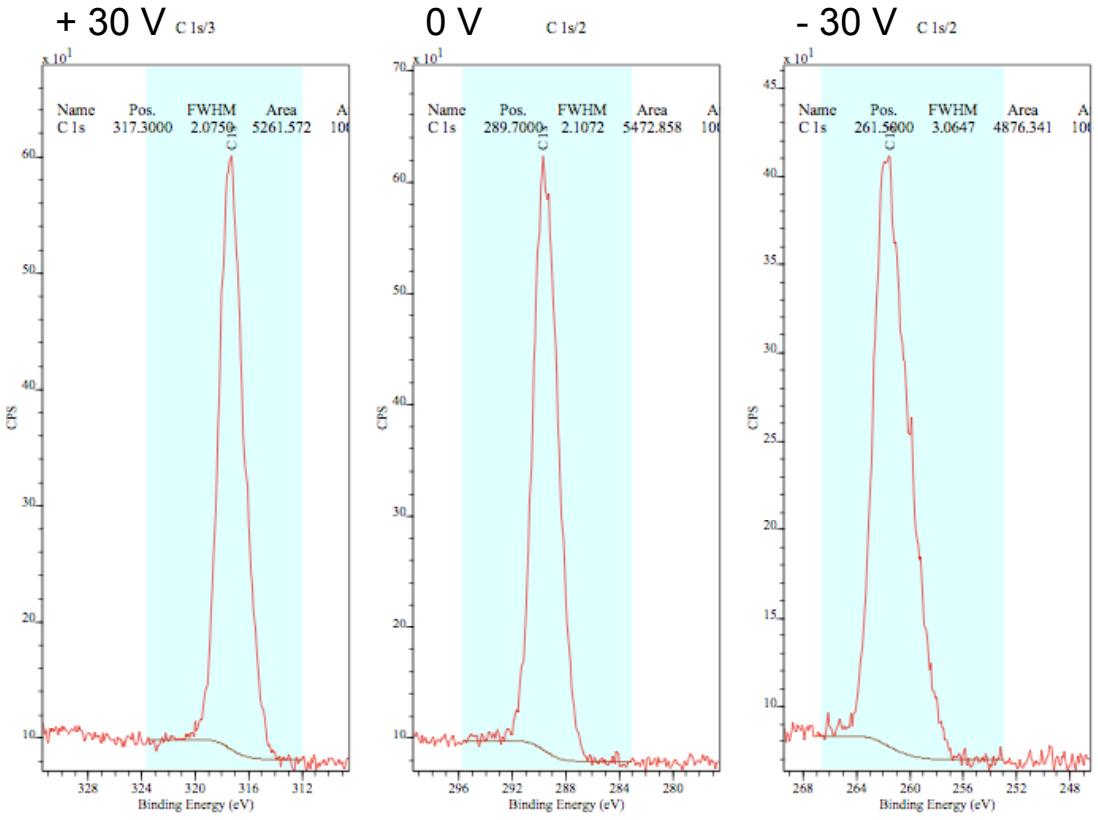

Figure 7.11 XPS bias measurements taken on the C1s of a phosphonate coated silicon nitride layer

The observed peak broadening suggests the presence of a multilayer phosphonate coating on the substrate despite sonication. While the multilayer forms during evaporation, its removal during sonication was expected. However, these findings suggest that perhaps sonication does not remove all of the multilayers that maybe present on a surface.

To further confirm the presence of a multilayer, the film thickness was estimated using the "thickogram" method, which has been used previously to calculate monolayer thicknesses.[31-33] Using this method a thickness of 1.5 monolayers was calculated for this sample. This result is in agreement with the above XPS, AFM and SEM data, and is also consistent with the absence of a detectable SFG signal.

7.3.5 Silanes

To test if a well-ordered silane molecular layer could be applied to a silicon nitride coated substrate, the substrate was functionalized with OTS and SFG spectra were acquired. Using PPP polarization mode a peak at 2971 cm^{-1} is observed and can be contributed to the in-plane, antisymmetric methyl stretching of the monolayer (Figure 7.12).[29] As a control, OTS functionalized quartz substrates were also

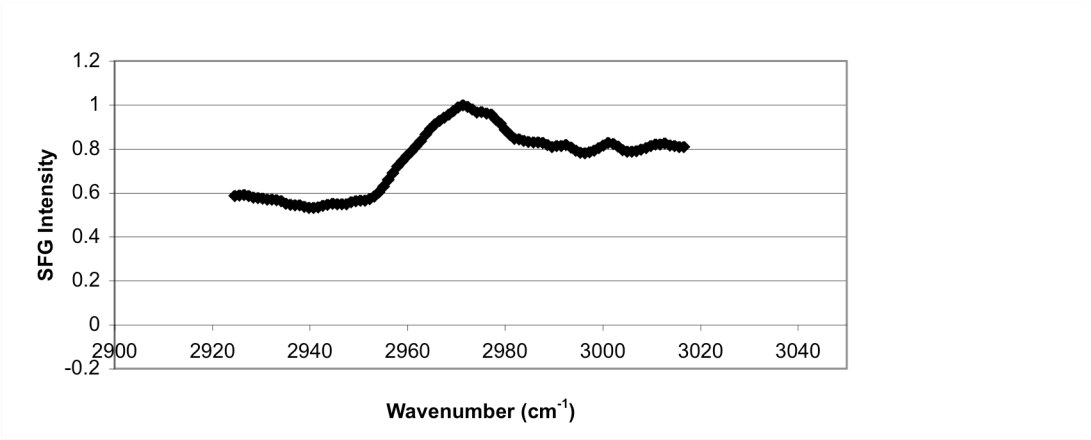

Figure 7.12 SFG spectra of an OTS coating on a silicon nitride wafer collected in PPP polarization.

measured and a peak at 2953 cm^{-1} can also be attributed to the antisymmetric methyl stretch (Figure 7.13).[29] These peaks could be shifted due to the differences in the two substrates and in how the silanes organize at the substrate.

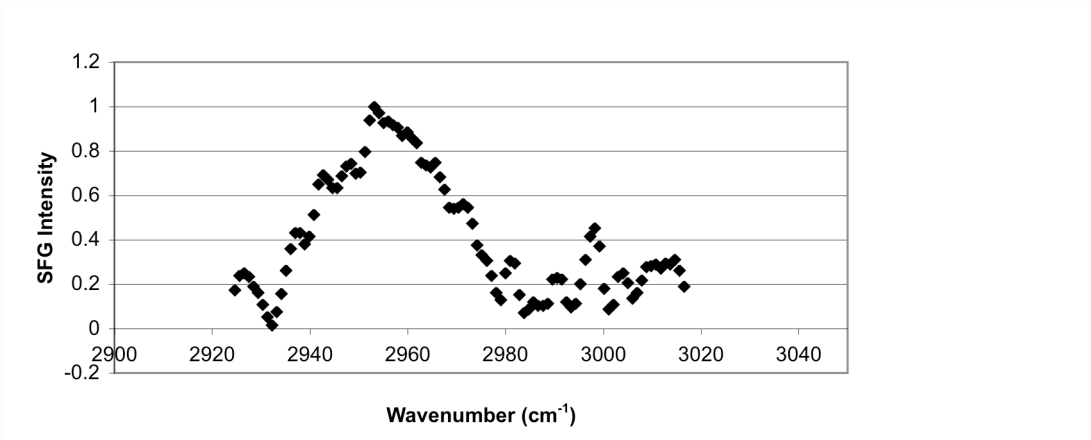

Figure 7.13 SFG spectra of an OTS coating on quartz glass collected in PPP polarization.

Spectra using SSP polarization were also taken on the silicon nitride and quartz substrates. The quartz spectra shows peaks at 2941 cm $^{-1}$ and ~ 2874 cm^{-1} that can be assigned to the Fermi resonance and the methyl symmetric stretch, respectively (Figure 7.14).[29, 34] The silicon nitride sample shows a slight shoulder at 2936 cm$^{-1,}$ which could correspond to the Fermi resonance between the methyl symmetric stretch or a C-H bending overtone (Figure 7.15).[29, 34]

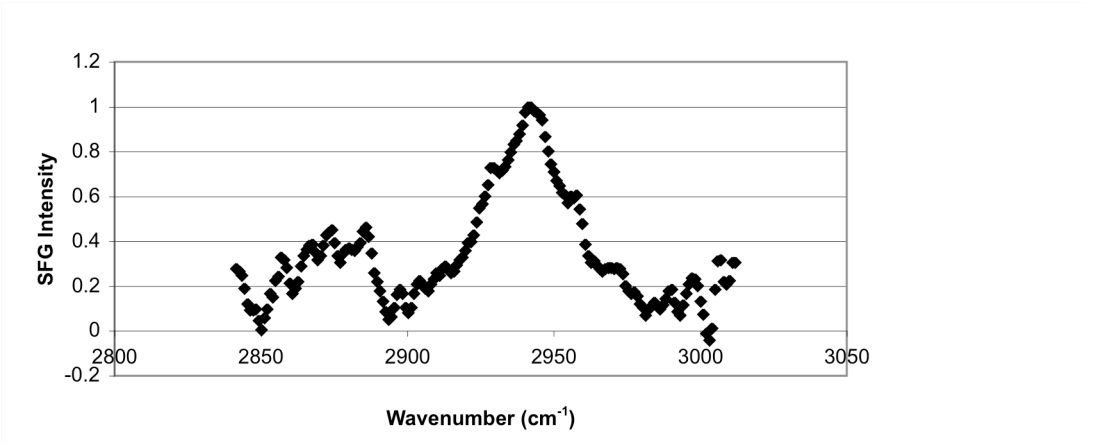

Figure 7.14 SFG spectra of a OTS coating on quartz glass collected in SSP polarization.

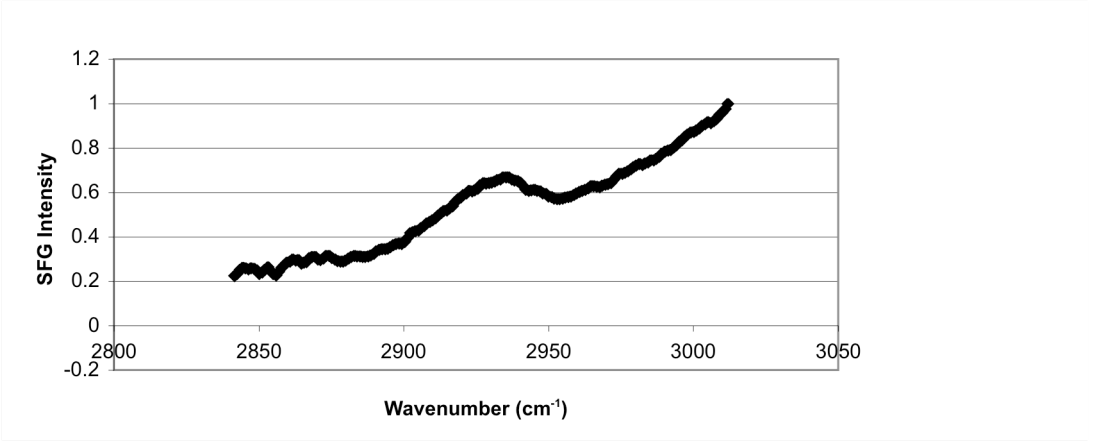

Figure 7.15 SFG spectra of a OTS coating on a silicon nitride wafer collected in SSP polarization.

The presence of sharper peaks in the spectra of OTS-modified silicon nitride coated substrates versus phosphonate substrates shows promise for the creation of a well-ordered molecular layer. Refinement of the deposition method for phosphonates is needed. Also, the sharper peaks observed from the OTS quartz vs. silicon nitride suggest that the substrate itself is causing the formation of a disordered monolayer, which is not surprising because the phosphonate layers were also not shown to be well organized. Future studies should focus on how silicon nitrite deposition affects molecular layer deposition as well as adsorption techniques.

7.4 Conclusions

The presence of phosphorus on the surface of silicon nitride coated substrates was confirmed using XPS. Unfortunately, the lack of distinct peaks in the SFG spectra and the presence of a textured region as observed by SEM and AFM suggests the absence of a well-organized monolayer. The presence of multilayers was confirmed using XPS measurements by applying a bias, which supports the inability to detect SFG peaks.

Coating OTS on silicon nitride surfaces may create a more organized layer than ODPA, as evidenced by much sharper features observed in the SFG spectra at both ppp and ssp polarizations. However, when compared to the signal detected OTS coated quartz, OTS on silicon nitride surfaces display slightly less sharp features, suggesting that the substrate itself leads to disordered molecular layers. Although all silicon nitride coated substrates discussed in this chapter utilize LSLPCVD silicon nitride, further investigations using other deposition methods for silicon nitride might

lead to improved SFG spectra. Results from these studies would also be applicable to ODPA deposition.

References

1. Schreiber, F., Structure and growth of self-assembling monolayers. *Prog. Surf. Sci.* **2000,** *65* (5-8), 151-256.

2. Love, J. C.; Estroff, L. A.; Kriebel, J. K.; Nuzzo, R. G.; Whitesides, G. M., Self-assembled monolayers of thiolates on metals as a form of nanotechnology. *Chem. Rev.* **2005,** *105* (4), 1103-1169.

3. Cox, J. D.; Curry, M. S.; Skirboll, S. K.; Gourley, P. L.; Sasaki, D. Y., Surface passivation of a microfluidic device to glial cell adhesion: a comparison of hydrophobic and hydrophilic SAM coatings. *Biomaterials* **2002,** *23* (3), 929-935.

4. Bruckbauer, A.; Zhou, D. J.; Kang, D. J.; Korchev, Y. E.; Abell, C.; Klenerman, D., An addressable antibody nanoarray produced on a nanostructured surface. *J. Am. Chem. Soc.* **2004,** *126* (21), 6508-6509.

5. Riepl, M.; Enander, K.; Liedberg, B.; Schaferling, M.; Kruschina, M.; Ortigao, F., Functionalized surfaces of mixed alkanethiols on gold as a platform for oligonucleotide microarrays. *Langmuir* **2002,** *18* (18), 7016-7023.

6. Xia, Y. N.; Zhao, X. M.; Whitesides, G. M., Pattern transfer: Self-assembled monolayers as ultrathin resists. *Microelectron. Eng.* **1996,** *32* (1-4), 255-268.

7. Hanson, E. L.; Schwartz, J.; Nickel, B.; Koch, N.; Danisman, M. F., Bonding self-assembled, compact organophosphonate monolayers to the native oxide surface of silicon. *J. Am. Chem. Soc.* **2003,** *125* (51), 16074-16080.

8. Ulman, A., Formation and structure of self-assembled monolayers. *Chem. Rev.* **1996,** *96* (4), 1533-1554.

9. Gawalt, E. S.; Lu, G.; Bernasek, S. L.; Schwartz, J., Enhanced bonding of alkanephosphonic acids to oxidized titanium using surface-bound alkoxyzirconium complex interfaces. *Langmuir* **1999,** *15* (26), 8929-8933.

10. Gawalt, E. S.; Avaltroni, M. J.; Koch, N.; Schwartz, J., Self-assembly and bonding of alkanephosphonic acids on the native oxide surface of titanium. *Langmuir* **2001,** *17* (19), 5736-5738.

11. Hauffman, T.; Blajiev, O.; Snauwaert, J.; van Haesendonck, C.; Hubin, A.; Terryn, H., Study of the Self-Assembling of n-Octylphosphonic Acid Layers on Aluminum Oxide. *Langmuir* **2008,** *24* (23), 13450-13456.

12. Gao, W.; Reven, L., SOLID-STATE NMR-STUDIES OF SELF-ASSEMBLED MONOLAYERS. *Langmuir* **1995,** *11* (6), 1860-1863.

13. Woodward, J. T.; Ulman, A.; Schwartz, D. K., Self-assembled monolayer growth of octadecylphosphonic acid on mica. *Langmuir* **1996,** *12* (15), 3626-3629.

14. Morkved, T. L.; Lopes, W. A.; Hahm, J.; Sibener, S. J.; Jaeger, H. M., Silicon nitride membrane substrates for the investigation of local structure in polymer thin films. *Polymer* **1998,** *39* (16), 3871-3875.

15. Green, E. D.; Kino, G. S., Atmospheric scanning electron-microscopy using silicon-nitride thin-film windows *J. Vac. Sci. Technol. B* **1991,** *9* (3), 1557-1558.

16. Petersen, K. E., Silicon as a mechanical material *Proc. IEEE* **1982,** *70* (5), 420-457.

17. Stutius, W.; Streifer, W., Silicon-nitride films on silicon for optical-waveguides. *Appl. Optics* **1977,** *16* (12), 3218-3222.

18. Barth, M.; Kouba, J.; Stingl, J.; Lochel, B.; Bensona, O., Modification of visible spontaneous emission with silicon nitride photonic crystal nanocavities. *Opt. Express* **2007,** *15* (25), 17231-17240.

19. Makarova, M.; Vuckovic, J.; Sanda, H.; Nishi, Y., Silicon-based photonic crystal nanocavity light emitters. *Appl. Phys. Lett.* **2006,** *89* (22), 3.

20. McCutcheon, M. W.; Loncar, M., Design of a silicon nitride photonic crystal nanocavity with a Quality factor of one million for coupling to a diamond nanocrystal. *Opt. Express* **2008,** *16* (23), 19136-19145.

21. Ropp, C.; Cummins, Z.; Probst, R.; Qin, S. J.; Fourkas, J. T.; Shapiro, B.; Waks, E., Positioning and Immobilization of Individual Quantum Dots with Nanoscale Precision. *Nano Lett.* **2010,** *10* (11), 4673-4679.

22. Ropp, C.; Probst, R.; Cummins, Z.; Kumar, R.; Berglund, A. J.; Raghavan, S. R.; Waks, E.; Shapiro, B., Manipulating Quantum Dots to Nanometer Precision by Control of Flow. *Nano Lett.* **2010,** *10* (7), 2525-2530.

23. Ding, F.; Zhong, Q.; Brindza, M. R.; Fourkas, J. T.; Walker, R. A., Ti:sapphire, broadband vibrational sum-frequency generation spectrometer with a counter-propagating geometry. *Opt. Express* **2009,** *17* (17), 14665-14675.

24. Briggs, D.; Seah, M. P., *Practical surface analysis: by auger and x-ray photoelectron spectroscopy*. Wiley: New York, 1983.

25. Gouzman, I.; Dubey, M.; Carolus, M. D.; Schwartz, J.; Bernasek, S. L., Monolayer vs. multilayer self-assembled alkylphosphonate films: X-ray photoelectron spectroscopy studies. *Surf. Sci.* **2006,** *600* (4), 773-781.

26. Lu, R.; Gan, W.; Wu, B. H.; Chen, H.; Wang, H. F., Vibrational polarization spectroscopy of CH stretching modes of the methylene goup at the vapor/liquid interfaces with sum frequency generation. *J. Phys. Chem. B* **2004,** *108* (22), 7297-7306.

27. Ding, F.; Hu, Z. H.; Zhong, Q.; Manfred, K.; Gattass, R. R.; Brindza, M. R.; Fourkas, J. T.; Walker, R. A.; Weeks, J. D., Interfacial Organization of Acetonitrile: Simulation and Experiment. *J. Phys. Chem. C* **2010,** *114* (41), 17651-17659.

28. Liu, Y.; Wolf, L. K.; Messmer, M. C., A study of alkyl chain conformational changes in self-assembled n-octadecyltrichlorosilane monolayers on fused silica surfaces. *Langmuir* **2001,** *17* (14), 4329-4335.

29. Keszthelyi, T.; Paszti, Z.; Rigo, T.; Hakkel, O.; Telegdi, J.; Guczi, L., Investigation of solid surfaces modified by Langmuir-Blodgett monolayers using sum-frequency vibrational spectroscopy and X-ray photoelectron spectroscopy. *J. Phys. Chem. B* **2006,** *110* (17), 8701-8714.

30. Dubey, M.; Weidner, T.; Gamble, L. J.; Castner, D. G., Structure and Order of Phosphonic Acid-Based Self-Assembled Monolayers on Si(100). *Langmuir* **2010,** *26* (18), 14747-14754.

31. Cumpson, P. J., The Thickogram: a method for easy film thickness measurement in XPS. *Surf. Interface Anal.* **2000,** *29* (6), 403-406.

32. Cumpson, P. J.; Seah, M. P., Elastic scattering corrections in AES and XPS .2. Estimating attenuation lengths and conditions required for their valid use in overlayer/substrate experiments. *Surf. Interface Anal.* **1997,** *25* (6), 430-446.

33. Merzlikin, S. V.; Tolkachev, N. N.; Strunskus, T.; Witte, G.; Glogowski, T.; Woll, C.; Grunert, W., Resolving the depth coordinate in photoelectron spectroscopy - Comparison of excitation energy variation vs. angular-re solved XPS for the analysis of a self-assembled monolayer model system. *Surf. Sci.* **2008,** *602* (3), 755-767.

34. Ye, S.; Nihonyanagi, S.; Uosaki, K., Sum frequency generation (SFG) study of the pH-dependent water structure on a fused quartz surface modified by an octadecyltrichlorosilane (OTS) monolayer. *Phys. Chem. Chem. Phys.* **2001,** *3* (16), 3463-3469.

Chapter 8: Conclusions and Future Work

8.1 Introduction

This dissertation makes contributions to the field of coatings by investigating patterns created in and on acrylate photoresists as well as exploring self-assembled monolayers (SAMs) of alkylphosphonates and chlorosilanes on silicon nitride surfaces. Photoresists have many applications that include integrated circuits and MEMS devices.[1, 2] Investigating new ways that photoresists can be used can provide alternative approaches to device production. One of these uses for photoresists was discussed in Chapter 5, in which a solid photoresist was tested as a way to transfer patterns created using multiphoton absorption polymerization (MAP).

Another kind of coating this dissertation discussed is SAMs. SAMs are of interest because they can alter the properties of a substrate, such as in attaching amine groups to introduce biocompatibility.[3] In Chapter 6, chlorosilane monolayers were investigated as a way to pattern a surface as preparation for use as a DNA microarray. The experiments discussed in this dissertation contribute to understanding of the processes that occur within a cured photoresist during ablation and investigate potential applications of SAMs in the creation of a DNA microarray. Below is a summary of each chapter and some potential directions for future exploration.

8.2 Chapter Summaries and Future Work

8.2.1 Chapter 2: Laser Ablation of Acrylate Polymers

Chapter 2 provided general observations of laser ablation on acrylate polymers. It described line resolutions with various microscope objectives (the smallest being 600 microns created with the 40× oil immersion objective) and a molding test to observe the texture of the ablated lines. A study on the optimal ablation conditions showed that above 200 mW and at velocities below 100 μm/s laser ablation should be observed. An area of future work is to test more power and velocity combinations to provide a better idea of where the ablation threshold lies. Additionally, a power vs. velocity study using different microscope objectives would further the understanding of the effect that the microscope objective has on ablation parameters.

The underlying mechanism of laser ablation was also explored indirectly in Chapter 2, with observations of a decrease in the power needed to observe ablation when near an already ablated area. A more direct approach was taken to determine if photothermal or photochemical processes dominate in the mechanism for laser ablation in acrylate polymers. It was determined that the ablation depends on the blend of acrylate polymer used. Exposure studies with different powers and objectives would provide further insight into the ablation mechanism.

8.2.2 Chapter 3: Laser Ablation's Role in the Formation of Dots

Characterization of raised dots formed on partially cross-linked acrylate films using laser ablation was presented in Chapter 3. These raised dots appear to be

created through a combination of polymerization and ablation. These dots are easily visible with the addition of an alcohol rinse after ablation. Some areas for future studies would include washing the partially cross-linked polymer surface prior to ablation. This wash would eliminate the unreacted monomers, decreasing the probability for polymerization to occur. Although the cross-section of one set of dots was performed, further exploration using laser ablation to cross-section dots created at various power and exposure times could provide a clearer idea of how these features form. Additionally, studying how the concentration of photoinitiator in the monomer blends affects the formation of dots may also contribute to understanding how these dots are formed.

8.2.3 Chapter 4: The Reduction of Stiction on Polymer Structures

Chapter 4 presented examples of how laser ablation can be used to prevent stiction of microcantilevers created using MAP. By including regions, such as support towers, to be removed later with laser ablation, stiction effects were avoided. An alternative approach to reducing stiction was also developed in which a fluorinated solution was applied to a structure. This solution was demonstrated on microwalls and used on a ring and post structure to decrease sticking on polymer surfaces. Further studies could expand on the kinds of surfaces the fluorinated solution could be applied to such as amino acids. Additionally, applying this solution to fields in which anti-sticking coatings would be desirable, such as microfluidics, could provide areas for future investigation.

8.2.4 Chapter 5: Investigations of PerMX as a Transferable Photoresist

In Chapter 5, pattern transfer to a substrate using PerMX photoresists was demonstrated. Both single and multiphoton absorption polymerizations were used to create patterns and structures for transfer. Glass, silicon, gold and silver substrates showed superb transfer using single-photon polymerization while PDMS and copper tape showed very little transfer. An area of future work for single-photon pattern transfer is to investigate other surfaces and textures that could be used, such as chromium and copper sputtered surfaces.

Using MAP, structures in the shape of an arch were made in PerMX photoresists. These arches showed promising success when transferred to glass substrates. Adhesion between the glass substrate and the MAP fabricated arches was investigated in Chapter 5 and revealed that including a soft bake provided some improvement.

Future studies are needed to improve the adhesion between the arches and the substrate and to investigate conditions in which defective arches are created. One possible way to improve adhesion of the structures would be to use a substrate other than glass. PerMX is designed for use with silicon wafers, which might provide better adhesion. Additionally, the manufacturer suggests the inclusion of an additional post-bake after development. This process could improve adhesion by increasing the amount of cross-linking in the photoresist.

Once adhesion is improved, further studies such as a system warm-up period could be more easily investigated. It is suspected that a system warm-up period is responsible for the appearance of a weakened first structure created using MAP but

further studies are needed to confirm this supposition. Another area for PerMX research is to explore the use of PerMX to pattern curved surfaces. Chapter 5 showed some preliminary results with transfer to curved surfaces, but further investigation and optimization could lead to promising applications.

8.2.5 Chapter 6: Efforts Towards the Creation of a DNA Microarray

The work presented in chapter 6 investigated the feasibility of steps in a photolithographic approach to create an amine and hydrophobic patterned substrate. It was discovered that a PDMS mold showed promising potential as a method to create this patterned surface. Although, DNA was not used in these experiments, this patterned substrate could ultimately be used as a DNA microarray for use in a label-free, diffraction based experiment.

The ability to create dual functionalities on the same surface was demonstrated by using a layer of UV cured polymer to protect an underlying functionalization. Exploring how small an area could be covered using cured polymer revealed that features sizes as small as 11 microns could be achieved with an Nd:YAG laser. It was also discovered that larger polymer features could be removed by sonication in dimethylformamide, but the same was not true for smaller features such as those created with the Nd:YAG laser. Future studies could investigate alternative methods or solvents that would allow the polymer to be removed from the substrate without damaging the underlying functionalizations.

Another method that showed promising results was using a polydimethylsiloxane (PDMS) mold to shield an amine substrate during plasma

cleaning. This method created amine squares that were visualized using a selective metallization technique that deposits copper metal only onto areas that are amine functionalized. The next experiments for this project involve functionalization of the amine patterned surface with a fluorinated silane and then to attach DNA. Additionally, an investigation of how small a feature size can be created using a PDMS mold would allow for a greater number of features to be created. Optimizing a mold design to allow for adequate surface exposure during plasma cleaning could contribute to exploring the appearance of copper metal in non amine functionalized areas. The projected path for this work continues towards the long-term goal of creating a DNA microarray for use in a label-free, diffraction based experiment.

8.2.6 Chapter 7: Investigations of Alkylphosphonate coatings on Silicon Nitride

In Chapter 7 alkylphosphonate coatings were deposited onto silicon nitride surfaces and examined using the surface analysis techniques of X-ray photoelectron spectroscopy (XPS), atomic force microscopy (AFM), scanning electron microscopy (SEM) and sum-frequency-generation spectroscopy (SFG), in an attempt to characterize the monolayer. Phosphonate coatings were selected for their ability to cross-link without the presence of water and thus to provide a more reproducible coating. These coatings would be applied to surfaces to reduce adhesion of quantum dots.

XPS confirmed the presence of phosphonate on the surface of our silicon nitrate substrate. However, XPS bias measurements ultimately established that a multilayer was present on the surface. SEM and AFM results observed the presence

of a textured region on the coated silicon nitride surface, and no distinct peaks were observed in the SFG spectra which all support the formation of a multilayer.

Comparisons of SFG spectra collected on another coating, octadecyltrichlorosilane, created on silicon nitride and quartz surfaces suggest that the silicon nitride substrate itself could be responsible for the uneven coating. Future work needs to be performed to analyze the substrate surfaces in order to determine the viability for monolayer coatings. By characterizing the various deposition methods used for creating silicon nitride surfaces the flattest ones can be selected for future coating experiments. The methods used in this chapter especially, AFM and SFG would be ideal for these investigations. Further studies can then go on to improve coating methods or find alternative deposition techniques.

References

1. Chiu, G. L.-T.; Shaw, J. M., Optical lithography: introduction. *IBM J. Res. Dev.* 1997, *41* (1-2), 3-6.

2. Zhang, J.; Tan, K. L.; Hong, G. D.; Yang, L. J.; Gong, H. Q., Polymerization optimization of SU-8 photoresist and its applications in microfluidic systems and MEMS. *J. Micromech. Microeng.* 2001, *11* (1), 20-26.

3. Chaki, N. K.; Vijayamohanan, K., Self-assembled monolayers as a tunable platform for biosensor applications. *Biosens. Bioelectron.* 2002, *17* (1-2), 1-12.

Appendix A

Supporting information for the figures presented in Chapter 2

Figure 2.3A, Line Comparison. A mixture of 55.3% SR499, 41.7% SR368 and 3% TPO-L by weight was spin-cast onto a coverslip at 1500 rpm for 30 seconds. The coverslip was UV cured for 5 minutes. The lines were ablated into the polymer at 100 μm/s using 250 mW of power through a 20× objective, NA=0.5.

Figure 2.3B, Line Comparison. A mixture of 55.3% SR499, 41.7% SR368 and 3% TPO-L by weight was spin-cast onto a coverslip at 1500 rpm for 30 seconds. The coverslip was UV cured for 5 minutes. The lines were ablated into the polymer at 100 μm/s using 250 mW of power through a 40× objective, NA=0.75.

Figure 2.3C, Fine Resolution. A mixture of 55.3% SR499, 41.7% SR368 and 3% TPO-L by weight was spin-cast onto a coverslip at 1500 rpm for 30 seconds. The coverslip was UV cured for 5 minutes. The lines were ablated into the polymer at 50 μm/s using 225 mW of power through a 40× oil-immersion objective, NA=1.3.

Figure 2.4, Line Spacing. A mixture of 55.3% SR499, 41.7% SR368 and 3% TPO-L by weight was spin-cast onto a coverslip at 1500 rpm for 30 seconds. The coverslip was UV cured for 5 minutes. The lines were ablated into the polymer at 50 μm/s

using 175 mW of power through a 20× objective with NA=0.5. Each line is 200 μm long.

Figure 2.5, Molded Lines. A mixture of 55.3% SR499, 41.8% SR368 and 3% TPO-L by weight was spin-cast onto an acrylate-functionalized coverslip at 1500 rpm for 30 seconds. The coverslip was UV cured for 5 minutes. The lines were ablated into the polymer at 200 μm/s using 250 mW of power through a 20× objective with NA=0.5. Each line is 150 μm long with 50 μm spacing between each. Sample was then molded in PDMS as described in the experimental for Chapter 2.

Figure 2.6, Power vs. Velocity Study. A mixture of 55.3% SR499, 41.8% SR368 and 3% TPO-L by weight was spin-cast onto an acrylate-functionalized coverslip at 1500 rpm for 30 seconds. The coverslip was UV cured for 5 minutes. 350 mW of power was used to create the grid that consisted of 200 μm × 200 μm squares. The 3 lines created for the study were centered in one of the grid squares. Tested velocities ranged from 1600 μm/s to 25 μm/s and the tested powers ranged from 300 mW to 150 mW. A 20× objective with NA=0.5 was used to create the lines that are 100 μm long.

Figure 2.7, Crossing Lines. One drop of a mixture of 53.8% SR399, 43.2% SR 368 and 3% TPO-L by weight was placed in an unfunctionalized #1 coverslip. A piece of tape was placed at each end of the coverslip as a spacer and another #1 coverslip was placed on top. The setup was then irradiated with a UV light for 20 minutes.

Subsequent ablation to form the lines was carried out with a 20× objective with NA=0.5 and a stage velocity of 500 μm/second.

Figure 2.8, Razor Lines. One drop of a mixture of 53.8% SR399, 43.2% SR 368 and 3% TPO-L by weight was placed in an unfunctionalized #1 coverslip. A piece of tape was placed at each end of the coverslip as a spacer and another #1 coverslip was placed on top. The setup was then irradiated with a UV light for 20 minutes. After curing, a razor blade was drug across the polymer surface by hand. Ablation was then carried out using a 20× objective with NA=0.5 and a stage velocity of 500 μm/s.

Figure 2.9 A and B, Mechanism Study in Photoresist I. A mixture of 55.3% SR499, 41.8% SR368 and 3% TPO-L by weight was spin-cast onto an acrylate-functionalized coverslip at 1500 rpm for 30 seconds. The coverslip was UV cured for 5 minutes. The 20× objective with NA=0.5 was used to expose the cured polymer surface with 200 mW of power.

Figure 2.9 A. Each of the 4 holes were created using 1 second of exposure.

Figure 2.9 B. Each of the 4 holes were created using 10, 0.1 second of exposure time. The time between each exposure was 100 seconds.

Figure 2.10. Mechanism Study in Photoresist II. A mixture of 53.7% SR399, 43.3% SR368 and 3% TPO-L by weight was spin-cast onto an acrylate-functionalized

coverslip at 1500 rpm for 30 seconds. The coverslip was UV cured for 5 minutes. The 20× objective with NA=0.5 was used to expose the cured polymer surface with 220 mW of power.

Figure 2.10 A. Each of the 4 holes were created using 1 second of exposure.

Figure 2.10 B. Each of the 4 holes were created using 10, 0.1 second of exposure time. The time between each exposure was 100 seconds.

Appendix B

Supporting Information for figures presented in Chapter 3

Figure 3.3A, Polymer Blends. A mixture of 50% SR499, 50% SR368 and 3% TPO-L by weight was spin-cast onto a coverslip at 1500 rpm for 30 seconds. The coverslip was UV cured for 5 minutes. The features were created using a 20× objective with NA = 0.5 and laser power was varied from 200 mW to 490 mW.

Figure 3.3B. Polymer Blends. A mixture of 25% SR499, 75% SR368 and 0.3% TPO-L by weight was spin-cast onto a coverslip at 1500 rpm for 30 seconds. The coverslip was UV cured for 5 minutes. The features were created using a 20× objective with NA = 0.5 and laser power was varied from 200 mW to 490 mW.

Figure 3.3C. Polymer Blends. A mixture of 99.7% SR368 and 0.3% TPO-L was spin-cast onto a piece of acrylate-functionalized glass at 4000 rpm for 30 seconds and UV cured for 5 minutes. The features were created using a 20× objective with NA = 0.5 and laser power was varied from 100 mW to 300 mW.

Figure 3.6, Investigating *z*. A mixture of 25% SR499, 75% SR368 and 0.3% TPO-L by weight was spin-cast onto a coverslip at 1500 rpm for 30 seconds. The coverslip was UV cured for 5 minutes. The features were created using a 20× objective with

NA = 0.5 and laser power of 175 mW. Exposure was allowed to proceed for a few seconds, until the dot was visible.

Figure 3.7, Investigating *z* with Rinsing. A mixture of 25% SR499, 75% SR368, and 0.3% TPO-L by weight was spin cast onto acrylate-functionalized glass at 4000 rpm for 30 seconds. The glass was UV cured for 10 minutes. The dots were ablated into the polymer at a spacing of 15 microns using a 20× objective with a 0.5 numerical aperture and 150 mW of power. Exposure was allowed to proceed for a few seconds, until the dot was visible. After ablation, the sample was washed in ethyl alcohol for 20 minutes and sonicated in methyl alcohol for 1 minute and then air-dried.

Figure 3.8, Ablation Dots. A mixture of 25% SR499, 75% SR368, and 0.3% TPO-L was spin cast onto acrylate-functionalized glass at 1500 rpm for 30 seconds and UV cured for 5 minutes. Dots were ablated into the polymer at a spacing of 15 microns using a 20× objective with a 0.5 numerical aperture and 150 mW of power. Exposure was allowed to proceed for a few seconds, until the dot was visible. After ablation, the sample was washed in ethyl alcohol for 10 minutes, sonicated in methyl alcohol for 1 minute, and then air-dried.

Figure 3.9, Spacing Study. A mixture of 25% SR499, 75% SR368, and 0.3% TPO-L was spin cast onto acrylate-functionalized glass at 1500 rpm for 30 seconds and UV cured for 5 minutes. Dots were ablated into the polymer using spacings of 5, 10, 12,

14, 16, 18, 20 and 25 μm using the 20× objective, 0.5=NA and 130 mW of power. Exposure was allowed to proceed for a few seconds, until the dot was visible. After ablation, the sample was washed in ethyl alcohol for 10 minutes, sonicated in methyl alcohol for 1 minute, and then air-dried.

Figure 3.10, Ablation Dots in Rings. A mixture of 25% SR499, 75% SR368, and 0.3% TPO-L was spin cast onto acrylate-functionalized glass at 1500 rpm for 30 seconds and UV cured for 5 minutes. Dots were ablated into the polymer in a ring formation with a spacing of 13 μm using the 20× objective, 0.5=NA and 130 mW of power. Exposure was allowed to proceed for a few seconds, until the dot was visible. After ablation, the sample was washed in ethyl alcohol for 10 minutes, sonicated in methyl alcohol for 1 minute, and then air-dried.

Figure 3.11, Cross-sections of Ablation Dots. A mixture of 25% SR499, 75% SR368, and 0.3% TPO-L was spin cast onto acrylate-functionalized glass at 1500 rpm for 30 seconds and UV cured for 5 minutes. Dots were ablated into the polymer with a spacing of 15 μm using the 20× objective, 0.5=NA and 130 mW of power. Exposure was allowed to proceed for a few seconds, until the dot was visible. After ablation, the sample was washed in ethyl alcohol for 10 minutes, sonicated in methyl alcohol for 1 minute, and then air-dried. Sample was then ablated using the 40× oil-immersion objective (1.3=NA) with 250 mW of power.

Figure 3.12, Ablation Dot Study. A mixture of 25% SR499, 75% SR368, and 0.3% TPO-L was spin cast onto acrylate-functionalized glass at 1500 rpm for 30 seconds and UV cured for 5 minutes. Dots were ablated into the polymer at a spacing of 15 microns using a 20× objective with a 0.5 numerical aperture and 150 mW of power. Exposure was allowed to proceed for 2 seconds. After ablation, the sample was washed in ethyl alcohol for 10 minutes, sonicated in methyl alcohol for 1 minute, and then air-dried.

Figure 3.13 A and B, Mechanism Study in Photoresist IV. A mixture of 25% SR499, 75% SR368 and 0.3% TPO-L was spin-cast onto an acrylate-functionalized coverslip at 1500 rpm for 30 seconds. The coverslip was UV cured for 5 minutes. The 20× objective with NA=0.5 was used to expose the cured polymer surface with 200 mW of power. After ablation, the sample was washed in ethyl alcohol for 10 minutes, sonicated in methyl alcohol for 1 minute, and then air-dried.

Figure 3.13 A. Each of the 4 holes were created using 1 second of exposure.

Figure 3.13 B. Each of the 4 holes were created using 10, 0.1 second of exposure time. The time between each exposure was 100 second.

Appendix C

Supporting information for the figures presented in Chapter 4

Figure 4.3, Cantilevers. A mixture of 55.4% SR499, 41.6% SR368, and 3% TPO-L by weight was used to fabricate cantilevers with a length of 60 μm. A 9.7 mW laser was focused through a 40× oil-immersion objective for the fabrication. After exposure, the sample was rinsed twice with ethanol. Subsequent ablation was performed with a 250 mW laser focused through a 40× oil-immersion objective with a 1.3 numerical aperture.

Figure 4.4A and B, Contact Angle Examples. These images were taken an alternate contact-angle goniometer (Ramé-Hart Instrument Co., 250-000). It was used to deliver a drop of distilled water from a syringe onto a treated surface. The drop was imaged using a drop-shape analysis program (DROPIMage, Ramé-Hart Instrument Co.) and the contact angle was measured between the solid-liquid interface and the line tangent to the drop shape at the liquid-vapor interface.

Figure 4.5, Contact Angles on Glass. A piece of acrylate-functionalized glass was treated for 30 minutes with a solution of 80% ethyl alcohol and 20% ethlyenediamine by volume. The glass was then rinsed three times with ethyl alcohol for 3 minutes each. The sample was then placed in a perfluorostearic acid solution containing hexafluorobenzene, as described in experimental, for 1 hour. Contact angles were

then measured as described in the experimental. The average for each sample was reported and the error bars are the standard deviation.

Figure 4.6, Contact Angles on Polymer Dots. A mixture of 53.6% SR399, 43.4% SR368, and 3% TPO-L was used to create polymer dots as described in the experimental and UV cured for 10 minutes. The dots were exposed to a solution of 80% ethyl alcohol and 20% ethlyenediamine by volume for 30 minutes. This treatment was followed by three rinses with ethyl alcohol. The sample was then placed in a perfluorostearic acid solution containing hexafluorobenzene, as described in experimental, for 1 hour. The average for each sample was reported and the error bars are the standard deviation.

Figure 4.7, Walls. A solution of 53.7% SR399, 43.4% SR368, and 3% TPO-L was used to create 40 micro tall walls. The walls were created with the 40× oil-immersion at a laser power of 9.2 mW for the non-fluorinated wall and 8.5 mW for the fluorinated walls. All walls were created at a speed of 20 microns/second in the *x* and *y* dimensions and 2 microns/second in the *z* dimension. The *y* and *z* step size was 0.5 microns. The walls in the first row were 1.5 microns thick and 4 microns apart while the second row shows walls that were 1.5 microns thick and 5 microns apart. All structures were developed and coated in a series of solvent rinses as follows. Two DMF rinses for 3 minutes each, two ethyl alcohol rinses for 3 minutes each, ethlyenediamine solution (80% ethyl alcohol, 20% ethlyenediamine) for 30 minutes, 3 ethyl alcohol rinses for 3 minutes each. The sample was then placed in a

perfluorostearic acid solution containing pentafluorobenzene for 1 hour followed by a hexane dip for 1 minute.

The control sample was washed in the first DMF and ethyl alcohol rinses followed directly by 1 minute in hexanes and air dried.

Figure 4.8, Ring-and-Post without Coating. The dimensions of the ring and post were 48 × 48 × 1 micron for the ring, 8 × 8 × 25 μm for the tower and 20 × 20 × 4 μm for the base. The structure was fabricated using MAP with 399/368 (53.7/43.3 weight percent respectively) 3% TPO-L resin. The 100× oil-immersion objective was used with a power of 25 mW to create the base and post at a speed of 50 microns/second. The ring was fabricated at a power of 20 mW and at a speed of 25 microns/second. The sample was rinsed in two, 3 minutes DMF rinses followed by two, 3 minutes ethyl alcohol rinses and a final rinse for 1 minute in hexamethyldisilazane (HMDS).

Figure 4.9, Ring-and-Post with Coating. The dimensions of ring and post structure were 25 × 25 × 1 μm for the ring, 8 × 8 × 25 μm for the tower and 20 × 20 × 4 μm for the base. The structure was fabricated using MAP with 399/368 (53.7/43.3 weight percent respectively) 3% TPO-L resin. A 40× oil-immersion objective, NA=1.3, and a power of 16 mW. Stage velocities for the base and post were 50 μm/second and the ring was fabricated with a 20 μm/second velocity. After fabrication unexposed prepolymer resin was rinsed away as described in the experimental. Immediately following the rinses structures were placed in an 80% ethyl alcohol, 20%

ethylenediamine solution for 1 hour. The sample was then transferred to a solution containing 4 mg perfluorooctadecanoic acid, 4.455 g pentafluorobenzene, 0.01 g methyl alcohol, 16 mL ethyl alcohol for 1 hour. Ablation was carried out using the 40× air objective (NA=0.75), and 130 mW of power.

Appendix D

Supporting information for figures in Chapter 5

Figure 5.4A, Silicon. The polyolefin separator sheet was removed from a piece of PerMX 3050 photoresist. The PerMX film was then exposed to UV light for 2 minutes through the negative mask with a glass slide spacer. After exposure the photoresist was transferred to a silicon substrate. Sample was developed at 65 °C for 5 minutes, cooled for a few minutes to remove mylar backing and followed with another baking at 95 °C for 5 minutes. Developed in SU-8 developer for 4 minutes.

Figure 5.4B, Gold. The polyolefin separator sheet was removed from a piece of PerMX 3050 photoresist. The PerMX film was then exposed to UV light for 2 minutes through the negative mask with a glass slide spacer. After exposure, the photoresist was transferred to a gold substrate with a 10 nm chromium adhesion layer. Sample was developed at 65 °C for 5 minutes, 95 °C for 5 minutes and 65 °C for 5 minutes, sample was cooled for a few minutes at room temperature and the mylar backing was removed. The photoresist was developed in SU-8 developer for 4 minutes.

Figure 5.4C, Copper. The polyolefin separator sheet was removed from a piece of PerMX 3050 photoresist. The PerMX film was then exposed to UV light for 2 minutes through a negative mask with a glass slide spacer. After exposure, the

photoresist was transferred to a copper tape substrate. Sample was developed at 65 °C for 5 minutes. The mylar backing was removed and then the sample was baked for another 5 minutes at 95 °C. After baking, the sample was developed in SU-8 developer for 4 minutes.

Figure 5.4D, Silver. The polyolefin separator sheet was removed from a piece of PerMX 3050 photoresist. The PerMX film was then exposed to UV light for 2 minutes through a negative mask with a glass slide spacer. After exposure, the photoresist was transferred to a silver sputtered substrate. Sample was developed at 65 °C for 5 minutes. The mylar backing was removed and the sample was baked for another 5 minutes at 95 °C. After baking, the sample was developed in SU-8 developer for 4 minutes.

Figure 5.5 Glass Rod. A glass rod was cleaned in acetone, isopropyl alcohol and distilled water for 3 minutes each. The rod was dried at 95 °C for 1 hour and oxygen plasma cleaned for 4 minutes at 300 mtorr. The PerMX film, with the polyolefin separator sheet removed, was exposed to UV light for 2 minutes through a negative mask. Glass slides were used as spacers. Standing in front of the oven (to warm the sample slightly making it flexible) wrapped the patterned PerMX film around the glass rod and secured with rubber bands. Developed at 95 °C for 5 minutes and removed mylar backing. Placed back in 65 °C for 5 minutes then developed in SU-8 developer for 4 minutes.

Figure 5.6A Unbaked (Not Soft-Baked) PerMX. An optical image of a unbaked PerMX film with the polyolefin separator sheet removed.

Figure 5.6B Soft-Baked PerMX. An optical image of soft-baked PerMX film with the polyolefin separator sheet removed. Soft-baking was done for 30 seconds at 95°C.

Figure 5.7A, Unbaked. The polyolefin separator sheet was removed from a piece of PerMX 3050. The PerMX film was then exposed to UV light for 1 minute through a negative mask with a glass slide spacer. After exposure the photoresist was transferred to a plasma cleaned glass substrate. The sample was then developed at 65 °C, 95 °C and 65 °C for 5 minutes each and let cool to room temperature for 10 minutes. The mylar backing was removed, and the sample was developed in two SU-8 developer rinses for 4 minutes, and 2 minutes followed by a 30 second dip in isopropyl alcohol and 1 minute in hexanes.

Figure 5.7B, Soft-Baked. The polyolefin separator sheet was removed from a piece of PerMX 3050. The PerMX film was then soft-baked at 65 °C for 3 minutes, 95 °C for 30 seconds and 65 °C for 3 minutes. The PerMX film was then exposed to UV light for 1 minute through a negative mask with a glass slide spacer. After exposure the photoresist was transferred to a plasma cleaned glass substrate. The sample was developed at 65 °C, 95 °C and 65 °C for 5 minutes each and let cool for 10 minutes at room temperature. The mylar backing was removed, and the sample was developed

in two SU-8 developer rinses for 4 minutes, and 2 minutes each, followed by a 30 dip in isopropyl alcohol and 1 minutes in hexanes.

Figure 5.8, Initial Arches. The polyolefin separator sheet was removed from a piece of PerMX 3050 photoresist. Arches with an outer diameter of 30 microns, a 5 × 5 foot and a line spacing of 1 micron were created in a PerMX photoresist using MAP. Fabrication was carried out with a 20 × air objective and 62 mW of power at a speed of 20 microns/second. After exposure the photoresist was transferred to an amine-functionalized glass rod and developed at 95 °C for 5 minutes. The sample was cooled to room temperature and the mylar backing was removed. The sample was then heated at 65 °C and rinsed in SU-8 developer for 4 minutes.

Figure 5.10, Arches shorter foot. The polyolefin separator sheet was removed from a piece of PerMX 3050 photoresist. Arches with an outer diameter of 47 microns, a 6 × 6 × 10 micron foot and a line spacing of 1.5 microns were then created in the PerMX 3050 photoresist, using MAP. Fabrication was carried out with a 20 × air objective and 30 mW of power at a speed of 20 microns/second. After exposure the photoresist was transferred to an amine-functionalized glass rod and developed at 95°C followed by 65 °C for 5 minutes each. The sample was cooled to room temperature, the mylar backing was removed and the sample was rinsed in SU-8 developer for 4 minutes. Arches were smaller than intended due to a restricted *z* value.

Figure 5.11A, Arches. The polyolefin separator sheet was removed from a piece of PerMX 3050 photoresist. Arches with an outer diameter of 47 microns, a 6 × 6 × 10 micron foot and a line spacing of 1.5 microns were created in a PerMX 3050 photoresist using MAP. Fabrication was carried out using a 20× air objective and 35 mW of power at a speed of 20 microns/second. After exposure the photoresist was transferred to an amine-functionalized glass slide and developed at 95 °C followed by 65 °C for 5 minutes each. The sample was cooled to room temperature, the mylar backing was removed and the sample was rinsed in SU-8 developer for 4 minutes. Arches were smaller than intended due to a restricted *z* value.

Figure 5.11B, Smoother Arches. The polyolefin separator sheet was removed from a piece of PerMX 3050 photoresist. Arches with an outer diameter of 40 microns, a 10 × 10 × 5 micron foot and a line spacing of 0.5 microns were created in a PerMX 3050 photoresist using MAP. Fabrication was carried out with a 20 × air objective and 17.5 mW of power at a speed of 20 microns/second for the *x* and *y* dimensions. The *z* dimension was fabricated at a speed of 10 microns/second. After exposure the photoresist was transferred to an amine-functionalized glass slide and developed at 65 °C, 95 °C and 65 °C for 5 minutes each with a 1/3 cut glass slide on top. The sample was cooled to room temperature, the mylar backing was removed and the sample was rinsed in SU-8 developer for 4 minutes.

Figure 5.11C, Smoothest Arches. Arches with two different diameters were fabricated on this sample. Larger arches have an outer diameter of 50 microns, a 10 ×

10 × 15 micron foot and a line spacing of 0.25 microns. Smaller arches have an outer diameter of 30 microns, a 5 × 5 × 15 micron foot and a line spacing of 0.25 microns. These arches were fabricated in PerMX 3050 photoresist, with the polyolefin separator sheet removed, using MAP. The fabrication was performed with a 100 × oil-immersion objective and a power of 18.3 mW with a speed of 20 microns/second. After exposure the photoresist was transferred to an amine-functionalized glass slide and developed at 65 °C, 95 °C and 65 °C for 5 minutes each. Sample was then cooled to room temperature, the mylar backing was removed and the sample was rinsed in two, SU-8 developer rinses for 4 and 2 minutes respectively, followed by an isopropyl alcohol rinse for 30 seconds and a hexane dip for 1 minute.

Figure 5.12A, Platform Arch. Four platform arches were made in PerMX 3050, with the polyolefin separator sheet removed, using MAP. The arches had an outer diameter of 30 microns, with a line spacing of 0.25 microns and a 5 × 5 × 10 micron foot with a line spacing of 0.5 microns. The platform the arches were fabricated on is 30 × 30 × 10 microns with a line spacing of 1 micron. Fabrication was carried out with a 20× air objective (0.5 NA), 17.8 mW of power at a speed of 20 microns/second. After exposure the photoresist was transferred to an amine - functionalized glass slide and developed at 65 °C, 95 °C and 65 °C for 5 minutes each. The sample was the cooled to room temperature, the mylar backing was removed and the sample was rinsed in two SU-8 developer rinses for 4 and 2 minutes respectively.

Figure 5.12B, Platform Arches Lower. Four platform arches were made in PerMX 3050, with the polyolefin separator sheet removed, using MAP. Arches had an outer diameter of 20 microns, with a line spacing of 0.25 microns and a 5 × 5 × 6 micron foot with a line spacing of 0.25 microns. The platform the arches were fabricated on is 30 × 30 × 10 microns with a line spacing of 0.5 microns in the *x* and *y* dimensions and a line spacing of 1 micron in the *z*. Fabrication was carried out using the 100× oil-immersion objective with 18.4 mW of power at a speed of 20 microns/second for the arches and foot, and 10 microns/second for the platform. After exposure the photoresist was transferred to an amine-functionalized glass slide and developed at 65 °C, 95 °C and 65 °C for 5 minutes each. The sample was cooled to room temperature, the mylar backing was removed and the sample was rinsed in two SU-8 developer rinses for 4 and 2 minutes respectively followed by a 30 second rinse in isopropyl alcohol and 1 minute in hexanes.

Figure 5.12C, Platform Arches Twisted. (Same as B) Four platform arches were made in PerMX 3050, with the polyolefin separator sheet removed, using MAP. Arches had an outer diameter of 20 microns, with a line spacing of 0.25 microns and a 5 × 5 × 6 micron foot with a line spacing of 0.25 microns. The platform the arches were fabricated on is 30 × 30 × 10 microns with a line spacing of 0.5 microns in the *x* and *y* dimensions and a line spacing of 1 micron in the *z*. Fabrication was carried out using the 100× oil-immersion objective with 18.4 mW of power at a speed of 20 microns/second for the arches and foot, and 10 microns/second for the platform. After exposure the arches were transferred to an amine-functionalized glass slide and

developed at 65 °C, 95 °C and 65 °C for 5 minutes each. Sample was cooled to room temperature, the mylar backing was removed and the sample was rinsed in two SU-8 developer rinses for 4 and 2 minutes respectively followed by a 30 second rinse in isopropyl alcohol and 1 minutes in hexanes.

Figure 5.12D, Platform Arches Fallen. (Same arch dimensions as B and C) Four platform arches were made in PerMX 3050, with the polyolefin separator sheet removed, using MAP. Arches had an outer diameter of 20 microns, with a line spacing of 0.25 microns and a 5 × 5 × 6 micron foot with a line spacing of 0.25 microns. The platform the arches were fabricated on is 30 × 30 × 10 microns with a line spacing of 0.5 microns in the *x* and *y* dimensions and a line spacing of 1 micron in the *z*. Fabrication was carried out using the 100× oil-immersion objective with 16.3 mW of power at a speed of 20 microns/second for the arches and foot, and 10 microns/second for the platform. After exposure the photoresist was transferred to an amine-functionalized glass slide and developed at 65 °C, 95 °C and 65 °C for 5 minutes each. The sample was cooled to room temperature and the mylar backing was removed. The sample was then rinsed in two SU-8 developer rinses for 4 and 2 minutes respectively followed by a 30 second rinse in isopropyl alcohol and 1 minute in hexanes.

Figure 5.13A and B, Underside of Platform arches. Same sample as figure 5.11D

Figure 5.14A-E, Arch Parameters. Four platform arches were made in PerMX 3050, with the polyolefin separator sheet removed, using MAP. Arches had an outer diameter of 20 microns, with a line spacing of 0.25 microns and a 5 × 5 × 6 micron foot with a line spacing of 0.25 microns. The platform the arches were fabricated on is 30 × 30 × 10 microns with a line spacing of 0.5 microns in the *x* and *y* dimensions and a line spacing of 1 micron in the *z*. Fabrication was carried out with the 100 × oil-immersion objective at a speed of 20 microns/second for the arches and foot, and 10 microns/second for the platform. After exposure the photoresist was transferred to an amine-functionalized glass slide and developed at 65 °C, 95 °C and 65 °C for 5 minutes each. Sample was cooled, the mylar backing was removed and the sample was rinsed in two SU-8 developer rinses for 4 and 2 minutes respectively followed by a 30 second rinse in isopropyl alcohol and 1 minute in hexanes.

Figure 5.14A. PerMX 3050, with the polyolefin separator sheet removed, was soft-baked for 20 seconds at 95 °C and used without cooling. Fabrication was done with 29.9 mW of power.

Figure 5.14B. PerMX 3050, with the polyolefin separator sheet removed, was soft-baked for 20 seconds at 95 °C and cooled for 10 minutes prior to use. Fabrication was done with 29.9 mW of power.

Figure 5.14C. PerMX 3050, with the polyolefin separator sheet removed, was soft-baked for 20 seconds and 95 °C and cooled for 20 minutes prior to use. Fabrication was performed with 29.9 mW of power.

Figure 5.14D, Same as C. PerMX 3050, with the polyolefin separator sheet removed, was soft-baked for 20 seconds and 95 °C and cooled for 20 minutes prior to use. Fabrication was performed with 29.9 mW of power.

Figure 5.14E. PerMX 3050, with the polyolefin separator sheet removed, was soft-baked for 30 seconds at 95 °C and let cool for 20 minutes prior to use. Fabrication was performed with 29.8 mW of power.

Figure 5.14F. PerMX 3050, with the polyolefin separator sheet removed, was soft-baked for 30 seconds at 95 °C and let cool for 2 hours and 21 minutes prior to use. Fabrication was performed with 29.9 mW of power.

Figure 5.15A-D Square Parameters and Development. PerMX 3020 films, with the polyolefin separator sheet removed, were soft-baked with a drop (< 5 micro liters) of gold nanobeads. Soft-baking was done at 65 °C for 3 minutes, 30 seconds at 95 °C and 65 °C for 3 minutes. The fabrication of 3 squares, 20 × 20 microns with heights moving from 5 to 10 to 15 microns, was carried out using MAP. The fabrication was performed with the 100× oil-immersion objective at a power of 25.5 mW and a speed of 20 microns/seconds. The line spacing is 0.5 microns in the *x* and *y* dimensions and

1 micron in the *z* dimension. The Spacing between the squares was 5 microns. After MAP the sample was transferred to a preheated (65 °C) amine-functionalized glass slide using a roller. The roller was also preheated to 65 °C. The sample was placed, photoresist side down, on the amine-functionalized substrate and the roller was used to press it against the substrate. The sample was developed at 65 °C, 95 °C and 65 °C for 5 minutes each. The sample was cooled to room temperature and the mylar layer was removed. The sample was then subjected to two SU-8 developer rinses for 4 and 2 minutes respectively followed by 30 seconds in isopropyl alcohol and hexanes of 1 minute.

Figure 5.15A, Light on. The microscope light was on the entire time during fabrication. Fabrication lasts a little less than 30 minutes.

Figure 5.15B, Light off. The microscope light was off during fabrication.

Figure 5.15C, Light on at Beginning. The microscope light was on at the beginning of fabrication. Turned off after the first square was complete, about 5 minutes.

Figure 5.15D, Light on at End. The microscope light was turned on for 20 minutes after fabrication was complete.

Appendix E

Supporting information for the "Thickogram" method used to calculate the film thickness presented in Chapter 7. The "Thickogram" (reference 24 in Chapter 7) calculation was performed using measurements collected at a take-off angle of 40°, on the same silicon nitride coated sample that was used for the bias work in Chapter 7. Original XPS spectra are provide at the end of this appendix, and the charge neutralizer was on during the experiments. In these calculations, the carbon 1s peak was used as the overlayer and the silicon 2p peak as the substrate.

Intensity of the overlayer signal: I_o = 4268.445 counts per second (cps)

Sensitivity of the overlayer signal: S_o = 0.278

Intensity of the substrate signal: I_s = 1826.776 cps

Sensitivity of the substrate signal: S_s = 0.328

$(I_o/S_o)/(I_s/S_s) = 2.76$

$KE = h\nu - (E_B + \Theta)$

KE = Kinetic energy

Work function: $\Theta = 0$ because the data is calibration

Photon energy $h\nu$ =1486.6 eV

Carbon 1s binding energy: E_{Bo} = 284.8 eV

Silicon 2p binding energy: E_{Bs} = 102.0 eV

KE_o / KE_s =0.868 eV

Value read from line C in the "Thickogram" = $t/\lambda\cos\theta$

Value read from line C on "Thickogram" graph = 2.1 for these calculations

Attenuation length of the photoelectrons in the overlayer as calculated by the CS1 method (see reference 25 in Chapter 7): λ = 19.8 monolayers

Take-off angle relative to the surface normal: $\theta = 90° - 40° = 50°$

t = thickness in monolayers

Values for CS1 method

Z for octadecylphosphonic acid = 3.12

E = KE_s = 1384.6 eV

t = 26.49 monolayers

26.49/18 carbon chain in our molecule = 1.48 monolayers

wide/2

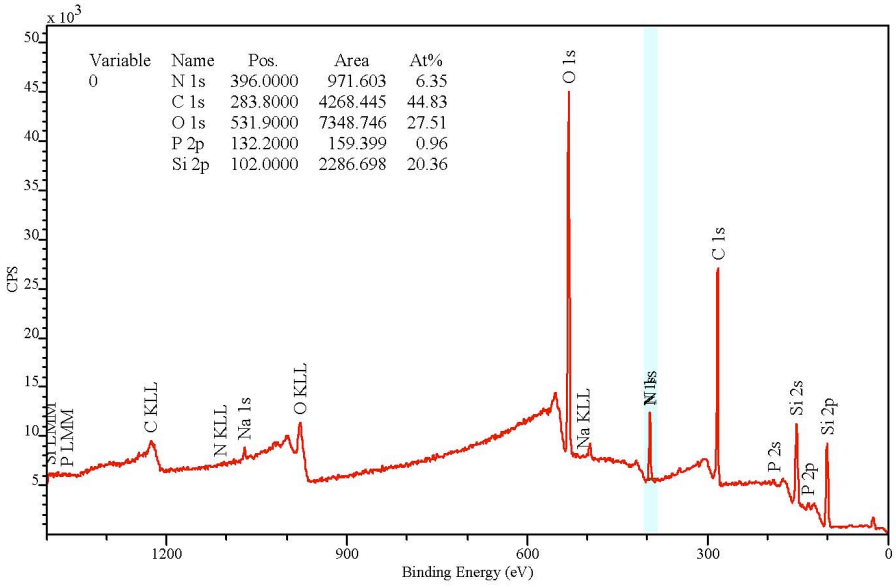

C 1s/3

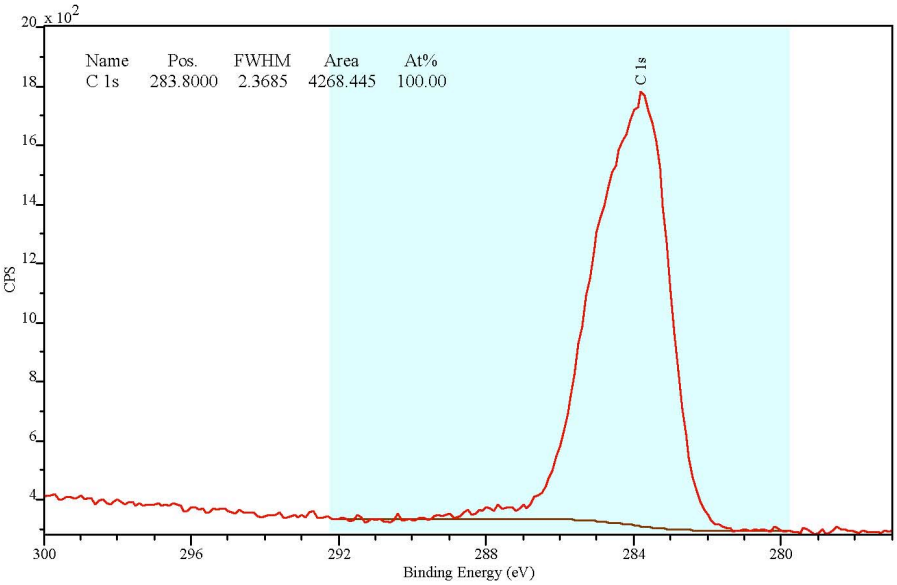

CasaXPS (This string can be edited in CasaXPS.DEF/PrintFootNote.txt)

O 1s/4

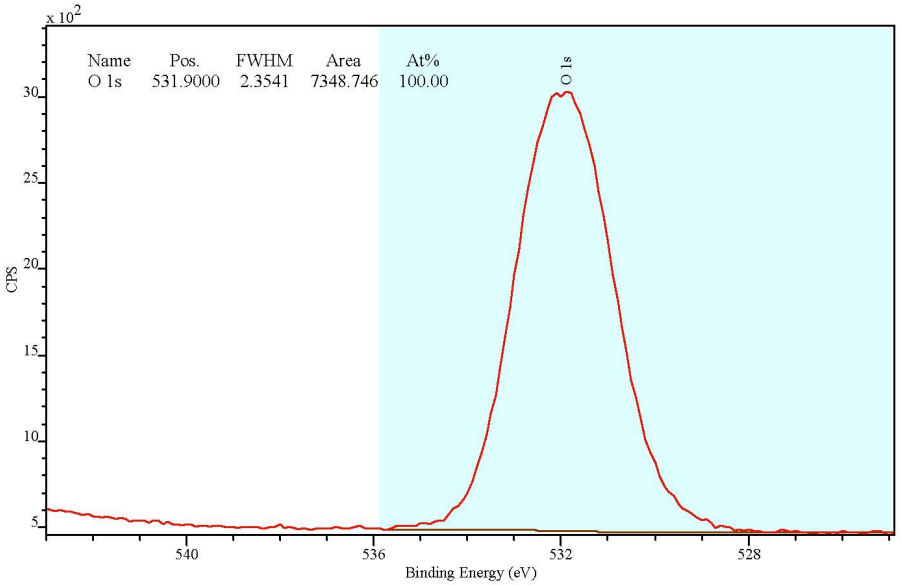

P 2p/5

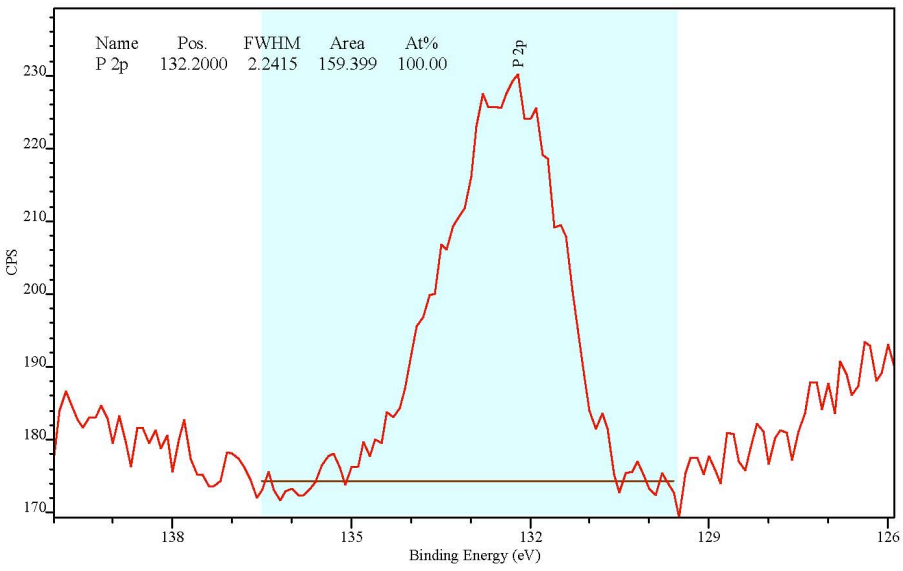

CasaXPS (This string can be edited in CasaXPS.DEF/PrintFootNote.txt)

P 2s/6

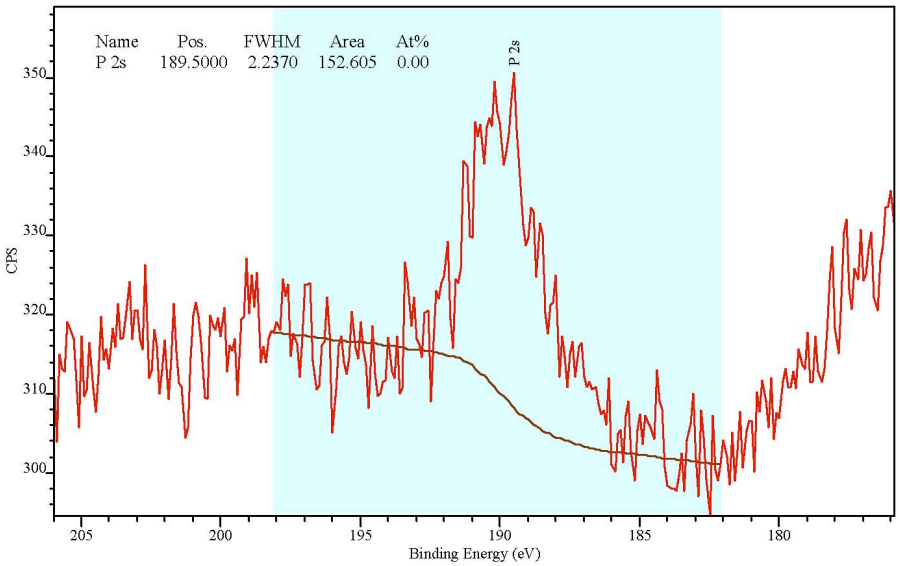

Si 2p/8

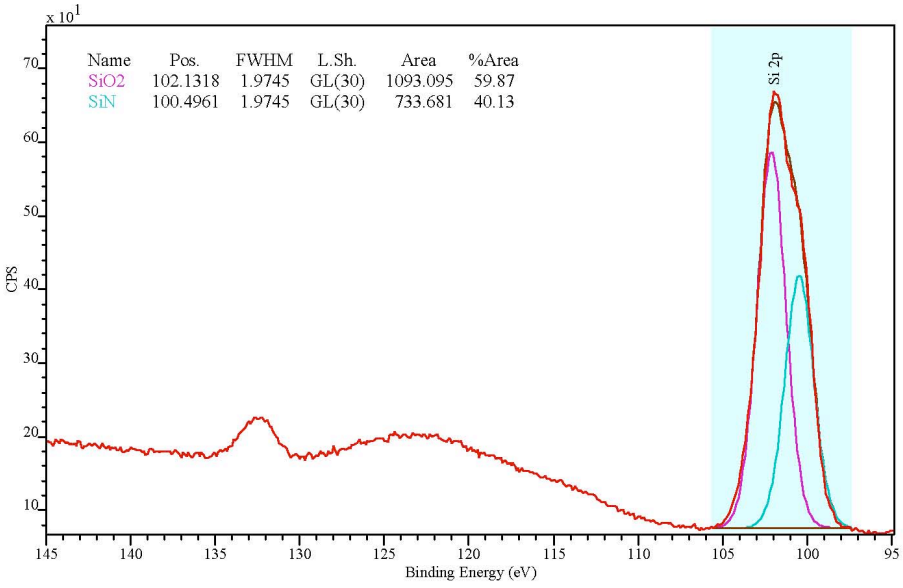

CasaXPS (This string can be edited in CasaXPS.DEF/PrintFootNote.txt)

References

1. Weiss, K. D., Paint and coatings: A mature industry in transition. *Prog. Polym. Sci.* **1997,** *22* (2), 203-245.

2. Nie, Z. H.; Kumacheva, E., Patterning surfaces with functional polymers. *Nat. Mater.* **2008,** *7* (4), 277-290.

3. Echlin, P., *Handbook of Sample Preparation for Scanning Electron Microscopy and X-Ray Microanalysis*. Springer: 2009.

4. Lewis, J., Material challenge for flexible organic devices. *Mater. Today* **2006,** *9* (4), 38-45.

5. Love, J. C.; Estroff, L. A.; Kriebel, J. K.; Nuzzo, R. G.; Whitesides, G. M., Self-assembled monolayers of thiolates on metals as a form of nanotechnology. *Chem. Rev.* **2005,** *105* (4), 1103-1169.

6. Biallozor, S.; Kupniewska, A., Conducting polymers electrodeposited on active metals. *Synth. Met.* **2005,** *155* (3), 443-449.

7. Kumar, A.; Biebuyck, H. A.; Whitesides, G. M., Patterning self-assembled monolayers- applications in materials science *Langmuir* **1994,** *10* (5), 1498-1511.

8. Chiu, G. L.-T.; Shaw, J. M., Optical lithography: introduction. *IBM J. Res. Dev.* **1997,** *41* (1-2), 3-6.

9. Adams, T. M.; Layton, R. A., *Introductory MEMS: Fabrication and Applications*. Springer: 2010.

10. Mortini, B., Photosensitive resists for optical lithography. *C. R. Phys.* **2006,** *7* (8), 924-930.

11. Shaw, J. M.; Gelorme, J. D.; LaBianca, N. C.; Conley, W. E.; Holmes, S. J., Negative photoresists for optical lithography. *Ibm Journal of Research and Development* **1997,** *41* (1-2), 81-94.

12. Reiser, A.; Huang, J. P.; He, X.; Yeh, T. F.; Jha, S.; Shih, H. Y.; Kim, M. S.; Han, Y. K.; Yan, K., The molecular mechanism of novotak-diazonaphthoquinone resists. *Eur. Polym. J.* **2002,** *38* (4), 619-629.

13. Abgrall, P.; Conedera, V.; Camon, H.; Gue, A. M.; Nguyen, N. T., SU-8 as a structural material for labs-on-chips and microelectromechanical systems. *Electrophoresis* **2007,** *28* (24), 4539-4551.

14. DuPont, DuPont PerMX 3000 Photodielectric dry film adhesive technical data sheet. DuPont, Ed. DuPont: 2010.

15. Microchem, SU-8 3000 Permanent Epoxy Negative Photoresist Microchem, Ed.

16. Ma, H.; Jen, A. K. Y.; Dalton, L. R., Polymer-based optical waveguides: Materials, processing, and devices. *Adv. Mater.* **2002,** *14* (19), 1339-1365.

17. Becker, H.; Gartner, C., Polymer microfabrication methods for microfluidic analytical applications. *Electrophoresis* **2000,** *21* (1), 12-26.

18. Zhang, J.; Tan, K. L.; Hong, G. D.; Yang, L. J.; Gong, H. Q., Polymerization optimization of SU-8 photoresist and its applications in microfluidic systems and MEMS. *J. Micromech. Microeng.* **2001,** *11* (1), 20-26.

19. Daly, D.; Stevens, R. F.; Hutley, M. C.; Davies, N., The manufacture of microlenses by melting photoresist. *Meas. Sci. Technol.* **1990,** *1* (8), 759-766.

20. McGall, G.; Labadie, J.; Brock, P.; Wallraff, G.; Nguyen, T.; Hinsberg, W., Light-directed synthesis of high-density oligonucleotide arrays using semiconductor photoresists. *Proc. Natl. Acad. Sci. U. S. A.* **1996,** *93* (24), 13555-13560.

21. Li, L.; Fourkas, J. T., Multiphoton polymerization. *Mater. Today* **2007,** *10* (6), 30-37.

22. LaFratta, C. N.; Fourkas, J. T.; Baldacchini, T.; Farrer, R. A., Multiphoton fabrication. *Angew. Chem.-Int. Edit.* **2007,** *46* (33), 6238-6258.

23. Sun, H. B.; Kawata, S., Two-photon photopolymerization and 3D lithographic microfabrication. In *Nmr - 3d Analysis - Photopolymerization*, Springer-Verlag Berlin: Berlin, 2004; Vol. 170, pp 169-273.

24. Maruo, S.; Ikuta, K.; Korogi, H., Force-controllable, optically driven micromachines fabricated by single-step two-photon micro stereolithography. *J. Microelectromech. Syst.* **2003,** *12* (5), 533-539.

25. Seet, K. K.; Mizeikis, V.; Matsuo, S.; Juodkazis, S.; Misawa, H., Three-dimensional spiral-architecture photonic crystals obtained by direct laser writing. *Adv. Mater.* **2005,** *17* (5), 541-+.

26. LaFratta, C. N.; Li, L. J.; Fourkas, J. T., Soft-lithographic replication of 3D microstructures with closed loops. *Proc. Natl. Acad. Sci. U. S. A.* **2006,** *103* (23), 8589-8594.

27. Serbin, J.; Egbert, A.; Ostendorf, A.; Chichkov, B. N.; Houbertz, R.; Domann, G.; Schulz, J.; Cronauer, C.; Frohlich, L.; Popall, M., Femtosecond laser-induced two-photon polymerization of inorganic-organic hybrid materials for applications in photonics. *Opt. Lett.* **2003,** *28* (5), 301-303.

28. Kawata, S.; Sun, H. B.; Tanaka, T.; Takada, K., Finer features for functional microdevices - Micromachines can be created with higher resolution using two-photon absorption. *Nature* **2001,** *412* (6848), 697-698.

29. Chaki, N. K.; Vijayamohanan, K., Self-assembled monolayers as a tunable platform for biosensor applications. *Biosens. Bioelectron.* **2002,** *17* (1-2), 1-12.

30. Schreiber, F., Structure and growth of self-assembling monolayers. *Prog. Surf. Sci.* **2000,** *65* (5-8), 151-256.

31. Guo, L. Y.; Zhao, Y. P., Effect of chain length of self-assembled monolayers on adhesion force measurement by AFM. *J. Adhes. Sci. Technol.* **2006,** *20* (12), 1281-1293.

32. Schwartz, D. K., Mechanisms and kinetics of self-assembled monolayer formation. *Annu. Rev. Phys. Chem.* **2001,** *52*, 107-137.

33. Onclin, S.; Ravoo, B. J.; Reinhoudt, D. N., Engineering silicon oxide surfaces using self-assembled monolayers. *Angew. Chem.-Int. Edit.* **2005,** *44* (39), 6282-6304.

34. Schreiber, F., Self-assembled monolayers: from 'simple' model systems to biofunctionalized interfaces. *J. Phys.-Condes. Matter* **2004,** *16* (28), R881-R900.

35. Ebner, A.; Wildling, L.; Zhu, R.; Rankl, C.; Haselgrubler, T.; Hinterdorfer, P.; Gruber, H. J., Functionalization of probe tips and supports for single-molecule recognition force Microscopy. In *Stm and Afm Studies On*, Springer-Verlag Berlin: Berlin, 2008; Vol. 285, pp 29-76.

36. Herzer, N.; Hoeppener, S.; Schubert, U. S., Fabrication of patterned silane based self-assembled monolayers by photolithography and surface reactions on silicon-oxide substrates. *Chem. Commun.* **2010,** *46* (31), 5634-5652.

37. Xia, Y. N.; Zhao, X. M.; Whitesides, G. M., Pattern transfer: Self-assembled monolayers as ultrathin resists. *Microelectron. Eng.* **1996,** *32* (1-4), 255-268.

38. Liu, C., Recent developments in polymer MEMS. *Adv. Mater.* **2007,** *19* (22), 3783-3790.

39. Kawamura, Y.; Toyoda, K.; Namba, S., Effective deep ultraviolet photoetching of poly methyl methacrylate by an excimer laser *Appl. Phys. Lett.* **1982,** *40* (5), 374-375.

40. Srinivasan, R.; Maynebanton, V., Self-developing photoetching of poly(ethylene-terephthalate) films by far ultraviolet excimer laser-radation *Appl. Phys. Lett.* **1982,** *41* (6), 576-578.

41. Baldacchini, T. Novel Techniques for the Fabrication of Two- and Three-Dimensional Microstructures. Boston College, 2004.

42. Lippert, T.; Dickinson, J. T., Chemical and spectroscopic aspects of polymer ablation: Special features and novel directions. *Chem. Rev.* **2003,** *103* (2), 453-485.

43. Lankard, J. R.; Wolbold, G., Excimer laser ablation of polyimide in a manufacturing facility. *Appl. Phys. A-Mater. Sci. Process.* **1992,** *54* (4), 355-359.

44. Gomez, D.; Tekniker, F.; Goenaga, I.; Lizuain, I.; Ozaita, M., Femtosecond laser ablation for microfluidics. *Opt. Eng.* **2005,** *44* (5), 8.

45. Zhang, Y.; Katoh, T.; Washio, M.; Yamada, H.; Hamada, S., High-aspect-ratio micromachining teflon by direct exposure to synchrotron-radiation *Appl. Phys. Lett.* **1995,** *67* (6), 872-874.

46. Belfield, K. D.; Schafer, K. J.; Liu, Y. U.; Liu, J.; Ren, X. B.; Van Stryland, E. W., Multiphoton-absorbing organic materials for microfabrication, emerging optical

applications and non-destructive three-dimensional imaging. *J. Phys. Org. Chem.* **2000,** *13* (12), 837-849.

47. Dyer, P. E., Excimer laser polymer ablation: twenty years on. *Appl. Phys. A-Mater. Sci. Process.* **2003,** *77* (2), 167-173.

48. Cain, S. R., A photothermal model for polymer ablation - chemical modification *J. Phys. Chem.* **1993,** *97* (29), 7572-7577.

49. Sinkovics, B.; Gordon, P.; Harsanyi, G., Computer modelling of the laser ablation of polymers. *Appl. Therm. Eng.* **2010,** *30* (16), 2492-2498.

50. Kuper, S.; Brannon, J.; Brannon, K., Threshold behavior in polyimide photoablation: single-shot rate measurements and surface-temperature modeling *Appl. Phys. A-Mater. Sci. Process.* **1993,** *56* (1), 43-50.

51. Kuper, S.; Stuke, M., Femtosecond UV excimer laser ablation *Applied Physics B-Photophysics and Laser Chemistry* **1987,** *44* (4), 199-204.

52. Sutcliffe, E.; Srinivasan, R., Dynamics of UV laser ablation of organic polymer surfaces *J. Appl. Phys.* **1986,** *60* (9), 3315-3322.

53. Kuper, S.; Stuke, M., UV-excimer-laser ablation of polymethylmethacrylate at 248 nm - characterization of incubation sites with fourier-transform IR-spectroscopy and UV-spectroscopy. *Appl. Phys. A-Mater. Sci. Process.* **1989,** *49* (2), 211-215.

54. Baudach, S.; Bonse, J.; Krautek, W., Ablation experiments on polyimide with femtosecond laser pulses. *Appl. Phys. A-Mater. Sci. Process.* **1999,** *69*, S395-S398.

55. Dyer, P. E.; Farley, R. J., Periodic surface-structures in the excimer laser ablative etching of polymers *Appl. Phys. Lett.* **1990,** *57* (8), 765-767.

56. Catry, C.; Jeuris, K.; Jackers, C.; Hofkens, J.; Bastin, L.; Gensch, T.; Grim, P. C. M.; De Schryver, F. C.; Van Damme, M., Confocal and scanning probe microscopy of surface modifications of thin polymer films induced by infrared diode laser irradiation. *Langmuir* **1999,** *15* (4), 1364-1372.

57. Znovena, J., Picture. Monaco, K., Ed. 2008; p 1.

58. Ortelli, E. E.; Geiger, F.; Lippert, T.; Wei, J.; Wokaun, A., UV-laser-induced decomposition of Kapton studied by infrared spectroscopy. *Macromolecules* **2000,** *33* (14), 5090-5097.

59. Parikh, M., Corrections to Proximity Effects in Electron-Beam Lithography .1. Theory *J. Appl. Phys.* **1979,** *50* (6), 4371-4377.

60. Chang, T. H. P., Proximity Effect in Electron-Beam Lithograpy. *Journal of Vacuum Science & Technology* **1975,** *12* (6), 1271-1275.

61. LaFratta, C. N.; Fourkas, J. T.; Baldacchini, T.; Farrer, R. A., Multiphoton fabrication. *Angew. Chem.-Int. Edit.* **2007,** *46* (33), 6238-6258.

62. Bustillo, J. M.; Howe, R. T.; Muller, R. S., Surface micromachining for microelectromechanical systems. *Proceedings of the IEEE* **1998,** *86* (8), 1552-1574.

63. Zhao, Y. P.; Wang, L. S.; Yu, T. X., Mechanics of adhesion in MEMS - a review. *J. Adhes. Sci. Technol.* **2003,** *17* (4), 519-546.

64. Bhushan, B., Adhesion and stiction: Mechanisms, measurement techniques, and methods for reduction. *J. Vac. Sci. Technol. B* **2003,** *21* (6), 2262-2296.

65. Tanaka, T.; Morigami, M.; Oizumi, H.; Ogawa, T., Freeze-drying process to avoid resist pattern collapse *Jpn. J. Appl. Phys. Part 1 - Regul. Pap. Short Notes Rev. Pap.* **1993,** *32* (12A), 5813-5814.

66. Shi, Y. Solvent study on micro towers fabricated via MAP. The University of Maryland, College Park, 2008.

67. BASF, Lucirin TPO-L. In *Technical Information, Coatings Raw Materials* BASF, Ed. 1999.

68. Williams, R.; Goodman, A. M., Wetting of Thin-Layers of SiO2 by Water. *Appl. Phys. Lett.* **1974,** *25* (10), 531-532.

69. Goeders, K. M.; Colton, J. S.; Bottomley, L. A., Microcantilevers: Sensing chemical interactions via mechanical motion. *Chem. Rev.* **2008,** *108* (2), 522-542.

70. Meyer, E., Atomic Force Microscopy. *Prog. Surf. Sci.* **1992,** *41* (1), 3-49.

71. LaFratta, C. Multiphoton Absorption Polymerization: Issues and Solutions University of Maryland, College Park, MD, 2006.

72. Ha, K.; Kim, J.-M.; Rabolt, J. F., Monolayer studies of perfluorostearic acid at air/water interface. *Thin Solid Films* **1999,** *347* (1-2), 272-277.

73. Bratton, D.; Yang, D.; Dai, J. Y.; Ober, C. K., Recent progress in high resolution lithography. *Polym. Adv. Technol.* **2006,** *17* (2), 94-103.

74. Geissler, M.; Xia, Y. N., Patterning: Principles and some new developments. *Adv. Mater.* **2004,** *16* (15), 1249-1269.

75. DuPont, DuPont PerMX 3000 Photodielectric dry film adhesive technical data sheet. DuPont, Ed. DuPont: 2010.

76. Nuzzo, R. G.; Allara, D. L., Adsorption of bifunctional organic disulfides on gold surfaces *J. Am. Chem. Soc.* **1983,** *105* (13), 4481-4483.

77. Ronse, K., Optical lithography - a historical perspective. *C. R. Phys.* **2006,** *7* (8), 844-857.

78. Maruo, S.; Fourkas, J. T., Recent progress in multiphoton microfabrication. *Laser Photon. Rev.* **2008,** *2* (1-2), 100-111.

79. Lockhart, D. J.; Winzeler, E. A., Genomics, gene expression and DNA arrays. *Nature* **2000,** *405* (6788), 827-836.

80. Debouck, C.; Goodfellow, P. N., DNA microarrays in drug discovery and development. *Nature Genet.* **1999,** *21*, 48-50.

81. Schena, M., *Microarray Analysis*. John Wiley & Sons: Hooken, New Jersey, 2003.

82. Duggan, D. J.; Bittner, M.; Chen, Y. D.; Meltzer, P.; Trent, J. M., Expression profiling using cDNA microarrays. *Nature Genet.* **1999,** *21*, 10-14.

83. Cheung, V. G.; Morley, M.; Aguilar, F.; Massimi, A.; Kucherlapati, R.; Childs, G., Making and reading microarrays. *Nature Genet.* **1999,** *21*, 15-19.

84. Bryant, P. A.; Venter, D.; Robins-Browne, R.; Curtis, N., Chips with everything: DNA microarrays in infectious diseases. *Lancet Infect. Dis.* **2004,** *4* (2), 100-111.

85. Robertson, B. H.; Nicholson, J. K. A., New microbiology tools for public health and their implications. *Annu. Rev. Public Health* **2005,** *26*, 281-302.

86. Niu, S.; Singh, G.; Saraf, R. F., Label-less fluorescence-based method to detect hybridization with applications to DNA micro-array. *Biosens. Bioelectron.* **2007,** *23* (5), 714-720.

87. Fei, Y. Y.; Landry, J. P.; Sun, Y. S.; Zhu, X. D.; Luo, J. T.; Wang, X. B.; Lam, K. S., A novel high-throughput scanning microscope for label-free detection of protein and small-molecule chemical microarrays. *Rev. Sci. Instrum.* **2008,** *79* (1), 7.

88. Tsay, Y. G.; Lin, C. I.; Lee, J.; Gustafson, E. K.; Appelqvist, R.; Magginetti, P.; Norton, R.; Teng, N.; Charlton, D., Optical biosensor assay (OBA). *Clin. Chem.* **1991,** *37* (9), 1502-1505.

89. Charbonnier, M.; Romand, M.; Harry, E.; Alami, M., Surface plasma functionalization of polycarbonate: Application to electroless nickel and copper plating. *J. Appl. Electrochem.* **2001,** *31* (1), 57-63.

90. Kumi, G.; Yanez, C. O.; Belfield, K. D.; Fourkas, J. T., High-speed multiphoton absorption polymerization: fabrication of microfluidic channels with arbitrary cross-sections and high aspect ratios. *Lab Chip 10* (8), 1057-1060.

91. Zaramella, S.; Yeheskiely, E.; Stromberg, R., A method for solid-phase synthesis of oligonucleotide 5 '-peptide-conjugates using acid-labile alpha-amino protections. *J. Am. Chem. Soc.* **2004,** *126* (43), 14029-14035.

92. Ellington, A.; Pollard, J. D., *Synthesis and Purification of Oligonucleotides*. John Wiley and Sons, Inc.: 2008.

93. McGall, G. H.; Barone, A. D.; Diggelmann, M.; Fodor, S. P. A.; Gentalen, E.; Ngo, N., The efficiency of light-directed synthesis of DNA arrays on glass substrates. *J. Am. Chem. Soc.* **1997,** *119* (22), 5081-5090.

94. Cox, J. D.; Curry, M. S.; Skirboll, S. K.; Gourley, P. L.; Sasaki, D. Y., Surface passivation of a microfluidic device to glial cell adhesion: a comparison of hydrophobic and hydrophilic SAM coatings. *Biomaterials* **2002,** *23* (3), 929-935.

95. Bruckbauer, A.; Zhou, D. J.; Kang, D. J.; Korchev, Y. E.; Abell, C.; Klenerman, D., An addressable antibody nanoarray produced on a nanostructured surface. *J. Am. Chem. Soc.* **2004,** *126* (21), 6508-6509.

96. Riepl, M.; Enander, K.; Liedberg, B.; Schaferling, M.; Kruschina, M.; Ortigao, F., Functionalized surfaces of mixed alkanethiols on gold as a platform for oligonucleotide microarrays. *Langmuir* **2002,** *18* (18), 7016-7023.

97. Hanson, E. L.; Schwartz, J.; Nickel, B.; Koch, N.; Danisman, M. F., Bonding self-assembled, compact organophosphonate monolayers to the native oxide surface of silicon. *J. Am. Chem. Soc.* **2003,** *125* (51), 16074-16080.

98. Ulman, A., Formation and structure of self-assembled monolayers. *Chem. Rev.* **1996,** *96* (4), 1533-1554.

99. Gawalt, E. S.; Lu, G.; Bernasek, S. L.; Schwartz, J., Enhanced bonding of alkanephosphonic acids to oxidized titanium using surface-bound alkoxyzirconium complex interfaces. *Langmuir* **1999,** *15* (26), 8929-8933.

100. Gawalt, E. S.; Avaltroni, M. J.; Koch, N.; Schwartz, J., Self-assembly and bonding of alkanephosphonic acids on the native oxide surface of titanium. *Langmuir* **2001,** *17* (19), 5736-5738.

101. Hauffman, T.; Blajiev, O.; Snauwaert, J.; van Haesendonck, C.; Hubin, A.; Terryn, H., Study of the Self-Assembling of n-Octylphosphonic Acid Layers on Aluminum Oxide. *Langmuir* **2008,** *24* (23), 13450-13456.

102. Gao, W.; Reven, L., SOLID-STATE NMR-STUDIES OF SELF-ASSEMBLED MONOLAYERS. *Langmuir* **1995,** *11* (6), 1860-1863.

103. Woodward, J. T.; Ulman, A.; Schwartz, D. K., Self-assembled monolayer growth of octadecylphosphonic acid on mica. *Langmuir* **1996,** *12* (15), 3626-3629.

104. Morkved, T. L.; Lopes, W. A.; Hahm, J.; Sibener, S. J.; Jaeger, H. M., Silicon nitride membrane substrates for the investigation of local structure in polymer thin films. *Polymer* **1998,** *39* (16), 3871-3875.

105. Green, E. D.; Kino, G. S., Atmospheric scanning electron-microscopy using silicon-nitride thin-film windows *J. Vac. Sci. Technol. B* **1991,** *9* (3), 1557-1558.

106. Petersen, K. E., Silicon as a mechanical material *Proc. IEEE* **1982,** *70* (5), 420-457.

107. Stutius, W.; Streifer, W., Silicon-nitride films on silicon for optical-waveguides. *Appl. Optics* **1977,** *16* (12), 3218-3222.

108. Barth, M.; Kouba, J.; Stingl, J.; Lochel, B.; Bensona, O., Modification of visible spontaneous emission with silicon nitride photonic crystal nanocavities. *Opt. Express* **2007,** *15* (25), 17231-17240.

109. Makarova, M.; Vuckovic, J.; Sanda, H.; Nishi, Y., Silicon-based photonic crystal nanocavity light emitters. *Appl. Phys. Lett.* **2006,** *89* (22), 3.

110. McCutcheon, M. W.; Loncar, M., Design of a silicon nitride photonic crystal nanocavity with a Quality factor of one million for coupling to a diamond nanocrystal. *Opt. Express* **2008,** *16* (23), 19136-19145.

111. Ropp, C.; Cummins, Z.; Probst, R.; Qin, S. J.; Fourkas, J. T.; Shapiro, B.; Waks, E., Positioning and Immobilization of Individual Quantum Dots with Nanoscale Precision. *Nano Lett.* **2010,** *10* (11), 4673-4679.

112. Ropp, C.; Probst, R.; Cummins, Z.; Kumar, R.; Berglund, A. J.; Raghavan, S. R.; Waks, E.; Shapiro, B., Manipulating Quantum Dots to Nanometer Precision by Control of Flow. *Nano Lett.* **2010,** *10* (7), 2525-2530.

113. Ding, F.; Zhong, Q.; Brindza, M. R.; Fourkas, J. T.; Walker, R. A., Ti:sapphire, broadband vibrational sum-frequency generation spectrometer with a counter-propagating geometry. *Opt. Express* **2009,** *17* (17), 14665-14675.

114. Briggs, D.; Seah, M. P., *Practical surface analysis: by auger and x-ray photoelectron spectroscopy*. Wiley: New York, 1983.

115. Gouzman, I.; Dubey, M.; Carolus, M. D.; Schwartz, J.; Bernasek, S. L., Monolayer vs. multilayer self-assembled alkylphosphonate films: X-ray photoelectron spectroscopy studies. *Surf. Sci.* **2006,** *600* (4), 773-781.

116. Lu, R.; Gan, W.; Wu, B. H.; Chen, H.; Wang, H. F., Vibrational polarization spectroscopy of CH stretching modes of the methylene goup at the vapor/liquid interfaces with sum frequency generation. *J. Phys. Chem. B* **2004,** *108* (22), 7297-7306.

117. Ding, F.; Hu, Z. H.; Zhong, Q.; Manfred, K.; Gattass, R. R.; Brindza, M. R.; Fourkas, J. T.; Walker, R. A.; Weeks, J. D., Interfacial Organization of Acetonitrile: Simulation and Experiment. *J. Phys. Chem. C* **2010,** *114* (41), 17651-17659.

118. Liu, Y.; Wolf, L. K.; Messmer, M. C., A study of alkyl chain conformational changes in self-assembled n-octadecyltrichlorosilane monolayers on fused silica surfaces. *Langmuir* **2001,** *17* (14), 4329-4335.

119. Keszthelyi, T.; Paszti, Z.; Rigo, T.; Hakkel, O.; Telegdi, J.; Guczi, L., Investigation of solid surfaces modified by Langmuir-Blodgett monolayers using sum-frequency vibrational spectroscopy and X-ray photoelectron spectroscopy. *J. Phys. Chem. B* **2006,** *110* (17), 8701-8714.

120. Dubey, M.; Weidner, T.; Gamble, L. J.; Castner, D. G., Structure and Order of Phosphonic Acid-Based Self-Assembled Monolayers on Si(100). *Langmuir* **2010,** *26* (18), 14747-14754.

121. Cumpson, P. J., The Thickogram: a method for easy film thickness measurement in XPS. *Surf. Interface Anal.* **2000,** *29* (6), 403-406.

122. Cumpson, P. J.; Seah, M. P., Elastic scattering corrections in AES and XPS .2. Estimating attenuation lengths and conditions required for their valid use in overlayer/substrate experiments. *Surf. Interface Anal.* **1997,** *25* (6), 430-446.

123. Merzlikin, S. V.; Tolkachev, N. N.; Strunskus, T.; Witte, G.; Glogowski, T.; Woll, C.; Grunert, W., Resolving the depth coordinate in photoelectron spectroscopy - Comparison of excitation energy variation vs. angular-re solved XPS for the analysis of a self-assembled monolayer model system. *Surf. Sci.* **2008,** *602* (3), 755-767.

124. Ye, S.; Nihonyanagi, S.; Uosaki, K., Sum frequency generation (SFG) study of the pH-dependent water structure on a fused quartz surface modified by an octadecyltrichlorosilane (OTS) monolayer. *Phys. Chem. Chem. Phys.* **2001,** *3* (16), 3463-3469.